Nanocomposite Electrodes for Electrochemical Supercapacitors

Fabrication and Characterization of High Mass-Loading Nanocomposite Electrodes for Electrochemical Supercapacitors

A Thesis Submitted to the School of Graduate Studies in Partial Fulfillment of the Requirements for the Degree Master of Applied Science

Written by:

Kaelan Jared Rorabeck B.Eng

April 4th, 2021

McMaster University

McMaster University MASTER OF APPLIED SCIENCE (2021) Hamilton, Ontario (Materials Science and Engineering)

TITLE: Fabrication and Characterization of High Mass-Loading Nanocomposite Electrodes for Electrochemical Supercapacitors

AUTHOR: Kaelan Jared Rorabeck, B.Eng. (McMaster University, Canada)

SUPERVISOR: Dr. Igor Zhitomirsky, Distinguished Engineering Professor, Ph.D., P.Eng.

NUMBER OF PAGES: 95

Lay abstract

The ever-growing realization that our energy consumption as a civilization is not sustainable, has fueled people around the globe to imagine and design new methods of energy storage, in attempts to mitigate this issue. From the foundational works of scientists, it has become clear to see that there is not “one right answer”. Instead, the unique benefits and drawbacks of energy storage technologies should be balanced and applied in situations where their properties permit a high efficacy. The intention of this work is to assist in the development of new materials to be used for energy storage devices called electrochemical supercapacitors. Novel colloidal processing techniques were developed, leading to the fabrication of high-performance electrodes, and providing further insight to the structure-properties relationship of organic extractors and co-dispersing agents for the design of nanocomposites.

Abstract

Supercapacitor electrodes were fabricated at a high active mass loading and exhibited enhanced electrochemical capacitance. A conceptually new salting-out extraction processing technique for the synthesis of dispersed Mn_3O_4-carbon nanotube (CNT) nanocomposites was developed, alleviating the need for hydrophobic solvents. The choice of isopropyl alcohol and NaCl for the extraction process offer advantages of an easy upscaling of this process. The salting out technique was shown to work with Octanohydroxyamic acid (OHA) and Lauryl Gallate (LG) as extractors and dispersants, critical to the success of the extraction. Mechanisms for surface adsorption on Mn_3O_4 and CNT for both OHA and LG are discussed. A secondary project was also undertaken, to investigate the use of chlorogenic acid and 3,4,5 – trihydroxybenzamide, as co-dispersing agents for MnO_2 and CNTs. These molecules are used due to their unique structural properties, which are discussed. The electrodes fabricated using these co-dispersants showed significant increases in their specific capacitances and SEM imaging indicated improved mixing, compared to samples prepared without dispersants. A specific capacitance of 6.5 F g^{-1} was achieve at low electrical resistance, attributed to the microstructure of electrodes prepared with the co-dispersant molecules.

Acknowledgements

1. Front and centre, I need to thank Dr Zhitomirsky for his unwavering patience and commitment to myself and the rest of the Zhitomirsky group during these challenging times during the COVID-19 pandemic. His knowledge of the development and workings of supercapacitor devices, his materials science background, as well as chemistry and physics proved to be an unparalleled boon. I am blessed to have had the opportunity to work with such a great scientist, and I sincerely hope I will be able to again in the future.
2. I would like to recognize the Mohammed Nawwar, Pamela Liang, Xuelin Li, Jessica Liu and Heyfer Zhao, as well as Ryan Poon and Amanda Clifford, for helping me with feeling comfortable and welcomed into the Zhitomirsky group, as well as guidance and fruitful scientific, and casual discussions. I wish you all the best in your futures.
3. Without the unconditional support of my family, financially and emotionally, there would have been no way this would have been possible. I would also like to give special thanks to my friends Jeromy Williams and Cal Siemens for their support, friendship, and comradery throughout my times here at McMaster. Words cannot describe my appreciation.
4. Jhoynner Martinez at the CCEM and Maureen Fitzpatrick at MAX, thank you both for your amazing insights and helpful discussions. Both facilities are fortunate to have you on board.

Table of Contents

Lay abstract iii

Abstract iv

Acknowledgements v

Declaration of academic achievements x

Chapter 1: Introduction 1

Chapter 2.0: Literature Review 5

2.1 Supercapacitor energy storage mechanisms 5

  2.1.1 Electrostatic Double Layer Capacitance 7

  2.1.2 Pseudocapacitance 10

2.2 Advanced Electrode Materials 15

  2.2.1 Conducting Polymers 15

  2.2.2 Carbon Materials 17

  2.2.3 Metal Oxides 19

  2.3 Supercapacitor electrolytes 22

Chapter 3 – Electrode Fabrication 28

References 33

Chapter 4 – Objectives 37

Chapter 5 –Application of Octanohydroxamic Acid for Salting out Liquid–Liquid Extraction of Materials for Energy Storage in Supercapacitors 38

1. Introduction 39

2. Results and Discussion 42

3. Materials and Methods 47

4. Conclusions 48

References 49

Chapter 6 – Salting-out aided dispersive extraction of Mn3O4 nanoparticles and carbon nanotubes for application in supercapacitors 52

Chapter 7 – Dispersant Molecules with Functional Catechol Groups for Supercapacitor Fabrication 69

1. Introduction 69

2. Results and Discussion 71

3. Materials and Methods 79

4. Conclusions 80

References 80

Chapter 8 – Conclusions and Future Works 83

List of Figures and Tables

Figure 1. Ragone Plot for various energy storage devices[2]. 1
Figure 2. Diagram of charge distribution within EDLC when discharged, and when charged.[19] 8
Figure 3. Depiction of (a) Helmholtz Model (b) Gouy-Chapman Model (c) Stern Model [21] 8
Figure 4. Illustration of two capacitors in series to represent capacitive contribution from Helmholtz layer and diffuse layer 9
Figure 5. Visualization of faradaic mechanisms of Pseudocapacitance as described by Conway [22] 10
Figure 6. Plot of Capacitance C ϕ , as a function of θ and V, for gθ=0 and gθ>0 [21]. 12
Figure 7. Intercalating mechanism of Akali metals in carbon matrix [30] 13
Figure 8. Schematic showing the mechanism of hydroxide intercalation in a $LaMnO_3$ lattice [31] 14
Figure 9. A) Polyaniline monomer B) Polypyrrole monomer 16
Figure 10. Polymorphs of Manganese Dioxide [49]. 21
Figure 11. Flow chart for possible supercapacitor electrolytes.[59] 22
Figure 12. Cases of potential vs time for GCD measurements of supercapacitor electrodes [64] 26
Figure 13. Cyclic voltagram with highlighted charge area from OHA dispersed Mn_3O_4 CNT electrode at a scan rate of 2 mV s^{-1} 27
Figure 14. Schematic of a liquid-liquid extraction [69]. 30
Figure 15. Carbon nanotubes fixed at the interface of a brine (bottom), and isopropanol (top). 31

Table 1. Relations for the three Faradaic charge mechanisms identified by Conway [21] 15
Table 2. Comparison of properties of carbon materials for use in EDLCs. [44] 19
Table 3. Summary of additives for different aqueous electrolytes 23

TABLE OF ABBREVIATIONS AND SYMBOLS

[ox]	Concentration of oxidized species
[red]	Concentration of reduced species
A (unit)	Amp
mL (unit)	Milliliter
V (unit)	Volt
F (unit)	Farad
g (unit)	Gram
m (unit)	Meter
C (unit)	Coulomb
J (unit)	Joule
K (unit)	Kelvin
s (unit)	Second
S (unit)	Siemens
Ω (unit)	Ohm
A	Area
AC	Alternating Current
C	Capacitance
C_{Φ}	Capacitance from pseudocapacitance
C^+	Cation
C’	Real component of capacitance calculated from EIS data
C”	Imaginary component of capacitance calculated from EIS data
$C_{Diffuse}$	Capacitance associated with diffuse layer
$C_{Helmholtz}$	Capacitance associated with the Helmholtz layer
C_{total}	The total calculated capacitance for a given equivalent circuit
CP	Conducting Polymer
CV	Cyclic voltammetry or cyclic voltammogram
d	The conducting surface separation distance
DI	Deionized
ε_d	Dielectric Constant
ε_o	Permeability of free space/vacuum
E	Electrode potential
e^-	Electron
E°	Standard electrode potential
Ecap	Energy stored in capacitor
EDLC	Electrical double layer capacitance/capacitor
EIS	Electrochemical Impedance Spectroscopy
ℱ	Faraday’s constant
ℊ	Constant accounting for the interaction between adjacent lead atoms during the underpotential deposition of lead on gold

H^+	Proton
HAM	High Active Mass
I	Current
I_{power}	Current when the capacitor shows max power
IR_{drop}	Voltage drop due to internal resistance of capacitor
K	Proportionality constant
LG	Lauryl gallate
LLE	Liquid-Liquid Extraction
MWCNT	Multi-wall carbon nanotube
MO	Metal Oxide
NEC	Nippon Electrical company
Θ_{pb}	Fractional surface area of lead
P	Power of a capacitor
P_{max}	Maximum power of a capacitor
PANi	Polyaniline
PPy	Polypyrrole
PVB	Poly(vinyl butyral-*co*-vinyl alcohol-*co*-vinyl acetate), Average M_w = 50000-80000
q	Charge
R	Ideal gas constant
$R_{internal}$	Internal resistance of capacitor
SCE	Standard Calomel Electrode
SEM	Scanning Electron Microscopy
T	Temperature
V	Voltage
V_{max}	Maximum capacitor voltage
V_{power}	Voltage that the capacitor shows max power
t	Time
XPS	X-Ray Photoelectron Spectroscopy
XRD	X-Ray Diffraction
z	Associated charge transfer for a given redox reaction
Z’	Real component of impedance
Z”	Imaginary component of impedance
ΔE	Change in electrode potential
Θ_{Pb}	Fractional surface coverage of lead during underpotential deposition of lead on gold
ω	Frequency of sinusoidal signal used in EIS

Declaration of academic achievements

This dissertation was used to fulfill the requirements of the degree: Master of Applied Science. The majority of research was conducted from September 2019 to March 2021. The results of this dissertation were published in 3 papers in peer-reviewed journals, which were listed below:

1. Rorabeck, K., & Zhitomirsky, I. (2021). Application of Octanohydroxamic Acid for Salting out Liquid-Liquid Extraction of Materials for Energy Storage in Supercapacitors. *Molecules (Basel, Switzerland)*, *26*,296. https://doi.org/10.3390/molecules26020296
2. Rorabeck, K., & Zhitomirsky, I. (2021). Salting-out aided dispersive extraction of Mn3O4 nanoparticles and carbon nanotubes for application in supercapacitors. *Colloids and Surfaces A: Physicochemical and Engineering Aspects*, *618*, 126451. https://doi.org/10.1016/j.colsurfa.2021.126451
3. Rorabeck, K., & Zhitomirsky, I. (2021). *Dispersant molecules with functional catechol groups for supercapacitor fabrication*. 26,1709, https://doi.org/10.3390/molecules26061709

As these published papers were a direct result of this research work, these journal articles are included in the body of this dissertation as Chapters 5,6 and 7.

Chapter 1: Introduction

A supercapacitor is essentially a capacitor that can offer high capacitances, often in the order of thousands of Farads. Consider motor capacitors that generally provide between 20-1000 μF[1], Maxwell Technologies produces supercapacitors that provide up to 3000F. This magnitude of 10^6 F difference is one reason why so much research is being done on supercapacitor devices and the materials used in them. The components of supercapacitor devices do not differ greatly from electrolytic capacitors, in the sense that they both and contain a positive and a negative electrode in an electrolyte, separated by an ion permeable membrane, however the material used for the components are significantly different.

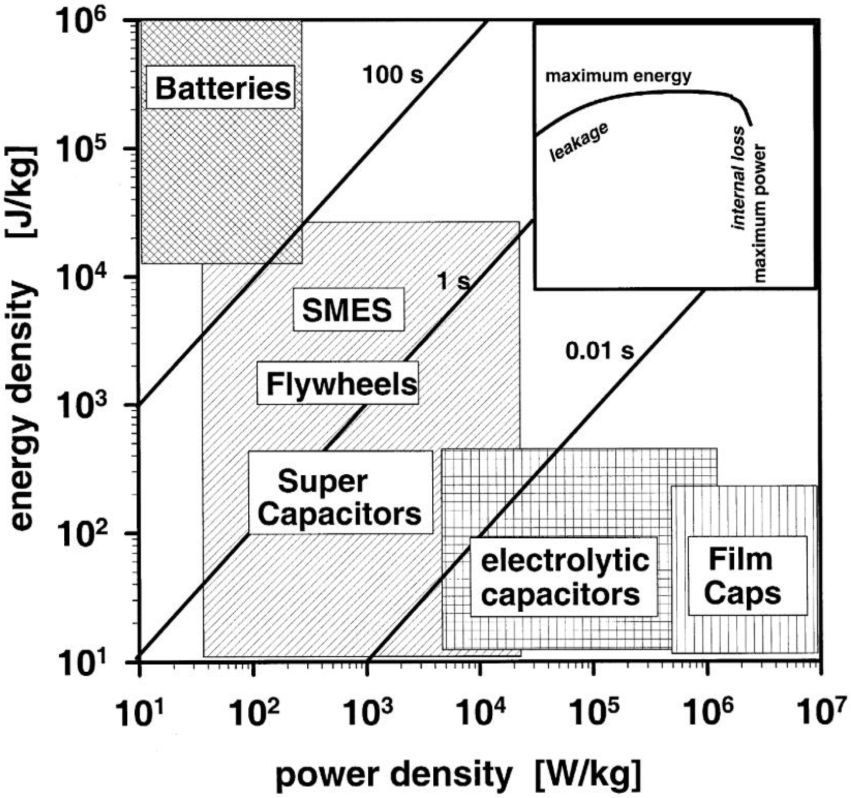

Figure 1. Ragone Plot for various energy storage devices[2].

Supercapacitors are not new technology, with the first patent coming from General Electric in 1957 for a “Low voltage electrolytic capacitor”, using carbon electrodes and providing a capacitance value of 6F at a range of 1-1.5V [3]. Initially these devices attracted very little attention, and no significant changes were seen until 1975, when the patent for an “Electrical Energy Storage Apparatus” was sold by the Standard Oil of Ohio Company to the Nippon Electric Company (NEC). This is when NEC began selling these electrochemical capacitors under the name “supercapacitors”. Soon afterwards, these devices were being tested as starters for automobiles and gained the attention of other companies such as Panasonic and Maxwell who began producing their own supercapacitors[4].

As energy storage devices, supercapacitors are subjected to the same criteria that batteries, fuel cells and capacitors are, namely energy to volume ratio, cycling life/stability, and rate of charge/discharge, when being selected for an application. Aside from these criteria, there are other aspects such as temperature range and overall ease of use, and materials with low toxicity and good environmental compatibility are becoming increasingly desirable [5]. Supercapacitors can be implemented as augmentations to energy systems, where they are paired with batteries to increase the efficiency of systems that have variable power demands, the Caterpillar 6120 hybrid is an example of this[6]. Countries have begun integrating supercapacitors into large public transport vehicles in China, Germany, France and the United States, with an example of the ISE hybrid-electric power train reporting a 25% improvement in fuel economy when compared to previous diesel powered buses[7]. These electrochemical devices are not limited to large scale applications, and can also be found in flashlights with variable power intensity[6], and capacitive de-ionization systems[5].

As stated previously, lots of research has been done on supercapacitors in recent years, so a few metrics have become commonplace to evaluate the performance of these devices. Gravimetric capacitance [F g^{-1}], areal capacitance [F cm^{-2}] and mass loading [mg cm^{-2}] are just a few metrics that are often mentioned. The first two are important for helping evaluate the economic feasibility of an active charge storage material. Mass loading is important for practical applications, to evaluate the mass ratio of active charge material to components that do not contribute to charge storage, such as the current collector and casing. Commercial supercapacitors are often sold with mass loadings greater than 20mg cm^{-2}. Often the mass loading is not stated explicitly, it can be easily calculated from product specifications. A Maxwell supercapacitor uses activated carbon at about 10% w/w, leading to a gravimetric capacitance of 60F g^{-1} at a mass loading of approximately 35mg/cm^{-2} [2,5]. One can easily find supercapacitors available commercially between 5-1000F, using carbon as an active material, from companies such as Maxwell or NEC.

Metal Oxides (MOs) and Conducting Polymers (CPs) have been a focus of recent research due to their high theoretical gravimetric capacitances. MnO_2 has been of interest due its theoretical capacitance of 1380 F g^{-1}, that makes it very appealing compared to carbon providing 300F g^{-1}. This value has been reached, however only using thin films[10], with one reason being the low electrical conductivity of MnO_2 , another being poor electrolyte permeability, that leads to significant reduction of capacitance at higher mass loadings [7,8]. For this reason, carbon materials are often combined with pseudocapacitive materials to increase conductivity [9–13]. The issue of agglomerates arises when combining MOs or CPs with conductive additives, where the reduction of surface area leads to a poor capacitive performance[17].

In this dissertation the focus was the development of new colloidal processing techniques to augment the dispersion of MWCNTs and promote mixing of the dispersed MWCNTs with MOs, specifically MnO_2 and Mn_3O_4. A secondary focus was put on the co-dispersion of MWCNTs with MnO_2 with the use of novel dispersants. As a result, 3 papers were published in peer reviewed journals, MDPI and Colloids and Surfaces A.

"Application of Octanohydroxamic Acid for Salting out Liquid-Liquid Extraction of Materials for Energy Storage in Supercapacitors" highlights the specific capacitance of Mn_3O_4-CNT electrodes at a mass loading of 40mg cm^{-2}, fabricated using the novel salting-out colloidal processing technique. Multi-functional OHA with Mn_3O_4, allowed for the dispersion of Mn_3O_4, as well as acting as a capping agent for the direct particle transfer to a 2-propanol phase for electrode processing. The nanocomposite showed a change in surface morphology after 1000 cycles, correlated with an increase in capacitance. The second publication, "Salting-out aided dispersive extraction of Mn_3O_4 nanoparticles and carbon nanotubes for application in supercapacitors" discusses the use of LG-Mn_3O_4 synthesized using another salting-out extraction method. These electrodes showed a higher capacitance and cycling stability after 1000 cycles than the electrodes fabricated using OHA. LG is used as a dispersant for MWCNTs with adsorption from π-π interactions, and adhesion to Mn_3O_4 from surface complexing, with SEM images indicating improved mixing. These works show the improvement in capacitive performance of Mn_3O_4-CNT electrodes, to a record high 6 F cm^{-2} for Mn_3O_4, based on the salting-out extraction method surpassing the limitation of other extraction processes, highlighting its advantages for fabrication of charge-storage nanocomposites.

"Dispersant molecules with functional catechol groups for supercapacitor fabrication" investigates the use of novel surfactants, chlorogenic acid and 3,4,5-trihydroxybenzamide, shown to have interesting optical and photovoltaic properties, as co-dispersing agents of MnO_2 and MWCNTs. This work showed the enhancement in electrode capacitance based on electrochemical testing and change in cyclic stability, and improved mixing and dispersion of both MnO_2 and MWCNT when compared to composites fabricated without the use of these co-dispersants.

Chapter 2.0: Literature Review

In this chapter, foundational topics will be addressed before proceeding into the published works in the subsequent chapters. First the energy storage mechanisms of supercapacitors will be discussed, followed by materials that are being used or are under consideration for supercapacitor applications, then electrolytes for supercapacitors, and concluding with electrochemical characterization techniques.

2.1 Supercapacitor energy storage mechanisms

In this section the two main energy storage mechanisms of supercapacitors will be discussed: electrostatic double layer capacitance (EDLC) and pseudocapacitance. Some supercapacitors exploit only one of these mechanisms, whereas some incorporate both and are aptly named hybrid supercapacitors[18].

Capacitance is described as charges of opposite polarity, stored on conducting surfaces, separated by some distance, and can be calculated using the following equation:

$$C = \frac{q}{V} \tag{1}$$

$$C = \varepsilon_d * \varepsilon_0 \frac{A}{d} \tag{2}$$

Where C is capacitance, q is the charge stored between the two conducting surfaces, V is the potential difference between the two surfaces in Equation (*1*). For a dielectric parallel plate capacitor, the capacitance is dependant on parameters represented by Equation (*2*), ε_d, is the dielectric constant of the material between the plates, ε_0, is vacuum permittivity, A is plate area, and d is the distance between the plates. Following Equation (*2*) therefore, the capacitance can be improved by increasing the dielectric constant, increasing surface area, and reducing the distance between charges.

Capacitance can also be related to the quantity of energy that can be stored by a capacitor which may be described using the following relationship:

$$E_{stored} = \int_0^{V_{max}} V dq \tag{3}$$

Combining Equation *(1)* and *(3)* gives:

$$E_{stored} = C \int_0^{V_{max}} V dV = \frac{1}{2} C V_{Max}^2 \tag{4}$$

This relationship shows that the amount of energy stored inside a capacitor would be increased by having a larger capacitance or using a higher maximum voltage.

Supercapacitors also need to be able to discharge their stored energy over a short time interval, also described as power, to be considered useful in many practical applications. A capacitor's maximum power (P_{max}) is related to the potential drop (V_{drop}) through the capacitor. The drop is described by maximum applied potential (V_{max}) minus $IR_{internal}$ due to the current (I) passing through the capacitor's electrical resistance ($R_{internal}$). To determine the maximum power output of a supercapacitor, consider the following equation for power (P):

$$P = V_{drop} * I = (V_{max} - IR_{internal}) * I \tag{5}$$

Taking the derivative of Equation *(5)* and setting it to 0 allows for the determination of the voltage and current that will provide the max power.

$$\frac{dP}{dI} = 0 = V_{max} - 2IR_{internal} \tag{6}$$

$$I_{power} = \frac{V_{max}}{2R_{internal}} \tag{7}$$

$$V_{power} = V_{max} - I_{power}R_{internal} = V_{max} - \frac{V_{max}}{2} = \frac{V_{max}}{2} \tag{8}$$

Substituting into Equation *(5)* this leads to the maximum power being described by:

$$P_{max} = \frac{V_{max}^2}{4R_{internal}} \tag{9}$$

Therefore, increasing the capacitance and the maximum potential drop across the electrodes, while keeping the internal resistances low would allow for more stored energy and high-power delivery.

2.1.1 Electrostatic Double Layer Capacitance

The electric double layer was first described by Hermann Von Helmholtz in the 1800’s, where two layers of opposite charge accumulate at the surface of metallic electrodes when submerged in an electrolyte under an applied potential. The distance between the two layers, characterized by the Debye length (≈ 1nm), was magnitudes smaller than the distance between charges in traditional capacitors (≈ 1µm), which contributes to the greater capacitance in EDLCs. The charge accumulation at the electrodes within the electrochemical cell can be seen in Figure 2.

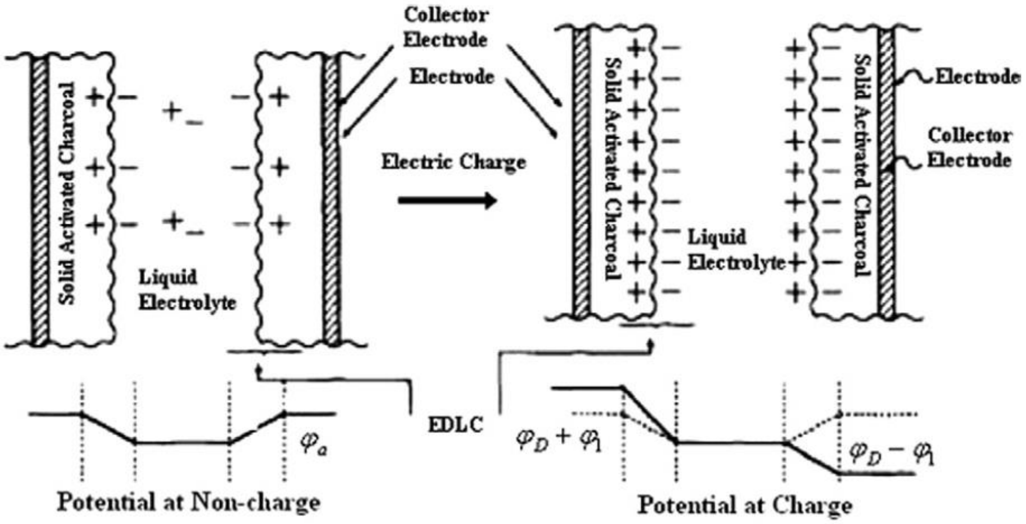

Figure 2. Diagram of charge distribution within EDLC when discharged, and when charged.[19]

In 1910 the Gouy-Chapman model was proposed, that accounted for diffusion in the electrolyte and highlighted the dependence of capacitance on the concentration of ions in the electrolyte[20]. Later the Stern model then combined the Helmholtz and Gouy-Chapman model, indicating that ions adhere to the surface of the electrode as described by Helmholtz, while a diffuse layer also existed past the Helmholtz layer boundary[21].

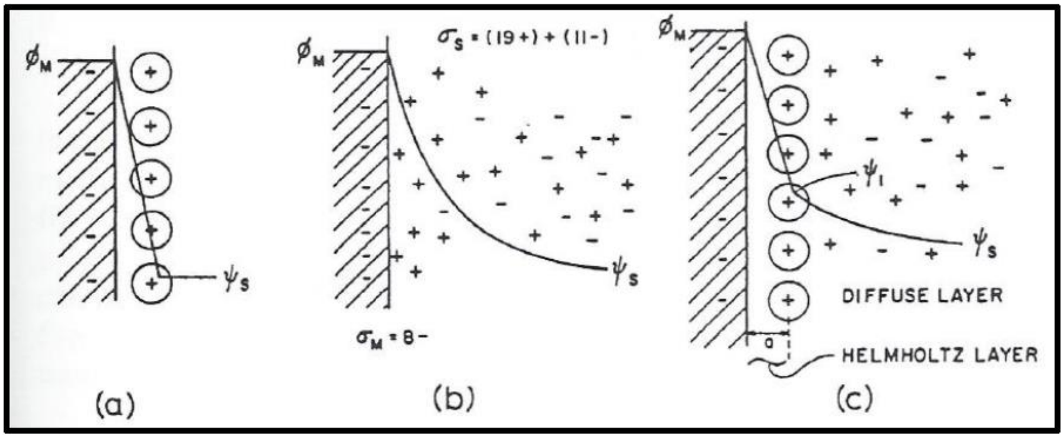

Figure 3. Depiction of (a) Helmholtz Model (b) Gouy-Chapman Model (c) Stern Model [21]

Using an equivalent circuit, a representation of the Stern model can be constructed to explain the capacitive contributions of the Helmholtz and the diffuse layer.

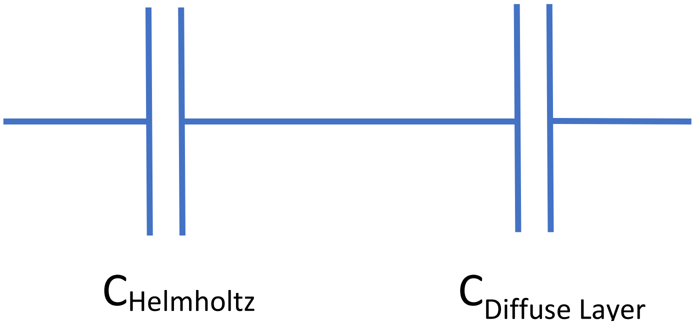

Figure 4. Illustration of two capacitors in series to represent capacitive contribution from Helmholtz layer and diffuse layer.

The total capacitance of capacitors in series is calculated as the inverse of the reciprocal sum of the components, where i indicates a different capacitive component and n is the total number of contributions to the capacitance:

$$C_{total} = \left(\sum_{i=1}^{n} \frac{1}{C_i}\right)^{-1} \tag{10}$$

Applying Equation (*10*), to the equivalent circuit in Figure 4, the following equation can be derived, where the mechanisms of capacitive component are stated in subscript.

$$C_{total} = \left(\frac{1}{C_{Helmholtz}} + \frac{1}{C_{Diffuse\ Layer}}\right)^{-1} \tag{11}$$

As capacitance values are in order of micro or nano Farads, the total in series capacitance will not be greater than the smallest of these two capacitances, based on Equation *(10)*. As stated earlier, the capacitance from the Helmholtz layer is dependent on the Debye length, which is usually much smaller than the distance between charges in the diffuse layer [20], making the limiting factor in the total capacitance $C_{\text{Diffuse Layer}}$. The capacitive contribution of the diffuse layer is reliant on the ability of ions in the electrolyte to diffuse away from the electrode surface. The Debye length and ion diffusion are both, linearly dependant on temperature and inversely dependant on ion concentration in the electrolyte [21]. Therefore, the selection of electrolyte can significantly change the capacitive behaviour of the electrochemical cell, which will be discussed in a later section.

2.1.2 Pseudocapacitance

In the 1990's Brian Conway published *Electrochemical Supercapacitors* [21], where he describes his work with ruthenium oxide electrochemical capacitors. He describes the ability of RuO_2 to hold charge as "Pseudocapacitance", due to its faradaic nature of charge transfer, to differentiate it from the electrostatic mechanisms described in EDLCs. Three mechanisms are identified for the faradaic charge storage of pseudocapacitive materials: Underpotential, Redox, and Intercalation[21].

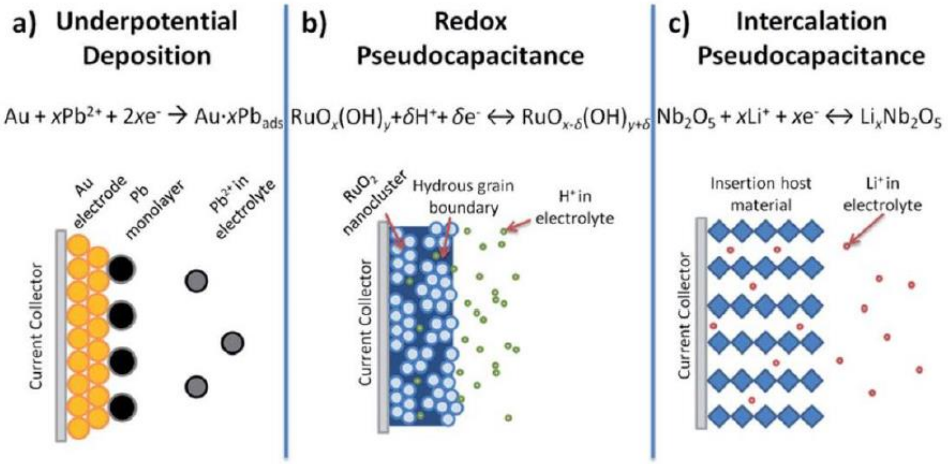

Figure 5. Visualization of faradaic mechanisms of Pseudocapacitance as described by Conway [22]

Underpotential deposition is a reversible reaction that can also be referred to as electrosorption, and can be seen in practical uses such as capacitive deionization technology[23]. The mechanism of underpotential was described using the deposition of lead atoms onto a gold substrate, as seen in Figure 5a). The theoretical electrosorption of lead atoms onto the gold substrate follows Langmuir's isotherm, with the major assumption that there are no interactions between the two species [24]. Equation*(12)* describes the fractional surface area of lead θ_{Pb} deposited onto the gold substrate based on the reaction in Figure 5a):

$$\frac{\theta_{Pb}}{1-\theta_{Pb}} = KC_{Pb}\exp\left(\frac{V\mathcal{F}}{RT}\right) \tag{12}$$

Where K is a constant and C_{Pb} is the concentration of lead ions in solution.

The capacitance from the separation of charge accumulated at the surface $C\phi$ can then be described using Equation *(13)*

$$C_{\phi} = q_{Pb}\frac{d\theta_{Pb}}{dV} = \frac{q_{Pb}\mathcal{F}}{RT}\theta_{Pb}(1-\theta_{Pb}) \tag{13}$$

However, the assumption that there is no interaction between the lead and the gold causes discrepancies with empirical data, where the value of C_{ϕ} is of the order of magnitude of $2000F\ cm^{-2}$, which 100x greater than that of EDLC[21]. Conway then introduced a term $g\theta$ to account for these interactions. This led to the formulation of Equation *(14)*

$$C_{\phi} = \frac{q_{Pb}\mathcal{F}}{RT}\frac{\theta_{Pb} * (1-\theta_{Pb)}}{1+g\theta_{Pb}(1-\theta_{Pb})} \tag{14}$$

Equation *(13)* and *(14)* both indicate a maximum capacitance when half of the gold surface is covered by lead. When plotted, Equation *(14)* creates a curve that indicates capacitance being spread over a larger potential window and reaching a lower maxima than Equation *(13)*, which can be seen in *Figure 6*. This correlates to the increase of the redox potential as the number of already oxidized adjacent lead atoms increases. This has been reported numerous times in literature, as symmetric cyclic voltammetry curves, that indicate pseudocapacitance changing with current and not voltage[15], [16], [22], [25]–[27].

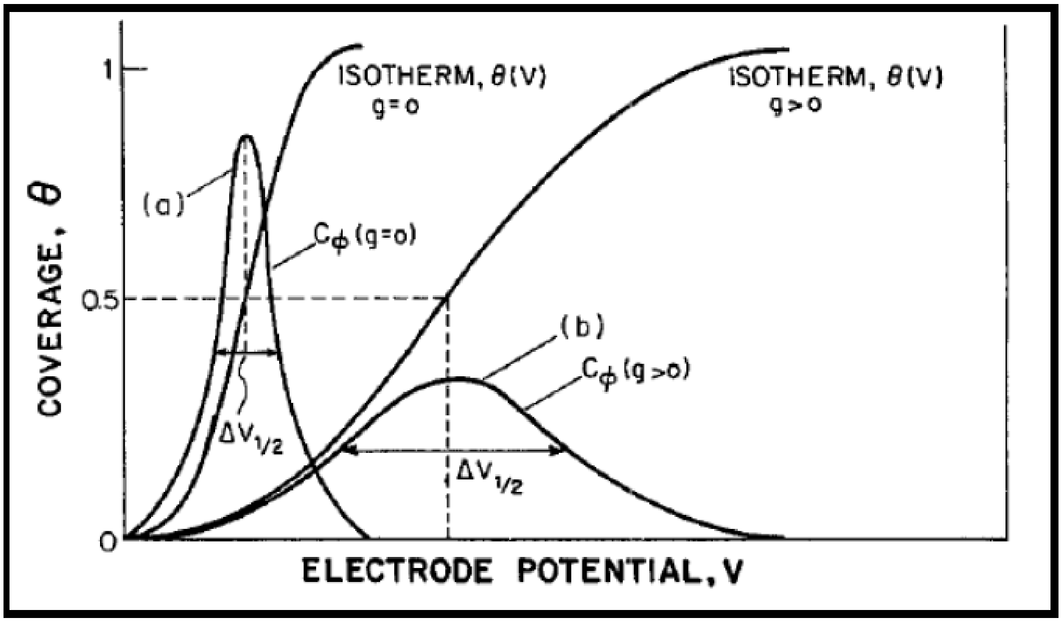

Figure 6. Plot of Capacitance C ϕ , as a function of θ and V, for gθ=0 and gθ>0 [21].

Redox pseudocapacitance transfers charge via fast surface reduction and oxidization reactions. The ions in solution are electrochemically adsorbed to the surface of the substrate creating chemical bonds, unlike those in underpotential depositions. These surface reactions are comparable to chemical reactions that occur in a battery yet without undergoing any phase changes and interactions only occurring at the surface[28]. The reactions taking place are reversible, leading to supercapacitors being able to undergo many charge-discharge cycles without experiencing degradation in performance [29]. Similarly to batteries, the energy in these reactions can be modelled using the Nernst Equation:

$$E = E_0 + \frac{z\mathcal{F}}{RT}\ln\left(\frac{\Re}{1-\Re}\right) \tag{15}$$

$$\Re = \frac{[ox]}{[ox]+[red]} \tag{16}$$

Where [ox] and [red] are the concentrations of oxidized or reduced species respectively, and z is the number of electrons transferred in a reaction. It can be seen in Equation *(15)* that the energy provided is logarithmically dependant on the extend of the redox reaction, which becomes important when considering that these reactions only occur at the surface.

Intercalating is a phenomenon in which a “host” matrix, changes to accompany a “guest” of another species. In recent years there have been discoveries in terms of the underlying principals behind intercalating and how it can be used to store energy. One method that intercalating stores energy is by expanding the lattice, bringing it to a higher energy state, through an applied potential; this mechanism is seen in carbon materials such as graphene, which will expand to accommodate cations such as potassium, like as seen in Figure 7.

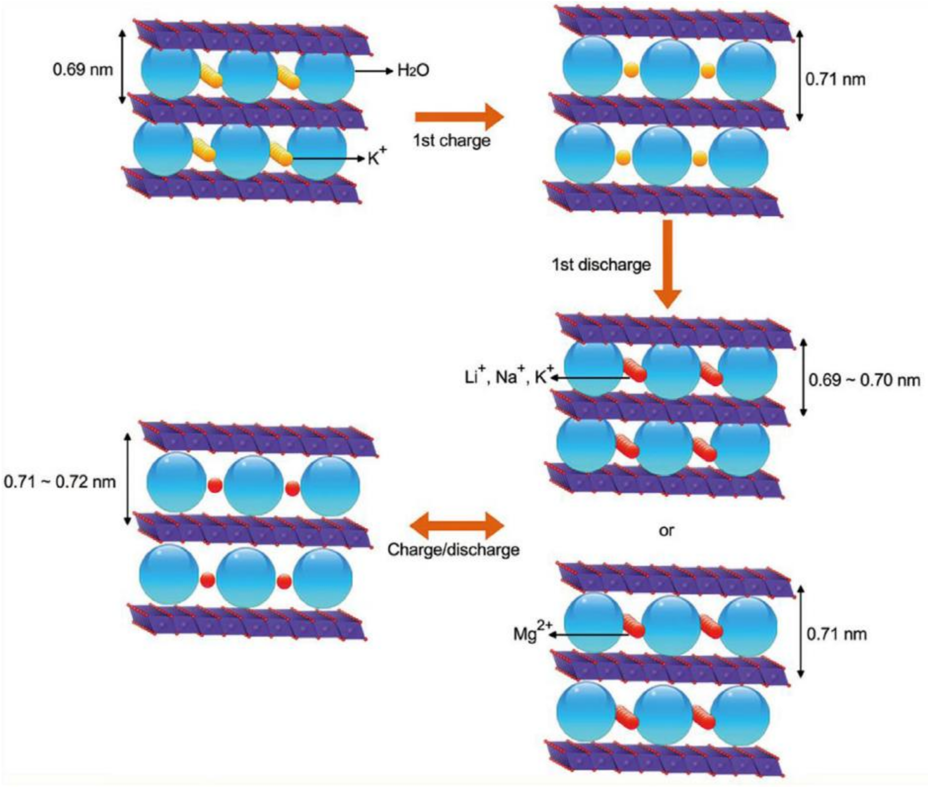

Figure 7. Intercalating mechanism of Akali metals in carbon matrix [30]

Another mechanism that has been recently investigated is the intercalating of oxygen in perovskite structures. This process involves the insertion of a charged molecule into a lattice defect, like a hydroxide seen in Figure 8, which then leads to the rearrangement of Mn atoms in the matrix and changing the oxidation state of a Mn atom from 3^+ to 4^+. This change in oxidation state attracts other hydroxide ions to sit inside interstitial lattice sites, where they can then be reduced by another hydroxide leaving a interstitial oxygen atom[31]. This interstitial oxygen atom elevates the oxidative state of surrounding Mn atoms, thus storing the energy of the applied potential.

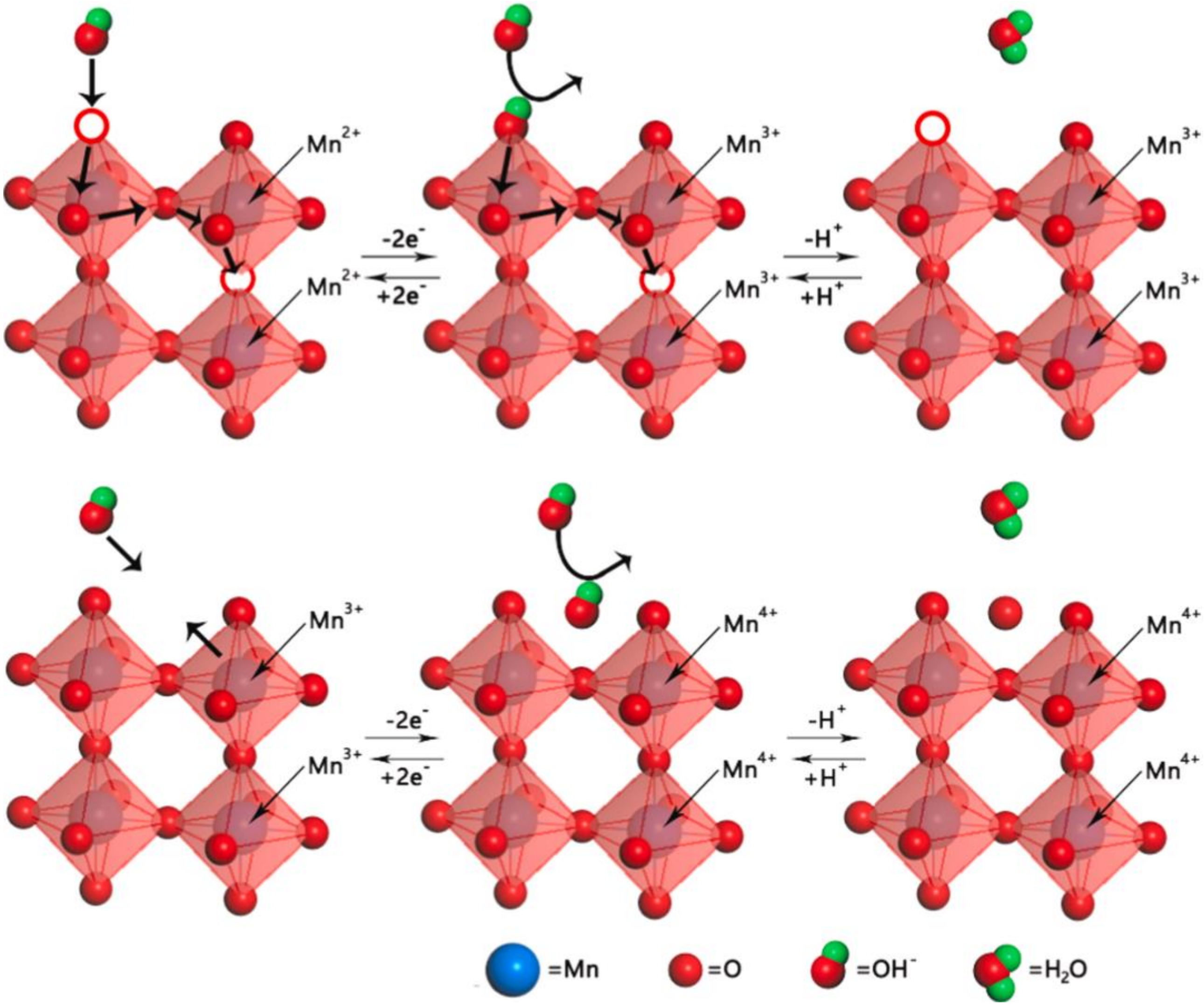

Figure 8. Schematic showing the mechanism of hydroxide intercalation in a $LaMnO_3$ lattice [31]

The energy stored via intercalating can be represented by the Nernst equation factoring in the fraction of intercalated lattice sites (X):

$$E = E_0 + \frac{zF}{RT} * Ln\left(\frac{X}{1-X}\right) \tag{17}$$

The energy storage relationship for each of these pseudocapacitive mechanisms can be seen in the summary provided in Table 1.

Table 1. Relations for the three Faradaic charge mechanisms identified by Conway [21]

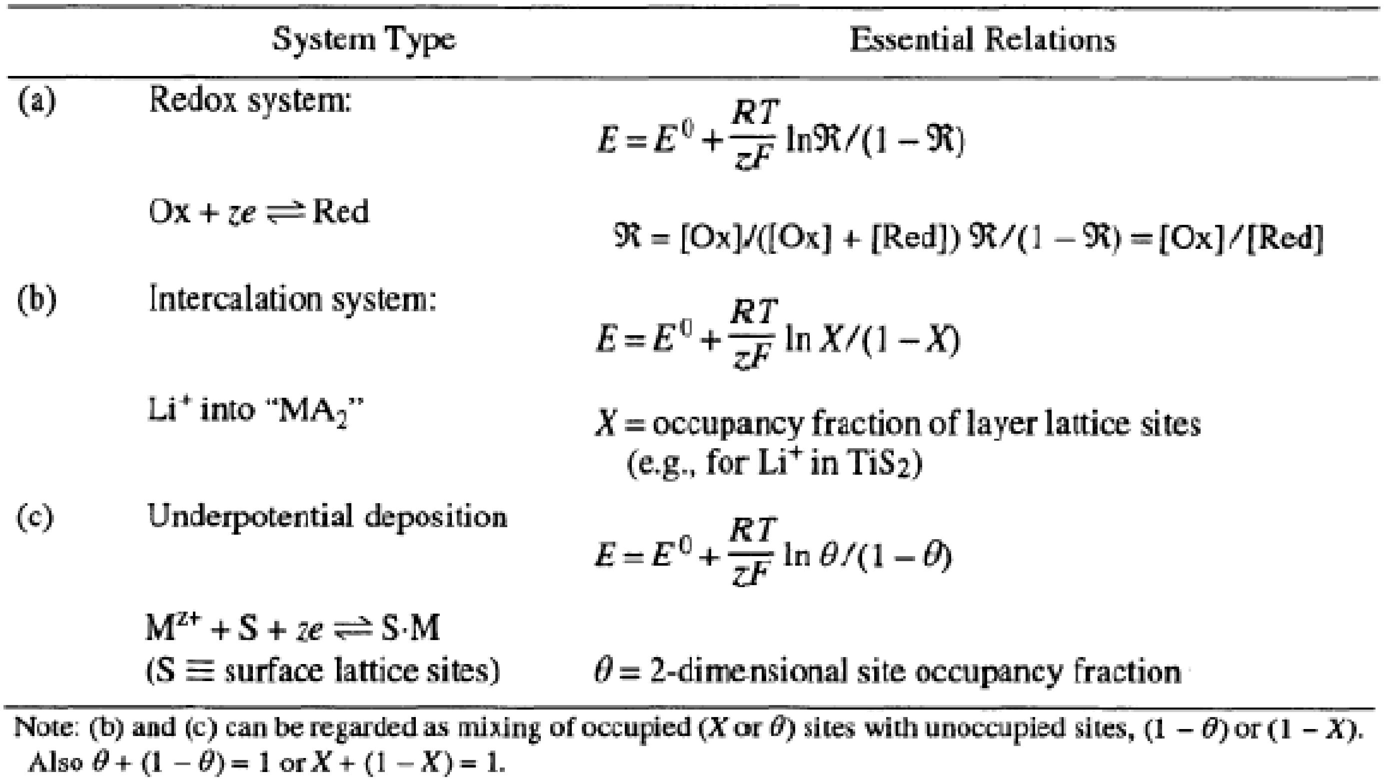

	System Type	Essential Relations
(a)	Redox system:	$E = E^0 + \frac{RT}{zF} \ln \Re/(1 - \Re)$
	$Ox + ze \rightleftharpoons Red$	$\Re = [Ox]/([Ox] + [Red])$ $\Re/(1 - \Re) = [Ox]/[Red]$
(b)	Intercalation system:	$E = E^0 + \frac{RT}{zF} \ln X/(1 - X)$
	Li^+ into "MA_2"	X = occupancy fraction of layer lattice sites (e.g., for Li^+ in TiS_2)
(c)	Underpotential deposition	$E = E^0 + \frac{RT}{zF} \ln \theta/(1 - \theta)$
	$M^{z+} + S + ze \rightleftharpoons S{\cdot}M$ ($S \equiv$ surface lattice sites)	θ = 2-dimensional site occupancy fraction

Note: (b) and (c) can be regarded as mixing of occupied (X or θ) sites with unoccupied sites, $(1 - \theta)$ or $(1 - X)$. Also $\theta + (1 - \theta) = 1$ or $X + (1 - X) = 1$.

2.2 Advanced Electrode Materials

In this section supercapacitor electrodes will be broken into three types of material classifications: conductive polymers, carbon-based compounds, metal oxides.

2.2.1 Conducting Polymers

Conducting polymers (CP) have strong potential to be used as bendable supercapacitor materials, due to their high flexibility compared to carbon and metal oxide materials, as well as low weight and cost[32]. Polymers of particular interest are polyaniline(PANi) and polypyrrole (PPy), due to their excellent conductivity [33] and high capacitance [12], and they will be the focus of this section. Other examples of potential CPs for supercapacitor applications include but are not limited to: Poly-acetylene, polythiophene, and poly(3,4-ethlyenedioxythiophene)[32].

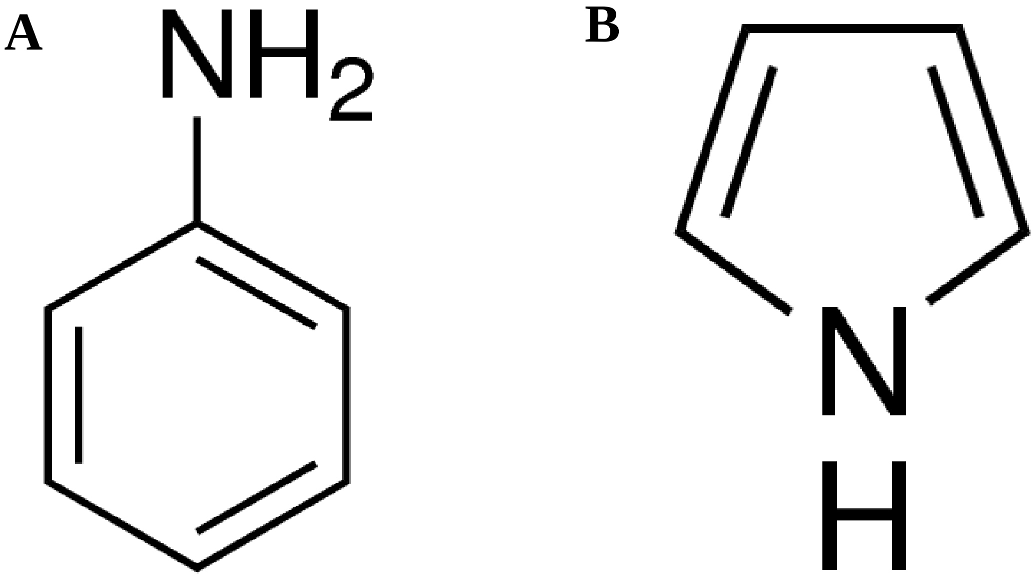

Figure 9. A) Polyaniline monomer B) Polypyrrole monomer

One of the earliest report of the synthesis of polyaniline was back 1862[33], meaning this polymer is no longer a new discovery. After its discovery little was reported on the polymer material, until the emergence of new characterization techniques in 1980s, after which it begun to gain popularity, where it was used in applications such as polyethylene welding, gas separation membrane, corrosion protective coatings. For supercapacitor applications, polyaniline has attractive properties such as high dopant compatibility, and electrochemical stability[5] at a cost that is generally lower than PPy[33]. Due to its high compatibility with dopants, PANi is often used in composite supercapacitor electrodes and literature shows a variation in capacitive results between 80 to 800 F g^{-1} [5].

Polypyrrole was first electrochemically synthesized in 1968, and later chemically synthesized in

1973 [33]. PPy has a theoretical gravimetric capacitance of 620 F g^{-1} , and as a CP its properties make it suiting as a material for supercapacitor electrodes. PPy also can show a very high conductivity for a polymer of around 600 S/cm [34], which makes its an appealing option from a versatility stand point such that it maybe be used a conductive additive or the charge storage material. PPy similarly to PANi, has also been used extensively in composite supercapacitor electrodes due to its compatibility with carbon-based compounds. Reports from literature have shown PPy based electrodes to have gravimetric capacitance values from between 30 to 400 F g^{-1} [5]. The monomers shown in Figure 9, do not intrinsically show high electrical conductivity. The electrical conductivity of these polymers is heavily dependant on the synthesis process, where conductivity is dependant on the amount of dopants and degree of background conjugation [35]. The main disadvantages of using CPs are that they have lower theoretical capacitance values than metal oxides and carbon compounds, and their poor cycling stability [12].

2.2.2 Carbon Materials

From section 2.1 it was identified that capacitance could be increased, by using materials with high surface area, low electrical resistance, and good thermal stability. Carbon materials can be manipulated into many different morphologies, varying from the buckminsterfullerene to diamonds, leading to carbon materials having a wide range of properties. Many carbon compounds have high electron mobility and can exhibit a very high specific surface area (1000-3000 m^2g^{-1}), such as graphene and activated carbon [36], that make them good candidates for use in supercapacitor electrodes.

Graphene was first created in 2004 by professors in Manchester, who discovered this single layered carbon material by using sticky tape to separate layers of graphite[37]. Since then, graphene has been tested extensively, with scientists finding applications for graphene in biomedicine, composites, coatings, and sensors. Graphene has the highest theoretical intrinsic capacitance of any carbon material at 550 F g^{-1}, that stems from a monolayer structure and high theoretical specific area of approximately 2600 m^2/g [38]. Graphene however has a tendency to stack and agglomerate leading to a reported capacitance value 190F g^{-1} [38] much lower than the theoretical 550F g^{-1}. Agglomeration is a challenge posed by use of nanomaterials and will be addressed in a later section. Graphene alone may not yield the best capacitance, however due to its honeycomb monolayer structure it makes it an excellent candidate for fabricating composite materials.

Activated carbon is a commonly used carbon material for supercapacitor electrodes, as it provides good gravimetric capacitance for its relative ease to synthesize, and is relatively inexpensive, when compared to materials such as RuO_2. Depending on the manufacturing procedure it can be manipulated to obtain an extremely high specific surface area, reported values of up to $3000m^2\,g^{-1}$. A 2009 article reported an areal capacitance of activated carbon as <10 μF cm^{-2}, less than half of the theoretical 25 μF cm^{-2} [39]. Zhang proposed that the diminished capacitance was likely due to restricted permeability of the electrolyte in the nanopores that would limit ion diffusion. This hypothesis was reinforced by the lower reported capacitance of high porosity carbon electrodes in organic electrolytes compared to aqueous electrolytes[39]; this discrepancy highlights the importance of diffusion kinetics in electrolytes.

Carbon nanotubes (CNT) are a cylindrical version of graphene, where single or multiple layers of graphene are wrapped into a tube shape. CNTs were actually discovered before graphene in 1991, and they were soon praised for their electric conducting capabilities (≈5S/cm) [40]. The specific surface area of CNT ranges greatly depending on it's structure which is influenced by the method of manufacturing, with a 2001 article reporting a range of 50-1315 m^2/g with

1315m^2/g being the theoretical maximum [41]. There have been reports of incredible increase in electrical conductivity (>10^{3}S/cm) of MOs with additions CNTs at less than 5wt% [40], and percolation theory may be helpful in describing this phenomenon. Percolation theory is used in statistical physics to investigate and describe the behaviour of networks when nodes are added or removed, in materials science it can help describe the transition from non-metal to metal electrical conductivity known as the percolation threshold[42]. The high aspect ratio of single walled CNTs imparts a low percolation threshold at around 0.1wt% [43], meaning that small quantities are needed to drastically increase conductivity in composite materials, making them a very appealing additive.

A summary of activated carbon, graphene, CNTs and other carbon materials for use in EDLC capacitor applications is shown below in Table 2.

Table 2. Comparison of properties of carbon materials for use in EDLCs. [44]

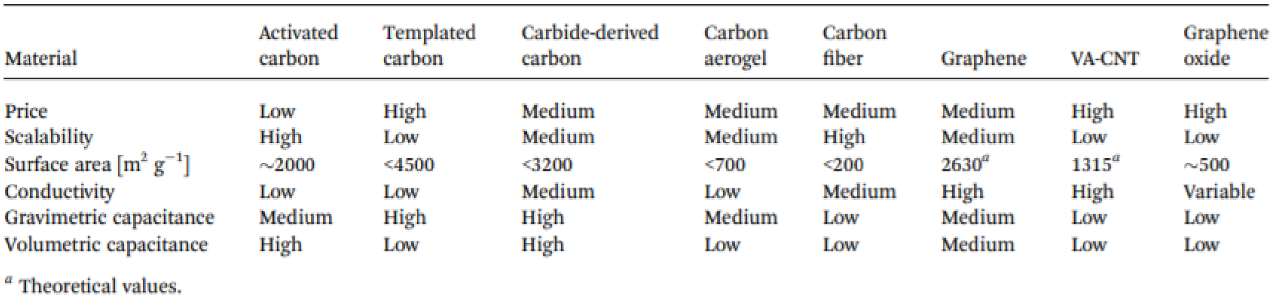

Material	Activated carbon	Templated carbon	Carbide-derived carbon	Carbon aerogel	Carbon fiber	Graphene	VA-CNT	Graphene oxide
Price	Low	High	Medium	Medium	Medium	Medium	High	High
Scalability	High	Low	Medium	Medium	High	Medium	Low	Low
Surface area [m^2 g^{-1}]	~2000	<4500	<3200	<700	<200	2630^a	1315^a	~500
Conductivity	Low	Low	Medium	Low	Medium	High	High	Variable
Gravimetric capacitance	Medium	High	High	Medium	Low	Medium	Low	Low
Volumetric capacitance	High	Low	High	Low	Low	Medium	Low	Low

^{a} Theoretical values.

2.2.3 Metal Oxides

Many MOs have been investigated as potential materials for supercapacitor electrodes, which include but are not limited to: Ni, Fe, Co, Mo, V, Bi, Mn, Ti and Ru oxides. For this chapter, the focus will be directed at Mn and Fe oxides, as they are considered as low cost, low toxicity and exhibit good capacitive performance[6, 36, 37] making them good candidates for supercapacitor electrodes.

In 1999 Lee and Goodenough, were one of the first to publish research on manganese oxides for use as a pseudocapacitive materials. They projected that its lower material cost and KCl electrolyte could make it a more commercially viable material for a supercapacitor compared to ruthenium oxides, even though it had less than half the capacitance[46]. Now MnO_2 and Mn_3O_4 are regarded as choice materials for pseudocapacitive electrodes because of their abundance in nature, high specific capacitance (1370 F g^{-1}) and low environmental impact [6, 9, 37]. These oxides exhibit poor electrical conductivity($\approx 10^{-5}$ S/cm) , which can lead to severe degradation in capacitance[47, 48].

The charge storage mechanism for MnO_2 is generally considered to stem from the change in the oxidation state Mn from 3^+ to 4^+, however as mentioned on page 10, pseudocapacitance can be attributed to 3 different mechanisms. MnO_2 has many possible morphologies, and the contribution of each of these mechanisms is dependant on the morphology. For example, the specific surface area of MnO_2 can vary from 20 to 300 m^2 g^{-1} based on its structural orientation[11], which can greatly vary the extent of surface redox reactions. The different polymorphs of MnO_2 can be seen in Figure 10, γ-MnO_2 offers good proton intercalation, and as such is often used in alkaline batteries[49]. The lattice parameters of these morphologies differ as well, leading to significant changes in ability for ions to insert and de-insert depending on spacing between lattice sites.

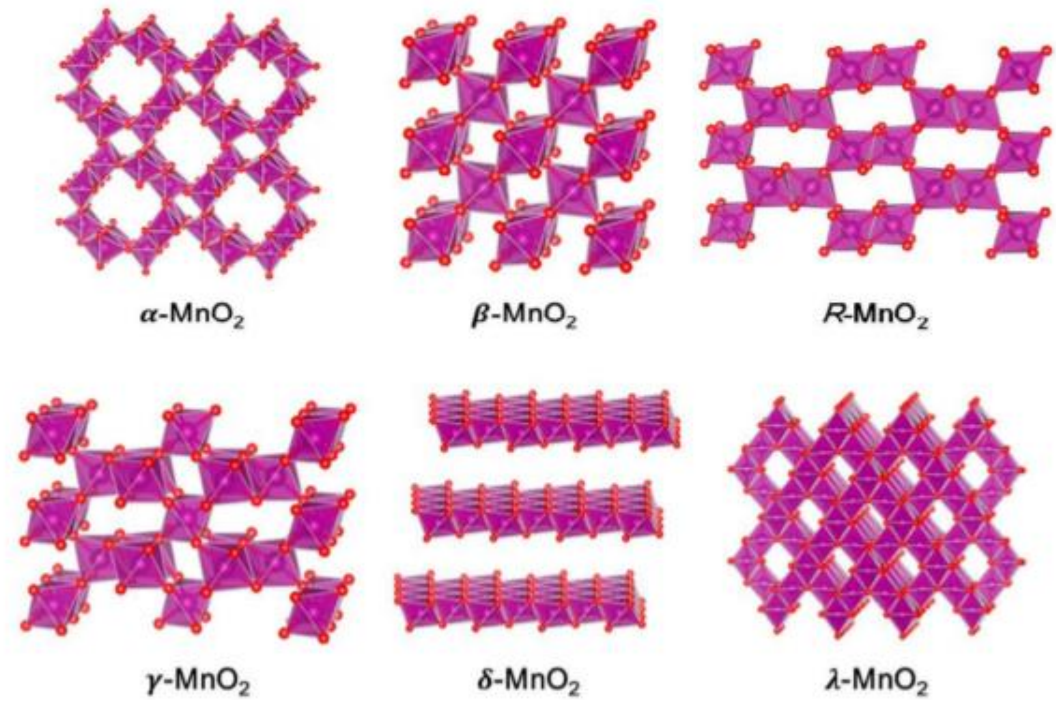

Figure 10. Polymorphs of Manganese Dioxide [49].

In 2004 Toupin reported XPS results for MnO_2 thin filmed electrodes[10], that indicated the role of Na^+ ions from the electrolyte engaging in the following surface reactions with MnO_2 *:*

$$MnO_2 + H^+ + e^- \leftrightarrow MnOOH \tag{18}$$

$$MnO_2 + C^+ + e^- \leftrightarrow MnOOC \tag{19}$$

$$(MnO_2)_{surface} + C^+ + e^- \leftrightarrow (MnO_2) \tag{20}$$

Where H^+ represents a proton and C^+ an alkali cation in Equations *(18)* and *(19)*, for the intercalation during reduction, after which the proton or ion becomes deintercalated during oxidation. Equation *(20)* specifically addresses the surface adsorption of C^+ , as described by the underpotential deposition.

Another oxide of manganese, Mn_3O_4 has also been probed for its electrochemical storage capabilities, however has historically shown lower capacitance than MnO_2 according to literature [41–45]. It has been hypothesized that due to the spinel structure of Mn_3O_4 it is less able to intercalate with electrolyte cations, resulting in lower capacitance values [11]. One large beneficial aspect of Mn_3O_4 is that it can be synthesized from a 2^+ state, rather than MnO_2 which is often synthesized from the 7^+ oxidation states. This would allow for the "in-situ" use of organic surfactants for Mn_3O_4 synthesis, which is not possible for syntheses using $KMnO_4$ as a precursor. The strong oxidizing properties of Mn^{7+} cause it to react with many organics and the use of surfactants is rendered ineffective from these oxidation reactions.

Iron oxides have gained interest in the scientific community, for their use as a negative electrode in supercapacitor devices, in particular Fe_3O_4. Based on Equation *(10)*, the in-series capacitance is limited by the lowest capacitance value in the series. There have been many reports of materials that have high capacitive properties as positive electrodes, however few have been reported with the same values for negative electrodes [6,41,46,47]. Similarly to Mn oxides, it is believed that surface redox reactions are main contributors to the capacitance of Fe oxide based electrodes, however there has been a study which also indicated that the magnetization also plays a role in the capacitive performance [56]. In a recent studies done by Nawwar [49,50], supercapacitor devices were fabricated using MnO_2 as a positive electrode and Fe_3O_4 as a negative electrode. In the studies, modifications of the Fe_3O_4 electrodes using polyaromatic dispersants resulted in good capacitive performance for negative electrodes When used in the fabrication of an asymmetric device with MnO_2, the specific capacitance dropped by nearly 50 % [58], which can be reasoned by Equation (*10*), as the two electrode are connected in series.

2.3 Supercapacitor electrolytes

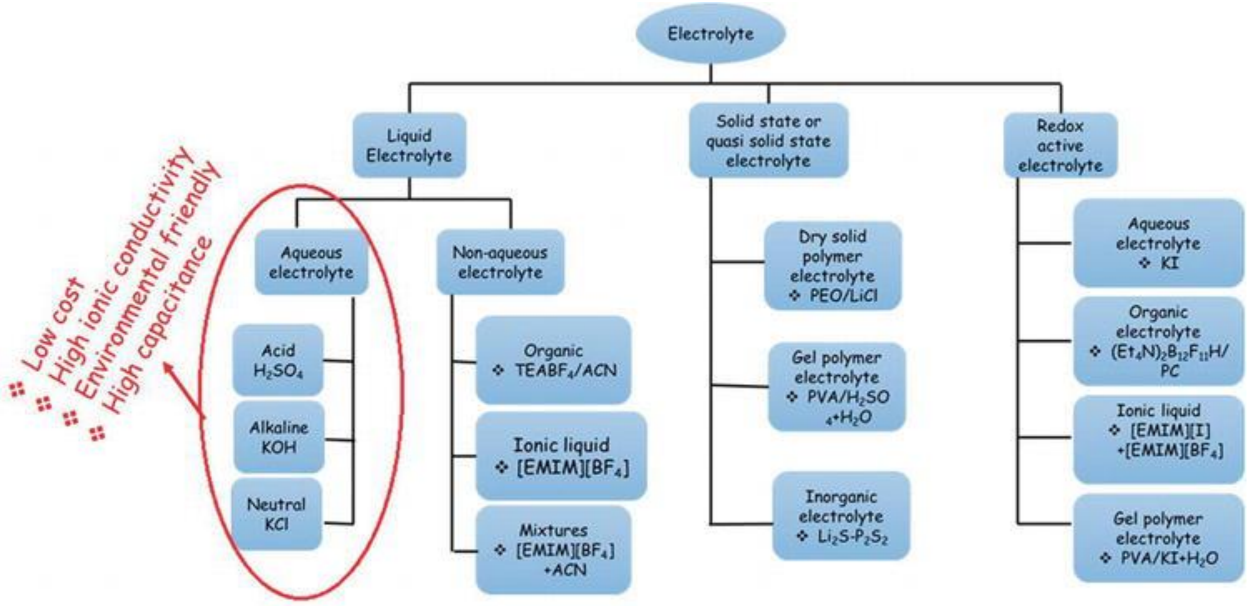

Figure 11. Flow chart for possible supercapacitor electrolytes.[59]

The selection of the electrolyte that is used for supercapacitor devices plays a critical role in the overall performance, due to factors such as the voltage stability and electrical resistance. These factors influence the electrochemical performance based on the parameters mentioned in Equations *(1)(9)*and *(15)*, and from which one can deduce some optimal characteristics for the ideal electrolyte; in terms of performance: high ionic conductivity, large voltage stability range, high thermal stability and overall compatibility with electrode materials. Though it should also be considered for the commercial production and viable of supercapacitor devices these electrolytes should also be: non toxic, non flammable, have a low environmental impact and low production cost[60]. Following a review by Zhang, the following types of electrolytes will be discussed: aqueous, organic and ionic.

Aqueous electrolytes are generally categorized by their pH, as acidic, basic or neutral. These electrolytes can have high ion conductivity and provide low equivalent electrical resistance, with aqueous sulfuric acid and sodium sulphate as examples. Researchers have looked into using redox additives to optimize the performance of supercapacitor devices, with two studies showing that using multiple redox additives can lead to notable increases in capacitive behaviour, and cyclic stability [60]. These additives varied depending on the pH of the electrolyte that was used and was summarized in Table 3:

Table 3. Summary of additives for different aqueous electrolytes

Aqueous Electrolyte Type	Possible additives
Acidic	KI, $NaMoO_4$, viologen substances, different moieties of hydroxybenzoic acid
Basic	$K_3Fe(CN)_6$ and phenylenediamine
Neutral	KI, $K_3Fe(CN)_6$, and viologens

As seen in Figure 11, aqueous electrolytes are often used due to their ease of access, low cost, low environmental impact, and high capacitance; and as such are the electrolyte of choice for many researchers. They do however have smaller voltage windows (usually less than 2V) than organic electrolytes due to the decomposition of water. Na_2SO_4 is a near pH neutral electrolyte, inert to many

MOs and CPs, that may be dissolved by acidic or basic environments, making it a good electrolyte for asymmetric devices. As well, it is an environmentally friendly option when compared to electrolytes like tetraethyl ammonium tetrafluoroborate. For reasons mentioned above, aqueous electrolytes were used for the entirety of this research project, specifically Na_2SO_4.

Organic electrolytes are composed of an organic solvent mixed with an ionic salt, where acetonitrile is a common solvent and tetraethyl ammonium tetrafluoroborate is often used as a salt[60]. A well-suited organic electrolyte can usually operate in a range of around 3V, meaning they will be able to store more energy according to Equation *(3)*, than aqueous electrolytes that would undergo hydrolysis. Although organic electrolytes offer better a larger voltage window leading to greater energy storage, they are toxic, flammable and costly [19]. Similarly, to aqueous electrolytes, redox additives may also be added into organic electrolytes to increase their electrochemical properties, however the options are more limited as the additives should only be active with certain functional groups.

Ionic liquids have the highest voltage stability of the three types of electrolytes, where they can operate from between 3 to 4V, meaning they have potential to significantly increase the energy and power density compared to aqueous electrolytes. Though for their better electrochemical stability, oxidation and high temperature resistance, liquid ionic electrolytes come with a plethora of problems. Their high viscosity leads to poor diffusion and low ionic conductivity, and these salts are highly toxic[61].

2.4 Electrochemical characterization

It is key to understand the electrochemical behaviour of materials to determine whether they exhibit properties that would make them suitable for supercapacitor applications. Three different methods were used in this research to test the energy storage properties of fabricated electrodes which are:

Electrochemical Impedance Spectroscopy(EIS), Cyclic Voltammetry(CV) and Galvanostatic Charge-Discharge (GCD). These methods all evaluate different aspects of electrochemical behaviour and thus give slightly different results when analyzing the capacitive properties of an electrode[5]. The equations used to calculate the specific capacitance of each method are provided in [5], and this section will focus on theoretical aspects of these three methods of electrochemical characterization.

EIS is a method of measuring the impedance in a material as a function of the AC frequency. A medium which exhibits only resistive properties will reduce the amplitude of the signal, while capacitive materials cause a phase shift in the wave of up to 90 degrees. The resulting measure can then be split into imaginary and real components, to allow for a meaningful comprehension of the output. This is done by using a 3-electrode set-up composed of a working, reference, and counter electrode. The reference electrode allows for the measure of potential while the counter electrode is used to measure the amount of current passed [62]. The results from the EIS measurements; the resistive (real) and capacitive (imaginary) contributions of impedance, are then often plotted on either a Bode (real/imaginary vs frequency) or a Nyquist plot (real vs imaginary). Based on the characteristics of these curves a few things can be determined about what is happening as the EIS measurements are being taken, such as estimate internal resistance and identify relaxation frequency.

GCD is a technique that is often used in the testing of Li-ion batteries, used to characterize their maximum capacity in Amp hours (Ah), by determining the amount of time to completely charge or discharge a cell with a given current. For example, a battery that charges to completion in 1 hour at a current of 2.2A would have a maximum capacity of 2.2Ah. This measurement can also be applied to the amount of time required to completely discharge the cell to determine the capacity[63].

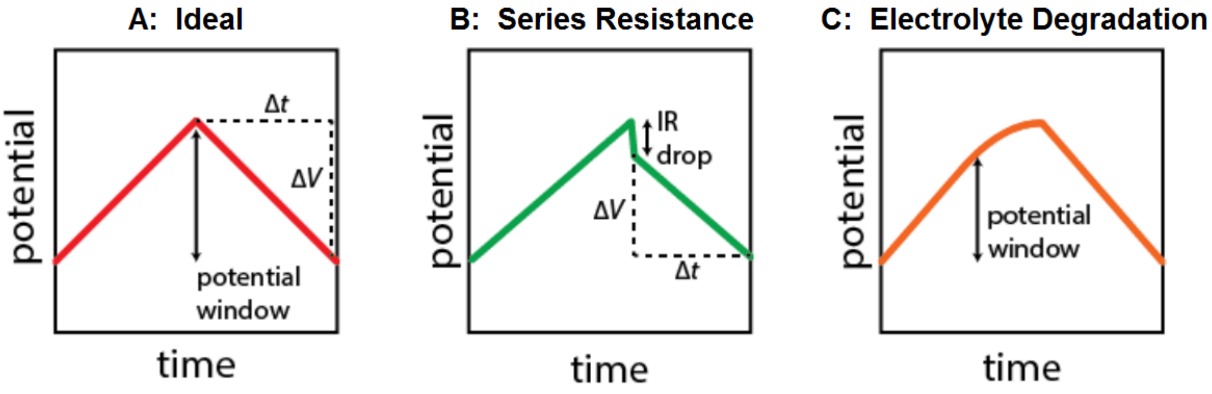

Figure 12. Cases of potential vs time for GCD measurements of supercapacitor electrodes [64]

In Figure 12, A represents the ideal case, where an electrode that is charged to some potential value then discharged, at a given current and exhibits only linear behaviour. When there are series resistances such as diffusional limitations at the electrode surface, they will be manifested as an IR drops at the peak voltage where the switch from charge to discharge occurs, that can be seen in B. If the cell is tested in a potential range that exceeds the electrochemical stability of the electrolyte used, the current will begin to drop as the electrolyte begins to decompose. This results in a change in the slope during charging, as seen in C. These factors considered, if capacitance is to be calculated using this method, the curves should exhibit linear behaviour, however correction factors can be used to adjust for deviations in linearity [5]. GCD is another useful tool for characterizing the electrochemical behaviour of cells as it allows researchers to easily determine if the potential window that is being used is appropriate for the electrolyte that was selected. GCD can also be helpful in identifying if non ideal resistive characteristics have manifested, that may stem from low electrical conductivity in the dielectric material, or low electrolyte permeability that may stem from high binder concentrations[64].

CV in contrast to GCD measures the current response of a cell when a varying potential is applied. Similarly, to GCD, the diffusion in the electrolyte is the only means mass transport to the electrode surface, while the electrolyte is not stirred. The cations from the electrolyte that are within the Nernst diffuse layer will be first to react with the electrode, as described in Equations *(19)* and *(20)*. As the reaction proceeds and more $Mn^{4+/3+}$ are converted, to the point where all the C^+ at the surface become intercalated or adsorbed, the distance that additional C^+ must diffuse to reach the electrode increases, a peak will be generated[65]. However, for supercapacitors their CV behaviour differs due to the nature of EDLC and pseudocapacitance as was described earlier. Instead, due to the nature of the reversible reactions surface reactions, a box shaped curve is used to describe the ideal capacitive behaviour of a supercapacitor. This box shape leads to a maximization of area for a given potential window, resulting in a higher calculated capacitance value. In Figure 13 a near box shape curve is displayed from an Mn_3O_4 sample that was tested during the course of this research project. The integrated value of the voltammogram curve is equal to the charge, represented in yellow and this area is then divided by the potential window to calculate the capacitance.

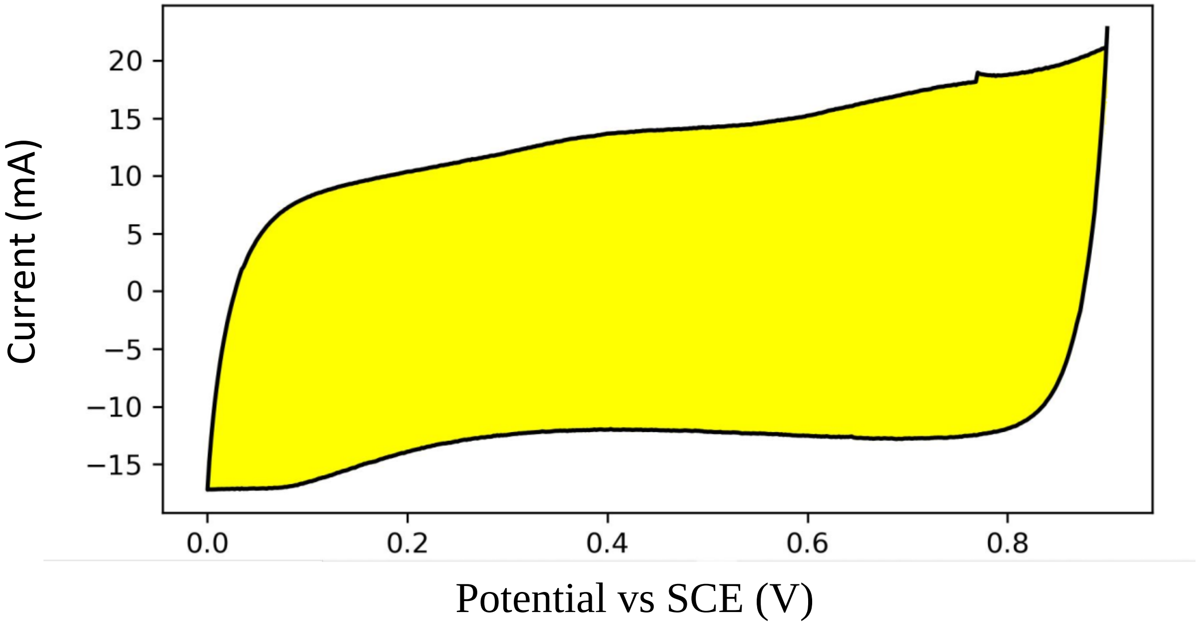

Figure 13. Cyclic voltagram with highlighted charge area from OHA dispersed Mn_3O_4 CNT electrode at a scan rate of 2 mV s^{-1}.

At scan rates of less than 5 mV s^{-1}, slower reactions can occur and contribute to the overall calculated charge, while at higher scan rates these reactions are “cut short” before the applied potential is switched, which often results in a lower calculated capacitance[5]. Cyclic voltammetry can give indications of the magnitude of the time constant depending on the rounding of the corners as is seen at 0.075V and 0.85V on Figure 13, as well as the occurrence of different redox reactions taking place at different potentials.

Chapter 3 – Electrode Fabrication

In this chapter methods of electrode fabrication will be discussed, including electrophoretic deposition, hydrothermal synthesis, chemical precipitation, surfactants and dispersant materials, and liquid-liquid extractions.

In the fabrication of a supercapacitor electrode, the active charge material should be deposited on a current collector, and there are a few methods of achieving this, one of which is electrophoretic deposition (EPD). EPD uses the motion of charged particles, inside a suspension under an applied potential, to cause the particles to form deposits on the electrode surface [17]. For this method to be applicable to the fabrication of supercapacitor electrodes, the active material that should be deposited onto the current collector needs to be charged. In the case of MOs such as MnO_2, the use of surfactants can be beneficial as to impart a charge so that nanoparticles may be deposited on a substrate using EPD, as well as improving their dispersion in solution. Electrodes fabricated using EPD often show uniform coating thicknesses, even for non-flat substrates, allowing for good electrolyte access. Literature shows that MnO_2 electrodes fabricated using EPD yield very good gravimetric capacitance when small amounts of mass are deposited[74,75]. The low active mass leads to low areal capacitance, highlighting the need for high mass loading electrodes.

Hydrothermal synthesis of oxide materials is another method of synthesizing active materials such as MOs for supercapacitor electrodes. This method of active materials synthesis allows for a well-controlled tuning of morphology, particles size and particle distribution[68]. This can be extremely beneficial as different nanoparticle morphologies have been shown to have varying specific capacitances [5]. Unlike in EPD the material must still be adhered to the surface of the current collector after it has been synthesized. Though this method allows for the fine tuning of nanostructures, it often requires expensive equipment (autoclaves and furnaces), high synthesis temperatures and can pose an issue that the material cannot easily be monitored when inside the autoclaves.

Chemical precipitation is a method that is used often in water purification; however, it may also be used to synthesize oxide materials for supercapacitor electrodes. By quickly adjusting the pH of a solution containing dissolved salts, like $Mn(NO_3)_2$, a precipitation reaction can be induced, allowing for the synthesis of nanoparticles. These nanoparticles however are energetically unfavourable due to their high surface area and will agglomerate without the use of a dispersing agent. Similarly, to using the hydrothermal method, after the material is synthesized it needs to be adhered to the current collector, and this is usually done using a polymer binder such as PTFE, PMMA or PVB. In traditional methods, the nanoparticles would be allowed to air dry, mixed with conducting additives, then the binder solution would be added. During this drying process, the nanoparticles can become agglomerated, reducing the effect of the conducting additives. In the case of PVB the binder is soluble in organic solvents, and has poor solubility in water, so the nanoparticles should be transferred from their aqueous synthesis medium to an organic solvent. To avoid the drying step, the transfer to the organic solvent can be done by performing a liquid-liquid extraction (LLE).

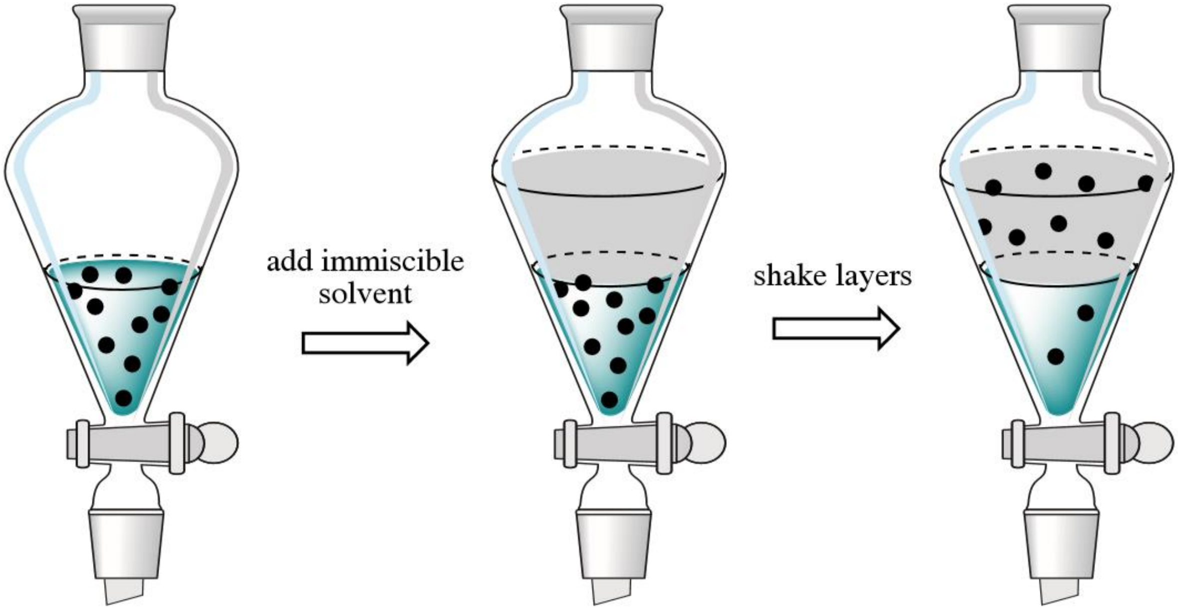

Figure 14. Schematic of a liquid-liquid extraction [69].

Figure 14 indicates the surface level simplicity of LLEs, where an immiscible solvent is poured into a separatory funnel with the liquid containing the desired substance(s), the flask gets shaken, is left to sit, the two liquids separate, and a solute enriched solution (extract-gray) and solute depleted solution (raffinate-blue) are left. The raffinate can then easily be poured out from the spout at the bottom of the funnel. In this simplified case, the desired substance is more soluble in the gray solution and is therefore easily extracted from the blue solution, however a couple issues arise if we consider the following possibilities that are addressed in this work:

1. There is more than one substance inside the blue solution, which may also be extracted.
2. The substance of interest is preferentially soluble in solvents like the blue solution (for example polar solvents).

To overcome these issues, organic extractor agents were used. An organic extractor can be used to selectively modify the surface of the desired substance, and in doing so, change its solubility[70]. Once modified, the desired substance will become hydrophobic and unstable in an aqueous environment and preferentially migrate into organic solvents, such as 1-butanol [71]. This modification and extraction has been successfully performed on a number of MO nanoparticles by the Zhitomirsky group[72], and has been coined as Particle Extraction through a Liquid-Liquid Interface (PELLI).

The PELLI technique has allowed the Zhitomirsky group to fabricate electrodes with high areal capacitances at high mass loadings (greater than 10mg/cm^2)[73]. The technique focuses on the aspect that particles behave differently at the interface of two immiscible liquids, where particles of small enough radius tend to become fixed to this interface, an image of this can be seen in Figure 15.

Figure 15. Carbon nanotubes fixed at the interface of a brine (bottom), and isopropanol (top).

The energies required to migrate the particles into either of the two liquids are represented below:

R is the radius of the particle

γ is the surface tension between two liquids

θ is the angle of particle contact, measured through water

$$E_o = \pi R^2 \gamma (1 + \cos\theta)^2 \tag{21}$$

E_o is the energy required for the particle to be desorbed from the LLI into the organic solution

$$E_w = \pi R^2 \gamma (1 + \cos\theta)^2 \tag{22}$$

E_w is the energy required for the particle to be desorbed from the LLI into the water.

Once bound by the liquid-liquid interface the particles will not have the energy required to overcome the surface tension of either liquid. The mobility of the particles at the interface is restricted[74], which allows the extractor to more easily adsorb to the surface of the particle. Once the extractor is adhered to the surface of the particle, it provides enough energy through repulsive forces to pull the particles into one of the two liquids dependant on the extractor used.

References

[1] C. Guide, “Motor Capacitors,” 2019. http://www.capacitorguide.com/motor-starting-capacitor/ (accessed Jun. 21, 2020).

[2] T. Christen and M. W. Carlen, “Theory of ragone plots,” *J. Power Sources*, vol. 91, no. 2, pp. 210–216, 2000, doi: 10.1016/S0378-7753(00)00474-2.

[3] H. I. Becker, “US2800616 Low voltage electrolytic capacitor patent,” 1954.

[4] E. Frackowiak and F. Beguin, *Supercapacitors: Materials, Systems, and Applications*. John Wiley and Sons.

[5] R. Chen, M. Yu, R. P. Sahu, I. K. Puri, and I. Zhitomirsky, “The Development of Pseudocapacitor Electrodes and Devices with High Active Mass Loading,” *Adv. Energy Mater.*, vol. 10, no. 20, pp. 1–33, 2020, doi: 10.1002/aenm.201903848.

[6] J. R. Miller, “Engineering electrochemical capacitor applications,” *J. Power Sources*, vol. 326, pp. 726–735, 2016, doi: 10.1016/j.jpowsour.2016.04.020.

[7] “Ultracapacitor Technologies and Application in Hybrid and Electric Vehicles Andrew Burke Institute of Transportation Studies University of California , Davis July 2009 Article published in the International Journal of Energy Research Research supported by,” *Development*, no. July, 2009.

[8] Maxwell and Maxwell Technologies, “Product Guide: BOOSTCAP Ultracapacitors,” *Doc. No. 1014627.1*, no. November, pp. 4–5, 2009.

[9] F. O. Safety and H. C. Standard, “Maxwell Material Safety Data Sheet,” no. 648, pp. 1–10, 2005.

[10] M. Toupin, T. Brousse, and D. Bélanger, “Charge storage mechanism of MnO2 electrode used in aqueous electrochemical capacitor,” *Chem. Mater.*, vol. 16, no. 16, pp. 3184–3190, 2004, doi: 10.1021/cm049649j.

[11] J. Zhang, Y. Cui, and G. Shan, “Metal oxide nanomaterials for pseudocapacitors,” 2019, [Online]. Available: http://arxiv.org/abs/1905.01766.

[12] R. Chen, I. K. Puri, and I. Zhitomirsky, “Polypyrrole-carbon nanotube-FeOOH composites for negative electrodes of asymmetric supercapacitors,” *J. Electrochem. Soc.*, vol. 166, no. 6, pp. A935–A940, 2019, doi: 10.1149/2.0281906jes.

[13] W.-S. Li, M.-L. Chang, K.-C. Chuang, Y.-S. Li, J.-D. Luo, and H.-C. Cheng, “ Electrochemical Properties of CNT/MnO 2 Hybrid Nanostructure with Low-Temperature Hydrothermal Synthesis as High-Performance Supercapacitor ,” *J. Electrochem. Soc.*, vol. 166, no. 10, pp. A2194–A2198, 2019, doi: 10.1149/2.1551910jes.

[14] C. Wallar, D. Luo, R. Poon, and I. Zhitomirsky, “Manganese dioxide–carbon nanotube composite electrodes with high active mass loading for electrochemical supercapacitors,” *J. Mater. Sci.*, vol. 52, no. 7, pp. 3687–3696, 2017, doi: 10.1007/s10853-016-0711-0.

[15] R. Mohan, R. Paulose, and V. Parihar, “Hybrid MnO2/CNT nanocomposite sheet with enhanced electrochemical performance via surfactant-free wet chemical route,” *Ionics (Kiel).*, vol. 23, no. 11, pp. 3245–3248, 2017, doi: 10.1007/s11581-017-2277-5.

[16] R. Chen, R. Poon, R. P. Sahu, I. K. Puri, and I. Zhitomirsky, “MnO2-carbon nanotube electrodes for supercapacitors with high active mass loadings,” *J. Electrochem. Soc.*, vol. 164, no. 7, pp. A1673–A1678, 2017, doi: 10.1149/2.1491707jes.

[17] M. S. Ata, Y. Liu, and I. Zhitomirsky, “A review of new methods of surface chemical modification, dispersion and electrophoretic deposition of metal oxide particles,” *RSC Adv.*, vol. 4, no. 43, pp. 22716–22732, 2014, doi: 10.1039/c4ra02218a.

[18] M. F. El-Kady *et al.*, “Engineering three-dimensional hybrid supercapacitors and microsupercapacitors for high-performance integrated energy storage,” *Proc. Natl. Acad. Sci. U. S. A.*, vol. 112, no. 14, pp. 4233–4238, 2015, doi: 10.1073/pnas.1420398112.

[19] P. Sharma and T. S. Bhatti, “A review on electrochemical double-layer capacitors,” *Energy Convers. Manag.*, vol. 51, no. 12, pp. 2901–2912, 2010, doi: 10.1016/j.enconman.2010.06.031.

[20] E. Gongadze, S. Petersen, U. Beck, and U. van Rienen, “Classical Models of the Interface between an Electrode and Electrolyte,” *Comsol Conf.*, 2009.

[21] B. . Conway, *Electrochemical Supercapacitors: Scientific Fundamentals and Technological Applications*. Springer US, 1999.

[22] V. Augustyn, P. Simon, and B. Dunn, “Pseudocapacitive oxide materials for high-rate electrochemical energy storage,” *Energy Environ. Sci.*, vol. 7, no. 5, pp. 1597–1614, 2014, doi: 10.1039/c3ee44164d.

[23] P. M. Biesheuvel *et al.*, “Capacitive Deionization -- defining a class of desalination technologies,” pp. 1–3,

2017, [Online]. Available: http://arxiv.org/abs/1709.05925.

[24] C. E. H. Bawn, "The adsorption of gases and vapors on plane surfaces," *J. Am. Chem. Soc.*, vol. 54, no. 1, pp. 72–86, 1932, doi: 10.1021/ja01340a008.

[25] R. Chen, I. K. Puri, and I. Zhitomirsky, "High areal capacitance of FeOOH-carbon nanotube negative electrodes for asymmetric supercapacitors," *Ceram. Int.*, vol. 44, no. 15, pp. 18007–18015, 2018, doi: 10.1016/j.ceramint.2018.07.002.

[26] J. Milne and I. Zhitomirsky, "Application of octanohydroxamic acid for liquid-liquid extraction of manganese oxides and fabrication of supercapacitor electrodes," *J. Colloid Interface Sci.*, vol. 515, pp. 50–57, 2018, doi: 10.1016/j.jcis.2018.01.021.

[27] C. J. Wallar, R. Poon, and I. Zhitomirsky, " High Areal Capacitance of V 2 O 3 –Carbon Nanotube Electrodes ," *J. Electrochem. Soc.*, vol. 164, no. 14, pp. A3620–A3627, 2017, doi: 10.1149/2.0661714jes.

[28] T. Brousse, *Supercapacitors Based on Carbon or Pseudocapacitive Materials*. John Wiley and Sons, 2017.

[29] A. Muza, M. B. Ahamed, K. Deshmukh, and J. Thirumalai, "A review on recent advances in hybrid supercapacitors : Design , fabrication and applications," vol. 101, no. October 2018, pp. 123–145, 2019, doi: 10.1016/j.rser.2018.10.026.

[30] Y. Liu, S. P. Jiang, and Z. Shao, "Intercalation pseudocapacitance in electrochemical energy storage: recent advances in fundamental understanding and materials development," *Mater. Today Adv.*, vol. 7, p. 100072, 2020, doi: 10.1016/j.mtadv.2020.100072.

[31] H. shan Nan, X. ying Hu, and H. wei Tian, "Recent advances in perovskite oxides for anion-intercalation supercapacitor: A review," *Mater. Sci. Semicond. Process.*, vol. 94, no. October 2018, pp. 35–50, 2019, doi: 10.1016/j.mssp.2019.01.033.

[32] Y. Wang, Y. Ding, X. Guo, and G. Yu, "Conductive polymers for stretchable supercapacitors," *Nano Res.*, vol. 12, no. 9, pp. 1978–1987, 2019, doi: 10.1007/s12274-019-2296-9.

[33] A. G. MacDiarmid, "Polyaniline and polypyrrole: Where are we headed?," *Synth. Met.*, vol. 84, no. 1–3, pp. 27–34, 1997, doi: 10.1016/s0379-6779(97)80658-3.

[34] D. Kumar and R. C. Sharma, "Advances in conductive polymers," *Eur. Polym. J.*, vol. 34, no. 8, pp. 1053–1060, 1998, doi: 10.1016/S0014-3057(97)00204-8.

[35] M. Khalid, A. M. B. Honorato, and H. Varela, "Polyaniline : Synthesis Methods, Doping and Conduction Mechanism," *Polyaniline - From Synth. to Pract. Appl.*, pp. 1–17, 2018.

[36] M. Natalia, Y. N. Sudhakar, and M. Selvakumar, "Activated carbon derived from natural sources and electrochemical capacitance of double layer capacitor," *Indian J. Chem. Technol.*, vol. 20, no. 6, pp. 392–399, 2013.

[37] "The University of Manchester :Graphene," 2017. https://www.graphene.manchester.ac.uk/learn/discovery-of-graphene/ (accessed Jun. 29, 2020).

[38] Y. Wang *et al.*, "Preventing graphene sheets from restacking for high-capacitance performance," *J. Phys. Chem. C*, vol. 115, no. 46, pp. 23192–23197, 2011, doi: 10.1021/jp206444e.

[39] L. Zhang and X. S. Zhao, "Carbon-based materials as supercapacitor electrodes," *Chem. Soc. Rev.*, vol. 38, no. 9, pp. 2520–2531, 2009, doi: 10.1039/b813846j.

[40] P. Cheng, B. Zhong, and J. Kim, "Effect of CNT decoration with silver nanoparticles on electrical conductivity of CNT-polymer composites," vol. 6, pp. 0–8, 2008, doi: 10.1016/j.carbon.2008.06.048.

[41] A. Peigney, C. Laurent, E. Flahaut, R. R. Bacsa, and A. Rousset, "Specific surface area of carbon nanotubes and bundles of carbon nanotubes," vol. 39, pp. 507–514, 2001.

[42] A. L. Efros and B. I. Shklovskii, "Critical Behaviour of Conductivity and Dielectric Constant near the Metal-Non-Metal Transition Threshold," no. 1, 1976.

[43] B. Earp *et al.*, "Electrically Conductive CNT Composites at Loadings below Theoretical Percolation Values," pp. 1–17, 2019, doi: 10.3390/nano9040491.

[44] L. Borchardt, M. Oschatz, and S. Kaskel, "Tailoring porosity in carbon materials for Supercapacitor applications," 2014, doi: 10.1039/c3mh00112a.

[45] R. Poon, X. Zhao, M. S. Ata, A. Clifford, and I. Zhitomirsky, "Phase transfer of oxide particles for application in thin films and supercapacitors," *Ceram. Int.*, vol. 43, no. 11, pp. 8314–8320, 2017, doi: 10.1016/j.ceramint.2017.03.167.

[46] H. Lee and J. . Goodenough, "Introduction of Mn as a pseudocapacitive material." 1999.

[47] R. Poon, W. Liang, and I. Zhitomirsky, "Mn3O4 and (ZnFe)OOH Composites for Supercapacitors with High

Active Mass," *Metall. Mater. Trans. A*, vol. 51, no. 2, pp. 855–862, Feb. 2020, doi: 10.1007/s11661-019-05561-x.
[48] C. Wan, L. Yuan, and H. Shen, "Effects of Electrode Mass-loading on the Electrochemical Properties of Porous MnO 2 for Electrochemical Supercapacitor," vol. 9, pp. 4024–4038, 2014.
[49] J. Shin, J. K. Seo, R. Yaylian, A. Huang, and Y. S. Meng, "A review on mechanistic understanding of MnO2 in aqueous electrolyte for electrical energy storage systems," *Int. Mater. Rev.*, vol. 65, no. 6, pp. 356–387, 2020, doi: 10.1080/09506608.2019.1653520.
[50] M. S. Ata, J. Milne, and I. Zhitomirsky, "Fabrication of Mn3O4–carbon nanotube composites with high areal capacitance using cationic and anionic dispersants," *J. Colloid Interface Sci.*, vol. 512, pp. 758–766, 2018, doi: 10.1016/j.jcis.2017.10.110.
[51] M. Aghazadeh, M. Asadi, M. R. Ganjali, P. Norouzi, B. Sabour, and M. Emamalizadeh, "Template-free preparation of vertically-aligned Mn3O4 nanorods as high supercapacitive performance electrode material," *Thin Solid Films*, vol. 634, pp. 24–32, 2017, doi: 10.1016/j.tsf.2017.05.008.
[52] D. P. M. D. Shaik, P. Rosaiah, and O. M. Hussain, "Fabrication of the Mn3O4 thin film electrodes by electron beam evaporation for supercapacitor applications," *J. Electroanal. Chem.*, vol. 851, p. 113409, 2019, doi: 10.1016/j.jelechem.2019.113409.
[53] H. W. Park, H. J. Lee, S. M. Park, and K. C. Roh, "Synthesis and electrochemical properties of Mn3O4 nanocrystals with controlled morphologies grown from compact ion layers," *RSC Adv.*, vol. 6, no. 22, pp. 18191–18197, 2016, doi: 10.1039/c5ra28110e.
[54] V. D. Nithya and N. Sabari Arul, "Progress and development of Fe3O4 electrodes for supercapacitors," *J. Mater. Chem. A*, vol. 4, no. 28, pp. 10767–10778, 2016, doi: 10.1039/c6ta02582j.
[55] G. Z. Chen, "Understanding supercapacitors based on nano-hybrid materials with interfacial conjugation," *Prog. Nat. Sci. Mater. Int.*, vol. 23, no. 3, pp. 245–255, 2013, doi: 10.1016/j.pnsc.2013.04.001.
[56] G. Wang, H. Xu, L. Lu, and H. Zhao, "Magnetization-induced double-layer capacitance enhancement in active carbon/Fe3O4 nanocomposites," *J. Energy Chem.*, vol. 23, no. 6, pp. 809–815, 2014, doi: 10.1016/S2095-4956(14)60216-3.
[57] I. Zhitomirsky, "High areal capacitance of Fe 3 O 4 - decorated carbon nanotubes for supercapacitor electrodes," no. July, pp. 1–10, 2019, doi: 10.1002/cey2.6.
[58] M. Nawwar, R. P. Sahu, I. K. Puri, and I. Zhitomirsky, "Functionally Decorated Carbon Nanotube Networks for Energy Storage in Supercapacitors," *Front. Energy Res.*, vol. 8, no. March, pp. 1–9, 2020, doi: 10.3389/fenrg.2020.00046.
[59] R. Ramachandran and F. Wang, "Electrochemical Capacitor Performance: Influence of Aqueous Electrolytes," *Supercapacitors - Theor. Pract. Solut.*, 2018, doi: 10.5772/intechopen.70694.
[60] L. Zhang *et al.*, "A Review of Redox Electrolytes for Supercapacitors," *Front. Chem.*, vol. 8, no. June, pp. 1–7, 2020, doi: 10.3389/fchem.2020.00413.
[61] "Sigma Aldrich- Ionic Liquids." https://www.sigmaaldrich.com/technical-documents/articles/chemfiles/ionic-liquids0.html.
[62] D. Macdonald and E. Barsoukov, *EIS -Theory , Experiment , and Applications*, vol. 125. 2013.
[63] A. Application and N. Bat, "Metrohm-Galvanostatic Charge-Discharge of a Li-Ion battery with Autolab," pp. 1–2, 2014.
[64] B. Hsia, "Materials Synthesis and Characterization for Micro-supercapacitor Applications," *Thesis*, 2013, [Online]. Available: http://digitalassets.lib.berkeley.edu/etd/ucb/text/Hsia_berkeley_0028E_13892.pdf.
[65] A. Quiroga, "Cyclic Voltammetry," 2020. https://chem.libretexts.org/Bookshelves/Analytical_Chemistry/Supplemental_Modules_(Analytical_Chemistry)/Instrumental_Analysis/Cyclic_Voltammetry#:~:text=Cyclic Voltammetry (CV) is an,and measuring the resulting current.
[66] W. Cong, R. Miao, F. Miao, and B. Tao, "Electrodeposition manganese oxide on Ni foam loaded graphene for high-performance supercapacitor," *Mater. Res. Express*, vol. 6, no. 11, 2019, doi: 10.1088/2053-1591/ab49e9.
[67] J. A. Argüello, J. M. Rojo, and R. Moreno, "Electrophoretic deposition of manganese oxide and graphene nanoplatelets on graphite paper for the manufacture of supercapacitor electrodes," *Electrochim. Acta*, vol. 294, pp. 102–109, 2019, doi: 10.1016/j.electacta.2018.10.091.
[68] N. Torres-Gómez, O. Nava, L. Argueta-Figueroa, R. García-Contreras, A. Baeza-Barrera, and A. R. Vilchis-Nestor, "Shape tuning of magnetite nanoparticles obtained by hydrothermal synthesis: Effect of temperature," *J. Nanomater.*, vol. 2019, 2019, doi: 10.1155/2019/7921273.

[69] L. Nichols, "4.2: Overview of Extraction," 2021. https://chem.libretexts.org/Bookshelves/Organic_Chemistry/Book%3A_Organic_Chemistry_Lab_Techniques_(Nichols)/04%3A_Extraction/4.02%3A_Overview_of_Extraction.

[70] R. M. E. Silva, R. Poon, J. Milne, A. Syed, and I. Zhitomirsky, "New developments in liquid-liquid extraction, surface modification and agglomerate-free processing of inorganic particles," *Adv. Colloid Interface Sci.*, vol. 261, pp. 15–27, 2018, doi: 10.1016/j.cis.2018.09.005.

[71] J. Milne and I. Zhitomirsky, "Application of octanohydroxamic acid for liquid-liquid extraction of manganese oxides and fabrication of supercapacitor electrodes," *J. Colloid Interface Sci.*, vol. 515, pp. 50–57, 2018, doi: 10.1016/j.jcis.2018.01.021.

[72] R. Chen, M. S. Ata, X. Zhao, I. Puri, and I. Zhitomirsky, "Liquid-liquid extraction of oxide particles and application in supercapacitors," *J. Mater. Res.*, vol. 32, no. 17, pp. 3242–3250, 2017, doi: 10.1557/jmr.2017.92.

[73] R. Chen, Z. Z. Wang, R. P. Sahu, I. K. Puri, and I. Zhitomirsky, "Influence of molecular structure of extractor molecules on liquid-liquid extraction of oxide particles and properties of composites," *Ceram. Int.*, vol. 44, no. 13, pp. 15714–15720, 2018, doi: 10.1016/j.ceramint.2018.05.244.

[74] R. M. E. Silva, R. Poon, J. Milne, A. Syed, and I. Zhitomirsky, "New developments in liquid-liquid extraction, surface modification and agglomerate-free processing of inorganic particles," *Adv. Colloid Interface Sci.*, vol. 261, pp. 15–27, 2018, doi: 10.1016/j.cis.2018.09.005.

Chapter 4 – Objectives

As shown in the literature review, there are different ways of improving the electrochemical performance of a supercapacitor. The testing of organic extractors, capping agents, dispersants, and surfactants containing different functional groups is one way the Zhitomirsky group is addressing the issue of poor mixing of manganese oxides with MWCNTs. Another is the development of colloidal processing techniques. The objectives for this work, are outlined below:

1. Investigate the use of novel dispersing agents to encourage mixing between metal oxides and MWCNTs
2. Develop a method of colloidal extraction that facilitates the synthesis of nanocomposite materials
3. Fabrication of high mass loading nanocomposite electrodes and testing their electrochemical performance
4. Materials characterization of the composite electrode surfaces, to investigate the influence of dispersants on structure and mixing.

Chapter 5 –Application of Octanohydroxamic Acid for Salting out Liquid–Liquid Extraction of Materials for Energy Storage in Supercapacitors

Author's Contributions:

1. Testing and documentation of new colloidal processing technique
2. Synthesis of nanocomposite active material
3. Electrode sample preparation and electrochemical testing
4. SEM imaging
5. Literature review
6. Preparation of manuscript draft

Application of Octanohydroxamic Acid for Salting out Liquid–Liquid Extraction of Materials for Energy Storage in Supercapacitors

Kaelan Rorabeck and Igor Zhitomirsky *

Citation: Rorabeck, K.; Zhitomirsky, I. Application of octanohydroxamic acid for salting out liquid-liquid extraction of materials for energy storage in supercapacitors. *Molecules* **2021**, *25*, x. https://doi.org/10.3390/xxxxx

Received: 16 November 2020
Accepted: 5 January 2021
Published: date

Department of Materials Science and Engineering, McMaster University, Hamilton, ON ,L8S 4L7, Canada; rorabeck@mcmaster.ca
* Correspondence: zhitom@mcmaster.ca

Abstract. The ability to achieve high areal capacitance for oxide-based supercapacitor electrodes with high active mass loadings is critical for practical applications. This paper reports the feasibility of the fabrication of Mn_3O_4-multiwalled carbon nanotube (MWCNT) composites by the new salting-out method, which allows direct particle transfer from an aqueous synthesis medium to a 2-propanol suspension for the fabrication of advanced Mn_3O_4-MWCNT electrodes for supercapacitors. The electrodes show enhanced capacitive performance at high active mass loading due to reduced particle agglomeration and enhanced mixing of the Mn_3O_4 particles and conductive MWCNT additives. The strategy is based on the multifunctional properties of octanohydroxamic acid, which is used as a capping and dispersing agent for Mn_3O_4 synthesis and an extractor for particle transfer to the electrode processing medium. Electrochemical studies show that high areal capacitance is achieved at low electrode resistance. The electrodes with an active mass of 40.1 mg cm^{-2} show a capacitance of 4.3 F cm^{-2} at a scan rate of 2 mV s^{-1}. Electron microscopy studies reveal changes in electrode microstructure during charge-discharge cycling, which can explain the increase in capacitance. The salting-out method is promising for the development of advanced nanocomposites for energy storage in supercapacitors.

Keywords: manganese oxide; supercapacitor; salting-out; dispersion; extraction; capacitance

---

1. Introduction

Supercapacitors are currently under development for various energy storage applications [1,2]. Investigations in this research area are focused on the synthesis of advanced electrode materials by different fabrication methods [3–8], optimization of electrolytes [9], design of nanocomposites [10–13], and modeling [14]. The synthesis of non-agglomerated particles of controlled shape and composition is of particular importance for supercapacitor technology [15–17]. Many investigations have focused on the manufacturing of wearable and flexible devices [18–20]. There has been significant progress in the development of advanced electrode microstructures [21–23], which facilitate charge-discharge reactions.

Recent studies have highlighted the need for the development of efficient electrodes with high active mass loading and the low mass of passive components [24]. It should be noted that high gravimetric capacitance is achieved only in thin films. However, the increase in active mass results in poor electrolyte access to the active material and high resistance. Therefore, the gravimetric capacitance decreases with increasing active mass. Improved material performance at high active mass is achieved using advanced techniques for the synthesis of porous materials and the design of advanced structures by template methods [24–26]. Novel research avenues have been proposed for the fabrication of nanoparticles of controlled size and shape [27,28]. The capacitive properties of electrodes are enhanced by the development of nanorods, nanowires, nanotubes, as well as lamellar, hollow, and core-shell particles of different capacitive materials [27,29,30]. New strategies have been developed for the fabrication of nanocomposites by heterocoagulation techniques, which involve electrostatic interactions or Schiff base reactions [24]. Significant progress has been achieved in the development of new dispersing agents for inorganic particles, graphene, carbon nanotubes, and other capacitive materials and conductive additives [31,32].

The need for supercapacitor electrodes with enhanced performance at high active mass has driven the development of particle extraction through a liquid–liquid interface (PELLI) method [33] for agglomerate-free processing of inorganic nanoparticles. The method allows direct particle transfer from the synthesis medium to a device processing medium, avoiding particle drying and re-dispersion stages. It has been shown [33] that the driving forces for particle agglomeration during the drying stage are the reduction of surface area and surface condensation reactions. Different PELLI strategies have been developed, such as bottom-up and top-down strategies. Various chelating organic molecules have been utilized as extractors, enabling particle transfer through the interface of two immiscible liquids [33]. The PELLI method has allowed for enhanced mixing of non-agglomerated particles of different capacitive materials with conductive additives and fabrication of electrodes with high areal capacitance and low resistance [24], which are achieved as a result of an enhanced material performance at high active mass. Despite the success in the application of PELLI in the development of advanced electrodes with high areal capacitance, the PELLI technique has limitations. Particle synthesis is usually achieved in an aqueous phase, and it is challenging to avoid agglomeration during synthesis. Extractor molecules are usually accumulated at the liquid–liquid interface with their hydrophilic groups exposed to water and hydrophobic hydrocarbon chains extending into the organic phase. Inorganic particles are modified at liquid–liquid extraction (LLI) and extracted into the organic phase after synthesis. Hydrophobic receiving liquids, such as 1-butanol, are immiscible with water. Moreover, 1-butanol has a relatively high boiling point. As a result, it is difficult to remove adsorbed 1-butanol molecules from the particle surface. The adsorbed hydrophobic 1-butanol molecules are detrimental to the access of an aqueous electrolyte to the particle surface.

The goal of this investigation was to develop Mn_3O_4-multiwalled carbon nanotube (MWCNT) electrodes using a new extraction strategy and avoid the limitations of the PELLI method. The approach was based on the use of 2-propanol as a receiving liquid instead of 1-butanol. It is important to note that 2-propanol is miscible with water. However, 2-propanol can be separated from an aqueous phase by the addition of salts, such as NaCl. The approach developed in this investigation involved the synthesis of Mn_3O_4 in an aqueous phase, the addition of a suspension of MWCNT in 2-propanol, co-dispersion, and mixing of Mn_3O_4 in the water-2-propanol mixture, salting out the 2-propanol phase, and extraction of Mn_3O_4 and MWCNT into the 2-propanol phase. The approach is conceptually different from the partitioning of organic compounds in a mixture of water and an organic solvent using a salting-out effect. In our investigation, Mn_3O_4 particles were synthesized in an aqueous phase. The synthesis was performed in the presence of an extractor, which acted as a capping agent for the synthesis and a dispersant for Mn_3O_4. The phase separation of aqueous and 2-propanol phases was achieved after synthesis by the addition of NaCl. The method allowed for the extraction of Mn_3O_4 and carbon nanotubes into the 2-propanol phase and their efficient dispersion and mixing. In this approach, the problem related to the adsorption of hydrophobic 1-butanol on the particle surface was avoided. The use of octanohydroxamic acid (OHA) as an extractor, capping, and the dispersing agent was a key for the successful fabrication of high active mass electrodes with high areal capacitance and low impedance by the salting-out particle extraction.

2. Results and Discussion

In this investigation, crystalline Mn_3O_4 material was prepared by a chemical precipitation method. Figure 1 shows the X-ray diffraction pattern of the obtained material. It exhibits diffraction peaks, corresponding to the JCPDS file 24-0734 of Mn_3O_4. For the fabrication of supercapacitor electrodes, Mn_3O_4 particles must be transferred from the aqueous synthesis media to an organic solvent containing a dissolved binder. A water-insoluble binder provides electrode stability in an aqueous electrolyte. Mn_3O_4 particles must be co-dispersed with conductive MWCNT in an organic solvent to achieve good mixing.

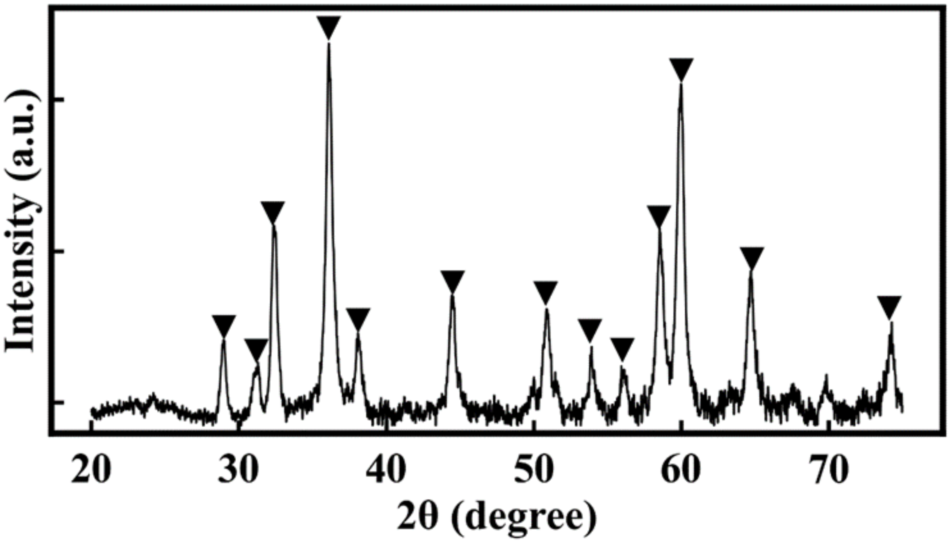

Figure 1. X-ray diffraction pattern of the as precipitated material (▼—peaks corresponding to JCPDS file 24-0734 of Mn_3O_4).

A traditional strategy involves washing, drying, and redispersion of particles in an organic solvent. However, as pointed out above, drying leads to particle agglomeration, which results in their poor mixing with conductive additives and poor electrode performance. PELLI method [33] allows for the direct transfer of oxide particles from an aqueous synthesis medium to an organic medium for electrode fabrication, thus avoiding particle agglomeration during the drying step. In many previous investigations, 1-butanol was used as a receiving liquid, which is immiscible with water. The superior capacitive behavior of electrodes, prepared using PELLI [33], was linked to the reduced agglomeration of capacitive materials and their improved mixing with conductive additives. However, there are difficulties related to the adsorption of hydrophobic 1-butanol on the surface of inorganic particles and carbon nanotube additives. The adsorbed hydrophobic 1-butanol limits the access of aqueous electrolyte to the active material surface. The relatively high boiling point of 1-butanol introduces problems with its removal. This reduces the benefits of PELLI for the fabrication of supercapacitor electrodes. To overcome these obstacles, we explored the salting-out method, which is conceptually different from the PELLI method. Figure 2 shows a schematic of the procedure used for Mn_3O_4

synthesis, mixing with MWCNT, and salting out of the mixture of Mn_3O_4 and MWCNT to the 2-propanol phase. Figure 3 shows a suspension of Mn_3O_4 and MWCNT dispersed using OHA in a mixture of water and 2-propanol before and after salting out.

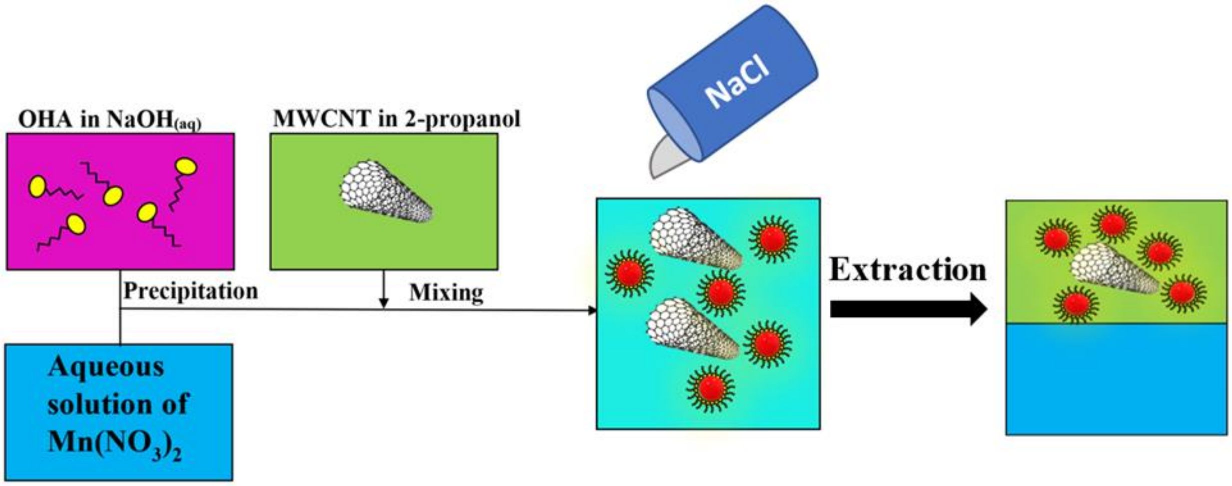

Figure 2. Schematic of Mn_3O_4 synthesis, mixing with multiwalled carbon nanotube (MWCNT), and salting-out method.

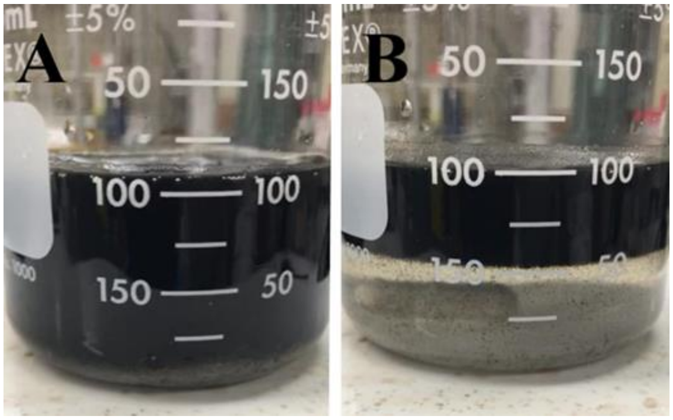

Figure 3. Suspension of Mn_3O_4 and MWCNT dispersed using octanohydroxamic acid (OHA) in a mixed water-2-propanol solvent (**A**) before and (**B**) after adding NaCl.

The salting-out method does not involve particle transfer through the liquid–liquid interface. It is based on the use of 2-propanol as a receiving liquid, which is miscible with water and has a relatively low boiling point. Moreover, 2-propanol and water form an azeotrope at a 2-propanol concentration of 87 wt% with a low boiling point of 80.3 °C [34]. The salting-out method was used for the separation of 2-propanol from an azeotropic water-2-propanol mixture [34]. It has previously been shown that salting out phase separation of 2-propanol and water can be used for the selective extraction of Co(II) [35] and Au(III) [36] ions. In our investigation, the salting-out method was developed for the extraction of Mn_3O_4 particles and MWCNT. In this approach, salting out resulted in a separation of 2-propanol, containing Mn_3O_4 and MWCNT from the aqueous phase. The co-extraction of Mn_3O_4 and MWCNT to 2-propanol allowed the fabrication of a composite electrode by impregnation of a current collector using a suspension of Mn_3O_4 and MWCNT.

In experiments performed without OHA, the hydrophobic MWCNT was extracted to the 2-propanol phase, whereas Mn_3O_4 remained in the aqueous phase. The modification of Mn_3O_4 particles with OHA was necessary for their extraction. Figure 4A shows a schematic of the chemical structure of OHA, which contains an alkyl chain, carbonyl, and NOH_2 groups. It has previously been shown that hydroxamic acids and their derivatives, such as OHA, exhibit metal chelating properties, which involve interactions of carbonyl and NOH_2 groups of the molecules with metal atoms, and facilitate their adsorption on surfaces of metal oxides [37–40]. Figure 4B shows a suggested mechanism of OHA adsorption on Mn_3O_4 particles, which involves the complexation of Mn atoms on the particle surface. In this investigation, OHA was used as a capping and dispersing agent for Mn_3O_4 synthesis. The hydrophobic alkyl chain of the adsorbed OHA molecule facilitated particle transfer into the 2-propanol phase. The transfer of Mn_3O_4 and MWCNT into the 2-propanol phase facilitated their co-dispersion and mixing, which allowed for the fabrication of electrodes with high areal capacitance at high active mass loading. The composite electrode was a mixture of Mn_3O_4 and MWCNT.

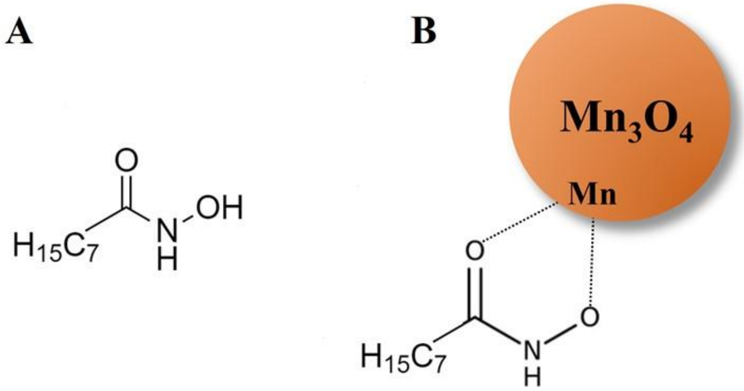

Figure 4. (**A**) The chemical structure of OHA, (**B**) OHA adsorption on Mn_3O_4 particles, involving complexation of surface Mn atoms.

Figure 5A shows Cyclic voltammetry(CV)curves for Mn_3O_4-MWCNT electrode with an active mass of 40.1 mg cm^{-2} prepared using the salting-out method. The nearly rectangular shape of the CVs and increase in the CV area with increasing scan rate indicate good capacitive behavior. The highest capacitance of 4.3 F cm^{-2} was achieved (Figure 5B) at a scan rate of 2 mV s^{-1}. The obtained capacitance was higher than literature data for Mn_3O_4-MWCNT electrodes, prepared by different advanced methods and summarized in a recent review [24]. The electrodes showed a high capacitance of 2.1 F cm^{-2} at a scan rate of 100 mV s^{-1} with capacitance retention of 48.8 %. The obtained areal capacitance was higher than that obtained in other investigations of electrodes with high active mass [41–43]. It is important to note that MWCNT was used as an additive, which enhanced the electrical conductivity of the composite electrodes. It was found that the capacitance of pure MWCNT electrodes with a mass of 8 mg cm^{-2} was 0.032 F cm^{-2} at a scan rate of 2 mV s^{-1}. Therefore, the contribution of the capacitance of MWCNT to the total capacitance was below 1%.

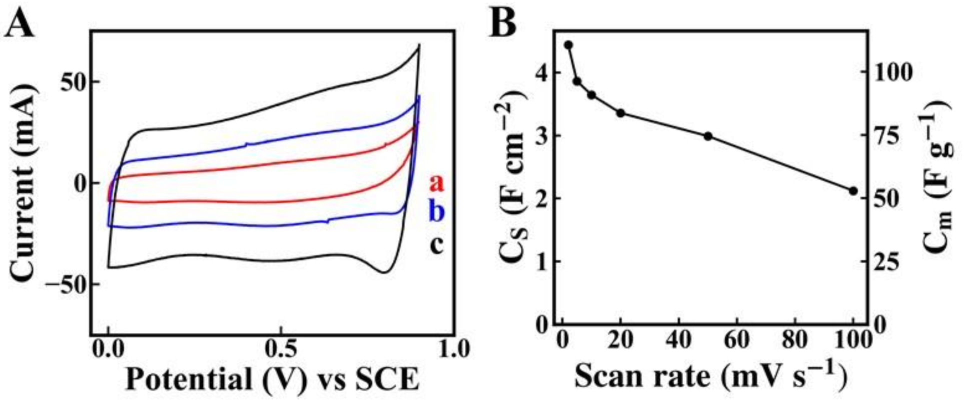

Figure 5. (**A**) CVs at scan rates of (a) 2, (b) 5, (c) 10 mV s^{-1}, and (**B**) C_S and C_m versus scan rate for Mn_3O_4-MWCNT electrodes.

Figure 6 shows charge-discharge data for the Mn_3O_4-MWCNT electrodes at different current densities. The time dependences of charge and discharge currents were nearly linear, and the charge-discharge curves were of a symmetric triangular shape. The capacitance C_S calculated at a discharge current of 3 mA cm^{-2} was 3.8 F cm^{-2}. It was found that C_s was nearly constant at discharge currents of 3–10 mA cm^{-2}.

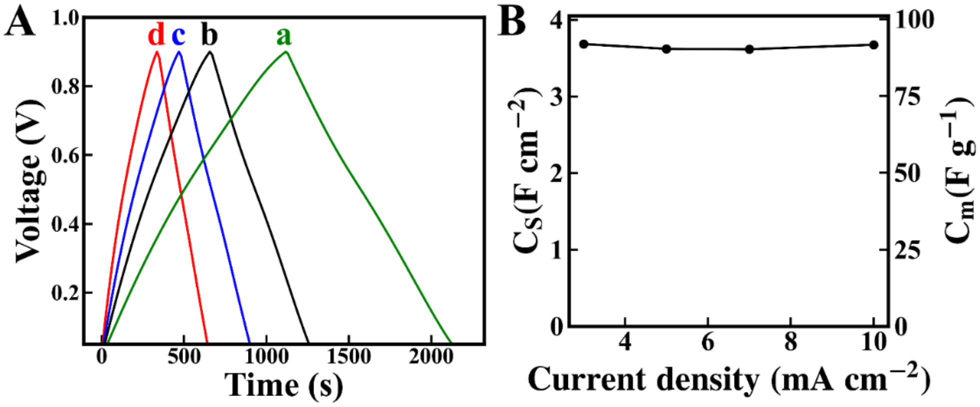

Figure 6. (**A**) Charge discharge behavior at current densities of (a) 3, (b) 5, (c) 7, and (d) 10 mA cm^{-2}, and (**B**) capacitance versus current density for Mn_3O_4-MWCNT electrodes.

The Nyquist plot of complex impedance showed a nearly vertical line, which indicated good capacitive behavior (Figure 7A). The low real part of impedance resulted from good mixing of Mn_3O_4 with conductive MWCNT.

The electrode resistance, represented by the real part of the complex impedance, decreased with increasing frequency. The highest resistance of 0.68 Ohm was obtained at a frequency of 10 mHz.

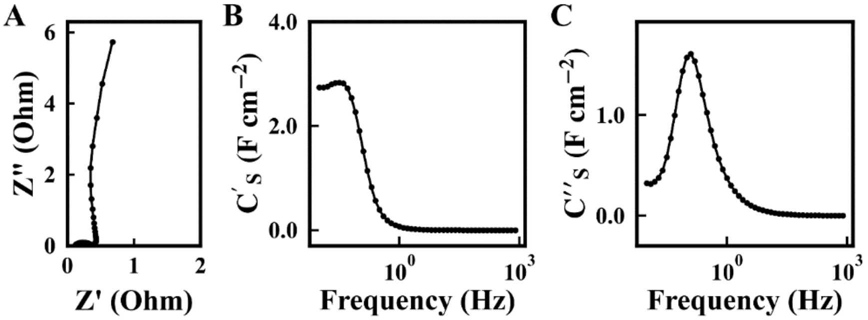

Figure 7. (**A**) Nyquist plot of complex impedance and (**B**,**C**) frequency dependences of (**B**) C_S' (**C**) C_S'' for Mn_3O_4-MWCNT electrodes.

The capacitance C_S' obtained at AC voltage of 5 mV (Figure 7B) was lower than C_S obtained from the CV data in a voltage window of 0.9 V. The difference can be attributed to limited electrolyte ion access to the active material at low voltages. The capacitance C_S' decreased with increasing frequency, and the frequency dependence of C_S'' showed a maximum (Figure 7C), which is typical for a relaxation type dispersion [15]. Figure 8 shows the cyclic behavior of the Mn_3O_4-MWCNT electrode. The capacitance showed an initial increase during the first 50 cycles and then remained nearly constant. The capacitance retention after 1000 cycles was 118%. It was hypothesized that the increase of capacitance during cycling could be attributed to the changing of the wetting behavior of the active material by the electrolyte. Figure 9 shows SEM images of the electrodes before and after cycling. The SEM image of the electrode before cycling showed composite particles with a typical size of 1–2 μm. The composite particles contained MWCNT dispersed in the Mn_3O_4 matrix. Such microstructure results from good mixing of the Mn_3O_4 particles and MWCNT in the suspension, prepared by the salting-out method for impregnation of current collectors, and explains the good capacitive behavior and low impedance of the electrodes. The SEM image of the electrodes after cycling shows a flaky morphology and large pores. It is suggested that such pores facilitated electrolyte access to the bulk of the electrodes and could be considered as an additional factor, which resulted in increased capacitance during cycling.

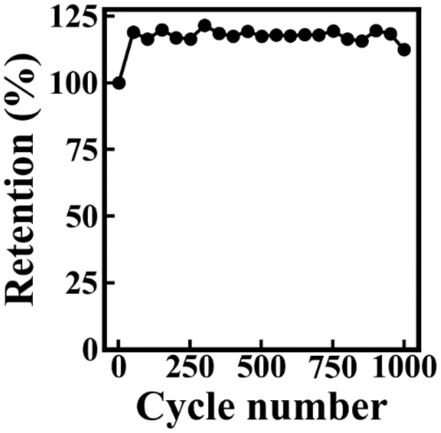

Figure 8. Capacitance retention versus cycle number for Mn_3O_4-MWCNT electrodes.

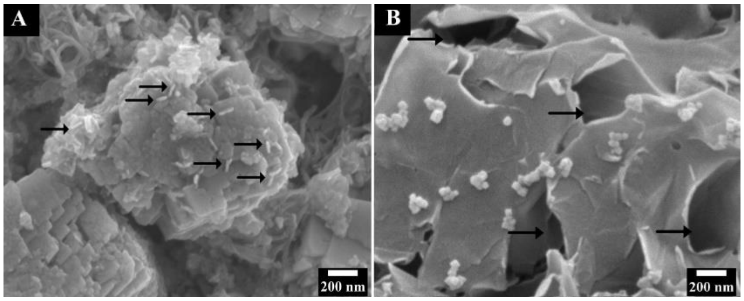

Figure 9. SEM images of the Mn_3O_4-MWCNT electrodes: (**A**) as prepared, arrows show MWCNT in the Mn_3O_4 matrix, (**B**) after cycling, arrows show large pores.

3. Materials and Methods

Octanohydroxamic acid (TCI America), $Mn(NO_3)_2{\cdot}4H_2O$, NaOH, Na_2SO_4, 2-propanol, NaCl, polyvinylbutyral (PVB) (Aldrich, Canada), multiwalled carbon nanotubes (Bayer, Germany) were used as starting materials. The 330 mg of $Mn(NO_3)_2{\cdot}4H_2O$ was dissolved into 20 mL of DI water, and then the pH was adjusted to 10 by the addition of aqueous NaOH solution, containing 33 mg of dissolved OHA. Obtained suspension of Mn_3O_4 particles modified with OHA as a capping and dispersing agent was ultrasonicated, and then 25 mg of MWCNT dispersed in 30 mL of 2-propanol was added. OHA improved dispersion of MWCNT, and a stable suspension was obtained. The addition of 6 g NaCl resulted in the separation of aqueous and 2-propanol phases. The phase separation resulted in a transfer of Mn_3O_4 and MWCNT into the 2-propanol phase (Figures 1 and 2) to form a composite suspension, containing Mn_3O_4 and MWCNT in a mass ratio of 4:1. The suspension of Mn_3O_4 and MWCNT in 2-propanol was separated from the aqueous phase, and the PVB binder was added to the suspension in order to achieve a ratio of PVB/(Mn_3O_4 +MWCNT) = 0.03.

The suspension was used for the impregnation of commercial Ni foam (Vale Canada) current collectors. The mass ratio of PVB:Mn_3O_4:MWCNT in the electrode was 3:80:20. Due to the low boiling point of 2-propanol, it was removed from the electrode material surface by drying of the electrode at 60 °C. The electrode area was 1 cm^2. The total mass of the material (active mass) impregnated into the current collector was 40.1 (±0.03) mg cm^{-2}. The electrode thickness was 0.4 mm.

X-ray diffraction (XRD) analysis (diffractometer Bruker D8, UK) was performed using Cu-Kα radiation in the 2θ range of 8–135 degrees, at the rate of 0.01 degrees per second. Electrode microstructures were analyzed using a JEOL SEM (scanning electron microscope, JSM-7000F) at an applied voltage of 5 keV and a working distance of 6 mm. Cyclic voltammetry (CV) and electrochemical impedance spectroscopy (EIS) studies were performed using a potentiostat-impedance analyzer PARSTAT 2273 (Ametek). Cyclic voltammetry data was obtained at sweep rates of 2–100 mV s^{-1}. EIS data was obtained at an open circuit potential using alternating voltage with an amplitude of 5 mV in the frequency range of 0.01–10 kHz. Galvanostatic charge-discharge (GCD) investigations in a fixed potential range were performed using BioLogic VMP 300 at current densities of 3, 5, 7, and 10 mA cm^{-2}. Testing was performed using a 3-electrode electrochemical cell containing a working electrode (impregnated Ni foam), counter-electrode (Pt mesh), and a reference electrode (SCE, saturated calomel electrode). Aqueous 0.5 M Na_2SO_4 solution was used as an electrolyte. Three different methods were used for the calculation of capacitance.

The integral capacitance C in the voltage window 0–0.9 V versus SCE was calculated from the CV data

$$C = \frac{\Delta Q}{\Delta U} = \frac{|\int_0^{t(Umax)} Idt| + |\int_{t(Umax)}^{0} Idt|}{2Umax} \quad (1)$$

where ΔQ denotes charge, I-current, t-time, and ΔU- the potential range.

The integral capacitance was also calculated from the GCD data in the same potential range:

$$C = I\Delta t/\Delta U \quad (2)$$

where I denotes the applied current, and Δt –discharge time.

The differential complex capacitance $C^*(\omega) = C'(\omega) - Ic''(\omega)$ was calculated at different frequencies (ω) from the complex impedance $Z^*(\omega) = Z'(\omega) + i\,Z''(\omega)$ data [44], where

$$C'(\omega) = \frac{-Z''(\omega)}{\omega|Z(\omega)|^2} \quad (3)$$

$$C''(\omega) = \frac{Z'(\omega)}{\omega|Z(\omega)|^2} \quad (4)$$

The capacitive properties of electrode material were presented in gravimetric (C_m) and areal (C_S) capacitance forms.

4. Conclusions

For the first time, the salting-out method was used for the extraction of particles from the aqueous synthesis medium to an electrode processing organic medium. OHA was used as a capping and dispersing agent for the synthesis as well as a particle extractor. The adsorption of OHA on Mn_3O_4 particles involved the complexation of Mn atoms on the particle surface. The surface modification of Mn_3O_4 particles with OHA facilitated the particle transfer into the 2-propanol phase. The method eliminated the particle drying stage, which resulted in particle agglomeration. The method facilitated co-dispersion of Mn_3O_4 and MWCNT in the 2-propanol phase and their enhanced mixing, which allowed for the fabrication of high active mass electrodes with enhanced performance. A capacitance of 4.3 F cm^{-2} was achieved at low impedance at active mass loading of 40.1 mg cm^{-2}. The electrodes showed good capacitance retention at high scan rates and good cyclic stability. The initial capacitance increase during cycling could be attributed to the changes in microstructure. The method opens a new and unexplored path for the fabrication of nanocomposites. Further progress in applications of the salting-out method will depend on the development of advanced extractor molecules.

Author Contributions: Conceptualization, K.R. and I.Z.; methodology, K.R.; validation, K.R.; formal analysis, K.R.; investigation, K.R.; resources, I.Z.; data curation, K.R.; writing—original draft preparation, K.R. and I.Z.; writing—review and editing, K.R. and I.Z.; supervision, I.Z.; project administration, I.Z.; funding acquisition, I.Z. All authors have read and agreed to the published version of the manuscript.

Funding: This research was funded by the Natural Sciences and Engineering Research Council of Canada, grant number RGPIN-2018-04014.

Institutional Review Board Statement: Not Applicable

Informed Consent Statement: Not Applicable

Data Availability Statement: The data presented in this study are available in : Application of Octanohydroxamic Acid for Salting out Liquid–Liquid Extraction of Materials for Energy Storage in Supercapacitors

Acknowledgments: SEM investigations were performed at the Canadian Centre for Electron Microscopy.

Conflicts of Interest: The authors declare no conflict of interest.

References

1. Attias, R.; Sharon, D.; Borenstein, A.; Malka, D.; Hana, O.; Luski, S.; Aurbach, D. Asymmetric supercapacitors using chemically prepared MnO2 as positive electrode materials. *J. Electrochem. Soc.* **2017**, *164*, A2231–A2237.
2. Brousse, T.; Bélanger, D. A Hybrid Fe3O4-MnO2 capacitor in mild aqueous electrolyte. *Electrochem. Solid State Lett.* **2003**, *6*, A244–A248.
3. Kierzek, K.; Gryglewicz, G. Activated Carbons and their evaluation in electric double layer capacitors. *Molecules* **2020**, *25*, 4255.
4. Chung, H.-Y.; Pan, G.-T.; Hong, Z.-Y.; Hsu, C.-T.; Chong, S.; Yang, T.C.-K.; Huang, C.-M. Biomass-derived porous carbons derived from soybean residues for high performance solid state supercapacitors. *Molecules* **2020**, *25*, 4050.
5. Kim, H.G.; Kim, Y.-S.; Kwac, L.K.; Shin, H.K. Characterization of activated carbon paper electrodes prepared by rice husk-isolated cellulose fibers for supercapacitor applications. *Molecules* **2020**, *25*, 3951.
6. Li, J.; Zhitomirsky, I. Cathodic electrophoretic deposition of manganese dioxide films. *Colloids Surf. A Physicochem. Eng. Asp.* **2009**, *348*, 248–253.
7. Yoon, S.; Kang, E.; Kim, J.K.; Lee, C.W.; Lee, J. Development of high-performance supercapacitor electrodes using novel ordered mesoporous tungsten oxide materials with high electrical conductivity. *Chem. Commun.* **2011**, *47*, 1021–1023.
8. Zhang, W.; Mu, B.; Wang, A. Halloysite nanotubes induced synthesis of carbon/manganese dioxide coaxial tubular nanocomposites as electrode materials for supercapacitors. *J. Solid State Electrochem.* **2015**, *19*, 1257–1263.

9. Ivol, F.; Porcher, M.; Ghosh, A.; Jacquemin, J.; Ghamouss, F. Phenylacetonitrile ($C_6H_5CH_2CN$) ionic liquid blends as alternative electrolytes for safe and high-performance supercapacitors. *Molecules* **2020**, *25*, 2697.
10. Pant, B.; Pant, H.R.; Park, M. Fe1−xS Modified TiO_2 NPs embedded carbon nanofiber composite via electrospinning: A Potential electrode material for supercapacitors. *Molecules* **2020**, *25*, 1075.
11. Wang, X.; Wu, D.; Song, X.; Du, W.; Zhao, X.; Zhang, D. Review on Carbon/Polyaniline Hybrids: Design and Synthesis for Supercapacitor. *Molecules* **2019**, *24*, 2263.
12. Shi, K.; Zhitomirsky, I. Electrophoretic nanotechnology of graphene–carbon nanotube and graphene–polypyrrole nanofiber composites for electrochemical supercapacitors. *J. Colloid Interface Sci.* **2013**, *407*, 474–481.
13. Xu, X.; Tang, J.; Qian, H.; Hou, S.; Bando, Y.; Hossain, M.S.A.; Pan, L.; Yamauchi, Y. Three-Dimensional Networked Metal–Organic Frameworks with Conductive Polypyrrole Tubes for Flexible Supercapacitors. *ACS Appl. Mater. Interfaces* **2017**, *9*, 38737–38744.
14. Conway, B.E.; Pell, W.G. Power limitations of supercapacitor operation associated with resistance and capacitance distribution in porous electrode devices. *J. Power Sources* **2002**, *105*, 169–181.
15. Zhu, Y.; Shi, K.; Zhitomirsky, I. Polypyrrole coated carbon nanotubes for supercapacitor devices with enhanced electrochemical performance. *J. Power Sources* **2014**, *268*, 233–239.
16. Athouël, L.; Moser, F.; Dugas, R.; Crosnier, O.; Bélanger, D.; Brousse, T. Variation of the MnO_2 birnessite structure upon charge/discharge in an electrochemical supercapacitor electrode in aqueous Na2SO4 electrolyte. *J. Phys. Chem. C* **2008**, *112*, 7270–7277.
17. Haldorai, Y.; Giribabu, K.; Hwang, S.-K.; Kwak, C.H.; Huh, Y.S.; Han, Y.-K. Facile synthesis of α-MnO_2 nanorod/graphene nanocomposite paper electrodes using a 3D precursor for supercapacitors and sensing platform to detect 4-nitrophenol. *Electrochim. Acta* **2016**, *222*, 717–727.
18. He, W.; Wu, B.; Lu, M.; Li, Z.; Qiang, H. Fabrication and Performance of Self-Supported Flexible Cellulose Nanofibrils/Reduced Graphene Oxide Supercapacitor Electrode Materials. *Molecules* **2020**, *25*, 2793.
19. Shi, K.; Yang, X.; Cranston, E.D.; Zhitomirsky, I. Efficient lightweight supercapacitor with compression stability. *Adv. Funct. Mater.* **2016**, *26*, 6437–6445.
20. Chang, Y.; Zhou, W.; Wu, J.; Ye, G.; Zhou, Q.; Li, D.; Zhu, D.; Li, T.; Nie, G.; Du, Y. High-performance flexible-film supercapacitors of layered hydrous RuO_2/poly (3, 4-ethylenedioxythiophene)-poly (styrenesulfonate) through vacuum filtration. *Electrochim. Acta* **2018**, *283*, 744–754.
21. Chen, G.; Zhang, X.; Ma, Y.; Song, H.; Pi, C.; Zheng, Y.; Gao, B.; Fu, J.; Chu, P.K. In-Situ Synthesis of Heterostructured Carbon-Coated Co/MnO Nanowire Arrays for High-Performance Anodes in Asymmetric Supercapacitors. *Molecules* **2020**, *25*, 3218.
22. Appadurai, T.; Subramaniyam, C.M.; Kuppusamy, R.; Karazhanov, S.; Subramanian, B. Electrochemical Performance of Nitrogen-Doped TiO_2 Nanotubes as Electrode Material for Supercapacitor and Li-Ion Battery. *Molecules* **2019**, *24*, 2952.
23. Zhang, D.; Shao, Y.; Kong, X.; Jiang, M.; Lei, X. Hierarchical carbon-decorated Fe_3O_4 on hollow CuO nanotube array: Fabrication and used as negative material for ultrahigh-energy density hybrid supercapacitor. *Chem. Eng. J.* **2018**, *349*, 491–499.
24. Chen, R.; Yu, M.; Sahu, R.P.; Puri, I.K.; Zhitomirsky, I. The Development of Pseudocapacitor Electrodes and Devices with High Active Mass Loading. *Adv. Energy Mater.* **2020**, *10*, 1903848.
25. Yang, S.; Wu, C.; Cai, J.; Zhu, Y.; Zhang, H.; Lu, Y.; Zhang, K. Seed-assisted smart construction of high mass loading Ni–Co–Mn hydroxide nanoflakes for supercapacitor applications. *J. Mater. Chem. A* **2017**, *5*, 16776–16785.
26. Fan, Z.; Wang, Y.; Xie, Z.; Xu, X.; Yuan, Y.; Cheng, Z.; Liu, Y. A nanoporous MXene film enables flexible supercapacitors with high energy storage. *Nanoscale* **2018**, *10*, 9642–9652.
27. Han, D.; Jing, X.; Xu, P.; Ding, Y.; Liu, J. Facile synthesis of hierarchical hollow ε-MnO_2 spheres and their application in supercapacitor electrodes. *J. Solid State Chem.* **2014**, *218*, 178–183.
28. Zhang, D.; Shao, Y.; Kong, X.; Jiang, M.; Lei, D.; Lei, X. Facile fabrication of large-area hybrid Ni-Co hydroxide/Cu $(OH)_2$/copper foam composites. *Electrochim. Acta* **2016**, *218*, 294–302.
29. Liu, Q.; Yang, J.; Wang, R.; Wang, H.; Ji, S. Manganese dioxide core–shell nanostructure to achieve excellent cycling stability for asymmetric supercapacitor applications. *RSC Adv.* **2017**, *7*, 33635–33641.
30. Shi, K.; Zhitomirsky, I. Fabrication of Polypyrrole-Coated Carbon Nanotubes Using Oxidant–Surfactant Nanocrystals for Supercapacitor Electrodes with High Mass Loading and Enhanced Performance. *ACS Appl. Mater. Interfaces* **2013**, *5*, 13161–13170.
31. Ata, M.S.; Poon, R.; Syed, A.M.; Milne, J.; Zhitomirsky, I. New developments in non-covalent surface modification, dispersion and electrophoretic deposition of carbon nanotubes. *Carbon* **2018**, *130*, 584–598.
32. Ata, M.; Liu, Y.; Zhitomirsky, I. A review of new methods of surface chemical modification, dispersion and electrophoretic deposition of metal oxide particles. *RSC Adv.* **2014**, *4*, 22716–22732.

33. Silva, R.M.E.; Poon, R.; Milne, J.; Syed, A.; Zhitomirsky, I. New developments in liquid-liquid extraction, surface modification and agglomerate-free processing of inorganic particles. *Adv. Colloid Interface Sci.* **2018**, *261*, 15–27.
34. Tang, Z.; Zhou, R.; Duan, Z. Separation of isopropanol from aqueous solution by salting-out extraction. *J. Chem. Technol. Biotechnol.* **2001**, *76*, 757–763.
35. Chung, N.H.; Tabata, M. Salting-out phase separation of the mixture of 2-propanol and water for selective extraction of cobalt (II) in the presence of manganese (II), nickel (II), and copper (II). *Hydrometallurgy* **2004**, *73*, 81–89.
36. Chung, N.H.; Tabata, M. Selective extraction of gold (III) in the presence of Pd (II) and Pt (IV) by salting-out of the mixture of 2-propanol and water. *Talanta* **2002**, *58*, 927–933.
37. Folkers, J.P.; Gorman, C.B.; Laibinis, P.E.; Buchholz, S.; Whitesides, G.M.; Nuzzo, R.G. Self-assembled monolayers of long-chain hydroxamic acids on the native oxide of metals. *Langmuir* **1995**, *11*, 813–824.
38. Sarvaramini, A.; Azizi, D.; Larachi, F. Hydroxamic acid interactions with solvated cerium hydroxides in the flotation of monazite and bastnäsite—Experiments and DFT study. *Appl. Surf. Sci.* **2016**, *387*, 986–995.
39. Eisenlauer, J.; Matijević, E. Interactions of metal hydrous oxides with chelating agents. II. α-Fe_2O_3—low molecular and polymeric hydroxamic acid species. *J. Colloid Interface Sci.* **1980**, *75*, 199–211.
40. Natarajan, R.; Fuerstenau, D. Adsorption and flotation behavior of manganese dioxide in the presence of octyl hydroxamate. *Int. J. Miner. Process.* **1983**, *11*, 139–153.
41. Ata, M.S.; Milne, J.; Zhitomirsky, I. Fabrication of Mn3O4–carbon nanotube composites with high areal capacitance using cationic and anionic dispersants. *J. Colloid Interface Sci.* **2018**, *512*, 758–766.
42. Poon, R.; Zhitomirsky, I. Application of Cyrene as a solvent and dispersing agent for fabrication of Mn_3O_4-carbon nanotube supercapacitor electrodes. *Colloid Interface Sci. Commun.* **2020**, *34*, 100226.
43. Poon, R.; Zhao, X.; Ata, M.S.; Clifford, A.; Zhitomirsky, I. Phase transfer of oxide particles for application in thin films and supercapacitors. *Ceram. Int.* **2017**, *43*, 8314–8320.
44. Taberna, P.; Simon, P.; Fauvarque, J.-F. Electrochemical characteristics and impedance spectroscopy studies of carbon-carbon supercapacitors. *J. Electrochem. Soc.* **2003**, *150*, A292–A300.

Chapter 6 – Salting-out aided dispersive extraction of Mn3O4 nanoparticles and carbon nanotubes for application in supercapacitors

Author's Contributions:

1. Testing and documentation of new colloidal processing technique
2. Synthesis of nanocomposite active material
3. Electrode sample preparation and electrochemical testing
4. SEM imaging
5. Preparation of manuscript draft
6. Literature review

Salting-out aided dispersive extraction of Mn_3O_4 nanoparticles and carbon nanotubes for application in supercapacitors

Kaelan Rorabeck and Igor Zhitomirsky*

Department of Materials Science and Engineering, McMaster University, Hamilton, ON, Canada

*E-mail: zhitom@mcmaster.ca

Phone: 1-905-525-9140

Abstract

In this study, results from a conceptually new method for the preparation of Mn_3O_4-multiwalled carbon nanotube (MCNT) composites are presented. High active mass (HAM) Mn_3O_4-MCNT cathodes are prepared and tested for supercapacitors. The method is based on a salting-out aided dispersive extraction of Mn_3O_4 particles precipitated in an aqueous phase to isopropanol and their co-dispersion with MCNT. The use of lauryl gallate as an extractor is a key factor for the phase transfer. Lauryl gallate is used as a co-dispersant for Mn_3O_4 and MCNT. The mechanisms of lauryl gallate adsorption on Mn_3O_4 and MCNT and the salting-out aided extraction mechanism are discussed. Enhanced electrochemical performance of the electrodes with HAM of 41 mg cm^{-2} is achieved due to enhanced mixing and co-dispersion of Mn_3O_4 and MCNT. The electrodes show a high capacitance of 6 F cm^{-2} in aqueous Na_2SO_4 and low electrical resistance. The obtained areal capacitance is substantially higher than that for Mn_3O_4-MCNT composites, prepared by other methods. The capacitance increase during initial cycling is linked to the microstructure changes. The salting-out aided extraction method overcomes the limitations of other extraction techniques and opens a new strategy for the manufacturing of nanocomposites with advanced functional properties.

Key words: manganese oxide, supercapacitor, carbon nanotube, capacitance, extraction, adsorption

1.Introduction

Manganese oxides, such as Mn_3O_4, MnO_2, as well as different polymorphs of MnO_2 have been considered as important cathode materials for supercapacitors[1-5]. The interest in manganese oxides is attributed to their various advantages, such as high theoretical capacitance, large voltage window and low cost[6,7]. Testing results showed nearly ideal preudocapacitive behavior of Mn_3O_4 and MnO_2. The use of manganese oxides as cathodes facilitated the development of asymmetric devices with enlarged operation voltage in aqueous electrolytes[6-8]. Such devices showed enhanced power-energy characteristics. Many important investigations focused on charge storage properties of complex oxides, containing manganese[9,10]. In previous studies, significant attention was given to the development of thin film electrodes[11-13]. Electrochemical testing revealed higher capacitance of MnO_2 films, than that of Mn_3O_4 films[14,15]. However, despite significant developments in the preparation of thin film supercapacitors, there is a need in the design of high active mass (HAM) bulk electrodes[16-18]. It is shown that an AM above 10 mg cm^{-2} is critical for the development of supercapacitor cells with low ratio of inactive components mass to the AM[19-22]. The major difficulty in the development of efficient HAM electrodes is reduction of specific capacitance with AM increase[16,17] due to diffusion limitations of an electrolyte. Wetting behavior of the electrodes by an electrolyte is an important factor, controlling the electrode performance. It is influenced by the nature of electrode material and its microstructure. However, the analysis of wetting behavior of HAM porous composite material impregnated into 3D current collectors presents difficulties.

Various colloidal techniques have been explored in the literature for the fabrication of HAM electrodes[16]. Main challenges for the fabrication of HAM electrodes by colloidal methods include synthesis of non-agglomerated nanoparticles, fabrication of stable suspensions of co-dispersed nanoparticles and conductive additives, development of advanced binders, impregnation of current collectors and formation of electrode structures with controlled porosity[18,23,24]. MnO_2 particles are usually produced by reduction of permanganate precursors[25,26], such as $KMnO_4$ and $NaMnO_4$. Such precursors react with various organic materials. Therefore, it is challenging to control size and dispersion of MnO_2 particles using organic capping agents for the particle synthesis. In contrast, various capping agents can be combined with Mn^{2+} salts for the preparation of non-agglomerated Mn_3O_4 particles. AM particle size reduction facilitates electrochemical reactions and allows for improved capacitive behavior. Moreover, Mn_3O_4 belongs to the large family of spinel compounds and the development of Mn_3O_4 based solid solutions can potentially lead to the fabrication of advanced electrode materials[27,28]. Therefore, Mn_3O_4 has generated interest for the fabrication of HAM electrodes[29].

Mn_3O_4 is usually combined with various conductive additives, which allow enhanced electronic conductivity[16,30]. In previous studies significant attention was given to dispersion of Mn_3O_4 nanoparticles and their enhanced mixing with MCNT[16,31]. Various co-dispersant molecules have been analyzed for the fabrication of stable suspensions of Mn_3O_4 and MCNT[16]. Heterocoagulation techniques[16,32] have emerged for the manufacturing of composites with enhanced mixing of Mn_3O_4 and MCNT. HAM electrodes were produced using slurries of Mn_3O_4 nanoparticles, conductive additives and water-insoluble polymer binders, which were impregnated into porous electrical current collectors.

Chemical precipitation from aqueous solutions offers a way to fabricate Mn_3O_4 particles[31]. Particle extraction through the interface of immiscible liquids has emerged in recent years as a versatile method for functionalization of nanoparticles and agglomerate-free manufacturing[31,33]. It has been shown that nanoparticle transfer to an organic liquid prevents agglomeration, which occurs during the traditional drying and redispersion method[31,33]. This strategy facilitates particle mixing with conductive additives on the nanometric scale and paves the way for the fabrication of electrodes with enhanced performance.

This investigation was motivated by achievements in the development of supercapacitor electrodes with HAM using particle extraction techniques. The objective of this study was the development of a conceptually new colloidal extraction technique, which is based on the salting-out effect of a water-miscible solvent, such as isopropanol. The formation of a biphasic system resulted from the addition of a salt, which facilitated phase separation. It was discovered that the use of a chelating surfactant for the surface modification of Mn_3O_4 particles in a mixed water-isopropanol phase is a key factor for the transfer of non-agglomerated Mn_3O_4 particles to the isopropanol phase. A record high capacitance of Mn_3O_4 -MCNT electrodes resulted from the good co-dispersion of Mn_3O_4 and MCNT. This investigation opens a new and unexplored colloidal method for the manufacturing of nanocomposites.

2.Experimental procedures

MCNT (US Nanomaterials Inc., 20-30nm diameter,), $MnN_2O_6 \cdot 4H_2O$, NaOH, isopropanol, a co-polymer of vinyl butyral, vinyl acetate and vinyl alcohol (PVBAA, 65 kDa) NaCl, lauryl gallate (MilliporeSigma), and Ni foam (Vale) were used.

A suspension of Mn_3O_4 nanoparticles was obtained by dissolving 330 mg of $MnN_2O_6 \cdot 4H_2O$ in 20 mL of water, then increasing the pH of the solution to pH=10 with aqueous NaOH. In a separate beaker, 33mg of LG was dissolved in 30mL of isopropanol, then 25mg of MCNT were added, and the solution was ultrasonicated. The nanoparticle suspension and the dispersed MCNT were then combined and stirred, which resulted in a stable suspension. After the addition of 6g NaCl the aqueous and isopropanol phases separated. The phase separation resulted in the transfer of MCNT and Mn_3O_4 into the isopropanol phase.

The aqueous phase, containing NaCl was removed with a separatory funnel, and PVBAA binder was added to the suspension at 3 wt % of the combined weight of Mn_3O_4 and MCNT. The use of the binder was critical for the fabrication of mechanically stable electrodes with HAM. Obtained mixture was impregnated into the foam, and then the foam was pressed to a final thickness of 0.38 mm, washed and dried. The total mass of the impregnated material after drying was 41 mg cm^{-2} for all samples tested in this investigation. The electrode area was 1 cm^2.

X-ray diffraction (XRD) analysis (Bruker D8, UK) was performed using Cu-Kα radiation, in the 2 theta range of 10-135°, with a step of 0.01° per second. Using a JEOL SEM (7000F), the fabricated electrode surface was imaged with a working distance of 10mm and an accelerating voltage of 5 keV. Cyclic voltammetry (CV) and electrochemical impedance spectroscopy (EIS) were performed using the Ametek potentiostat (model 2273), while galvanostatic charge-discharge (GCD) was done using the BioLogic VMP 300. Testing was performed using a 3-electrode set up containing a working electrode (Ni foam with active material), a counter electrode of a Pt mesh, and a saturated calomel electrode (SCE) as a reference, in a solution of 0.5 M Na_2SO_4 as an aqueous electrolyte. EIS data was obtained using an AC voltage with an amplitude of 5mV. Areal C_S (F cm^{-2}) and gravimetric C_g (F g^{-1}) capacitances were calculated from CV and GCD data as it was described in literature[16]. Cyclic stability testing was performed by analysing CVs at a scan rate of 50 mV s^{-1} in 0.5M Na_2SO_4 electrolyte for electrodes with mass of 41 mg cm^{-2}.

3.Results and Discussion

The success of Mn_3O_4 applications for energy storage in supercapacitors will depend on the ability to exploit advanced pseudocapacitive properties of this material for electrodes with HAM. Mn_3O_4

is an attractive charge storage material due to its high C_g. The major difficulty in utilizing high C_g of Mn_3O_4 in bulk electrodes is poor electrolyte access to the particle surface in the bulk electrodes and increase of electrode resistance with increasing AM. The equivalent circuit of HAM electrodes includes a highly capacitive surface layer, connected in series with a bulk electrode, which can have a lower capacitance[16]. Therefore, it is not surprising that in many experiments the increase in AM resulted in reduction of total capacitance at fast charging rates[16]. Experimental C_g of very thin films can be close the theoretical capacitance value of a material, which represents its fundamental charge storage properties. However, the increase in active mass results in decreasing C_g. Therefore, measured C_g shows the degree of utilization of capacitive properties of the material. It is challenging to increase C_S using higher AM due to the decrease in C_g[16]. Previous studies[16] showed that C_S is an important parameter, which must be considered together with C_g for the characterization of HAM electrodes. C_S measurements are important for matching capacitances of cathodes and anodes of asymmetric supercapacitor devices and optimization of the total device capacitance.

In this investigation, Mn_3O_4 was synthesized by an aqueous precipitation technique. XRD testing showed the crystallization of the spinel Mn_3O_4 structure (Figure 1). The traditional strategy for creation of a slurry for impregnation of porous electric current collectors involves washing and drying of Mn_3O_4 precipitates, and Mn_3O_4 particle co-dispersion with MCNT in a solution of a binder in an organic solvent. The principal drawback of this approach is agglomeration of the particles and their poor mixing with conductive additives. Indeed, drying promotes agglomeration resulting from the condensation of OH surface groups and formation of oxo-bridges between particles.

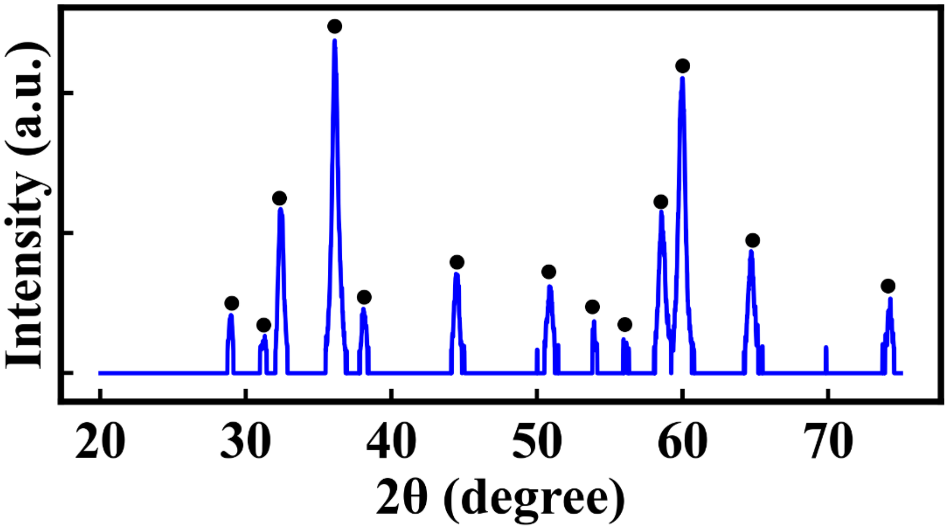

Figure 1. XRD pattern of as prepared material (●- peaks, matching Mn_3O_4, JCPDS file 24-0734).

The high surface energy of Mn_3O_4 nanoparticles is another factor, which facilitates their agglomeration. One way to overcome this difficulty is to modify particles with a surfactant at the liquid-liquid interface of an aqueous phase with water-immiscible organic solvent and transfer the modified particles to the organic medium[33]. However, this approach has several drawbacks. It is challenging to achieve modification of particles with a surfactant by the diffusion of particles from an aqueous phase and surfactant molecules from an organic phase to the liquid-liquid interface, where their interaction occurs. In many studies 1-butanol was used as a water-immiscible organic receiving liquid[33]. Therefore, another difficulty is related to hydrophobic properties of 1-butanol and relatively high boiling point of this solvent. It is obvious that adsorbed hydrophobic 1-butanol must be removed from the AM surface, because it limits diffusion of electrolyte in pores of AM.

The approach developed in this investigation is conceptually different from other particle extraction techniques, described in a recent review[33]. Isopropanol is a hydrophilic alcohol[34], which is miscible with water and has a relatively low boiling point. In this investigation, we applied a salting-out aided extraction for the separation of an isopropanol phase, containing co-dispersed Mn_3O_4 and MCNT, from a suspension in a mixed water-isopropanol solvent. It is known that salting-out method allows separation of isopropanol from water-isopropanol mixtures[34,35]. The addition of a salt, such as NaCl, to the water-isopropanol mixture results in enhanced interactions between the salt ions and water molecules, which reduces the number of water molecules interacting with isopropanol. Therefore, separation of water and isopropanol phases was observed. Salting-out aided extraction methods have been developed for the extraction of organic molecules and ions to the isopropanol phase[36-38]. The extraction of organic molecules was based on their hydrophobic interactions with an organic solvent[36]. The mechanism of ion extraction was based on the formation ion-pair complexes[38]. It will be shown below that the mechanism of Mn_3O_4 particle extraction is conceptually different. It is based on the use of LG as an extractor. The experimental results of our investigation indicate that salting-out aided extraction can be used for the extraction of Mn_3O_4 particles and MCNT. In our approach, Mn_3O_4 particles were modified with LG extractor and co-dispersed with MCNT in the mixed water-isopropanol solvent (Figure 2). The addition of NaCl resulted in separation of isopropanol from the aqueous phase. The modified particles and MCNT were transferred to the isopropanol phase. Figure 3 shows separated aqueous and isopropanol phases.

The use of LG was a key factor for the particle transfer. The chemical structure of LG (Figure 4A) contains a chelating galloyl group, which can be involved in a strong bonding to the surface atoms by a catecholate-type[39] bonding mechanism (Figure 4B). Recent review[39] on catecholate-type dispersants provides evidence of strong bonding of various catecholate surfactants to manganese oxides. In experiments performed without LG and MCNT it was found that Mn_3O_4 remained in the aqueous phase after salting out of isopropanol. In contrast, Mn_3O_4 particles were extracted in the presence of LG. Therefore, the surface modification of Mn_3O_4 by LG bonding to the particle surface was one of the key factors governing the particle extraction. LG is soluble in isopropanol and in isopropanol-water mixtures.

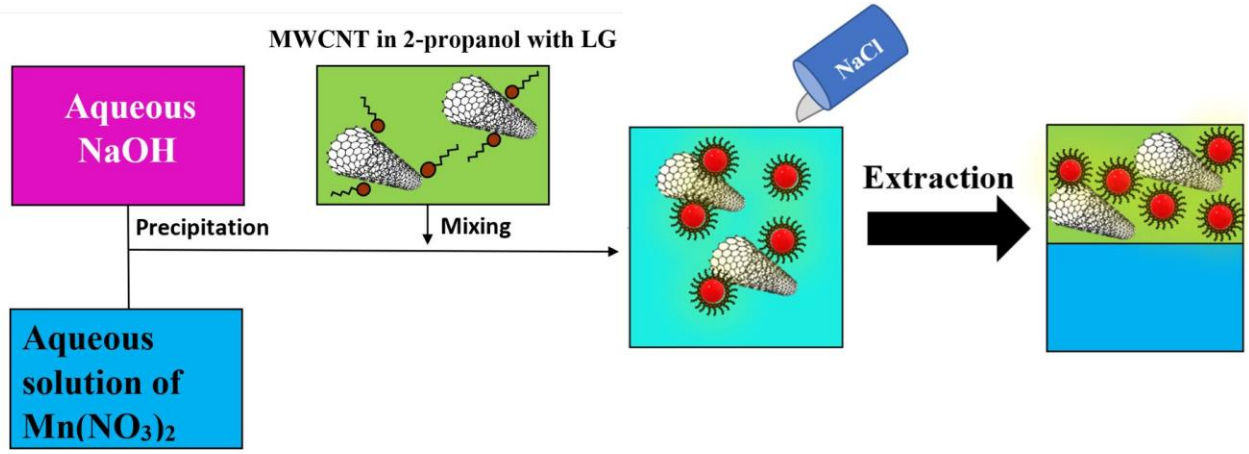

Figure 2. Schematic of Mn_3O_4 synthesis and salting-out aided extraction mechanism.

Figure 3. Salting out aided extraction of Mn_3O_4 and MCNT to the isopropanol phase

The solubility of LG in a water-isopropanol mixture was beneficial for LG adsorption on the Mn_3O_4 particles. The $C_{12}H_{25}$ group of adsorbed LG facilitated particle dispersion. In experiments performed without LG and Mn_3O_4, MCNT were transferred to the isopropanol phase. However, we found that LG improved MCNT dispersion. It was suggested that the LG adsorption on the MCNT surface involved hydrophobic interactions of the hydrocarbon chain and π-π interactions (Figure 4). The transfer of Mn_3O_4 and MCNT from the water-isopropanol mixture to the salted-out isopropanol phase resulted in their improved co-dispersion and mixing. As a result, obtained electrodes showed enhanced electrochemical performance.

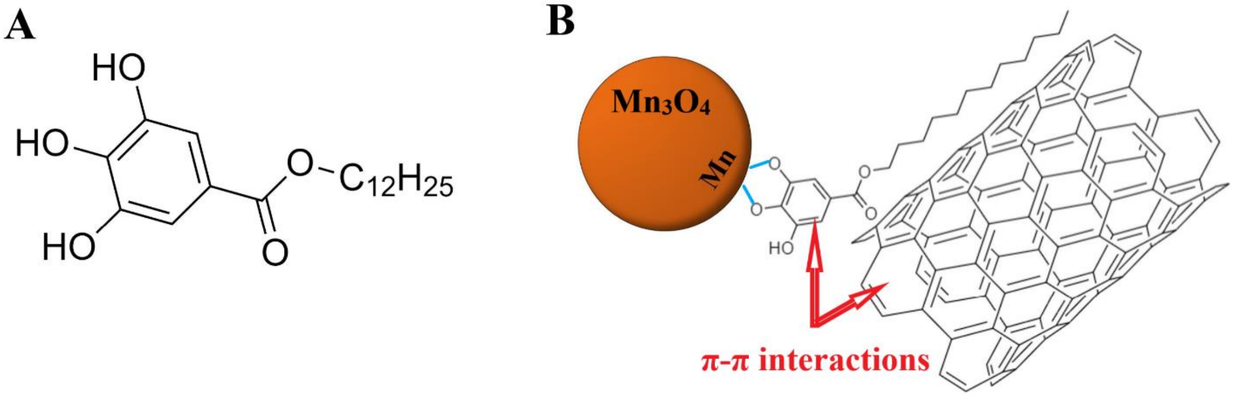

Figure 4. (A) LG structure, (B) LG adsorption on Mn_3O_4 and MCNT

Figure 5 shows the results of cyclic voltammetry for the Mn_3O_4 -MCNT nanocomposite electrode with AM of 41.0 mg cm^{-2}, prepared via the salting-out aided dispersion method. There is an indication of pseudocapacitive behaviour from the nearly box shape of the CV curves, with a correlation between CV area and scan rate. The highest calculated capacitance was 6.0 F cm^{-2} (147 F g^{-1}) at 2 mV s^{-1}, whereas C_S was 1.5 F cm^{-2} at 100 mV s^{-1} and C_S retention was 25%. Several previous investigations of Mn_3O_4 based electrodes with HAM, described in a recent review[16], reported C_S of 2.8-4.2 F cm^{-2}, which were obtained from the CV data at similar conditions in the same scan rate range. Therefore, the method developed in this investigation resulted in a record-high capacitance of the Mn_3O_4 based electrodes. The measurements at lower scan rates showed small C_S variations. The C_S values at 1 and 0.5 mV s^{-1} were found to be 6.2 and 6.3 F cm^{-2}, respectively. In this study, high C_S was achieved at very low electrical resistance, which is presented by the real impedance component in the EIS Nyquist plot (Figure 6) for the electrode. Capacitive response is also indicated by nearly vertical line (Figure 6) of the EIS plot and by a triangular shape of the GCD plot (Figure 7). The C_S value, calculated from the GCD data at 3 mA cm^{-2} was 5.0 F cm^{-2}. The capacitance showed small changes with current density variations from 3 to 10 mA cm^{-2}. Relatively small C_S variations were reported in the same range in previous investigations[40] of electrodes with a comparable AM. It is important to note that capacitances measured by different methods must be compared at similar charge-discharge times. Therefore, the small variations in the capacitance for CV scan rates of 0.5-2 mV s^{-1} correlate with small variations in capacitances at GCD current densities of 3-10 mA cm^{-2}. The difference in absolute values of capacitances obtained by different methods in the same potential range can result from deviations from the ideal shapes of the CV or GCD curves.

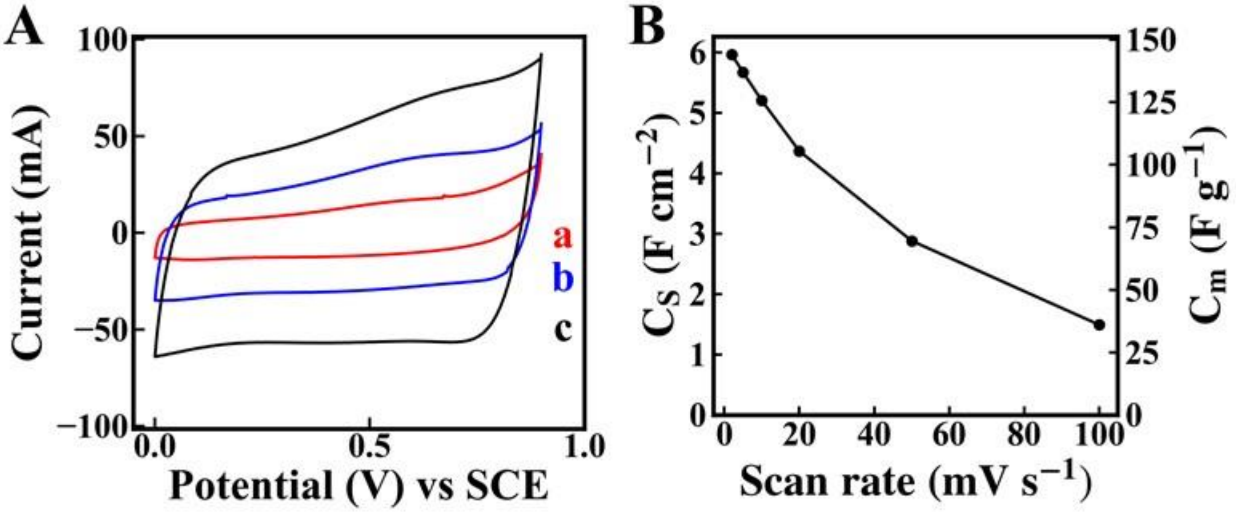

Figure 5. (A) CVs at (a)2, (b) 5, and (c) 10 mV s^{-1}, (B) capacitances versus scan rate

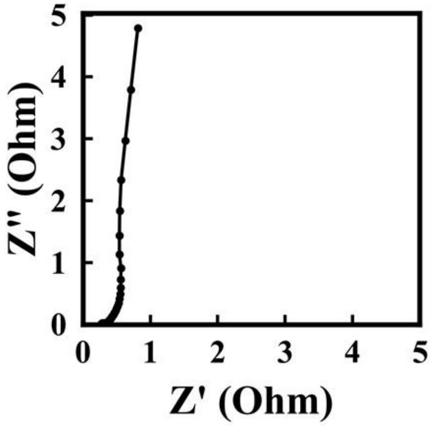

Figure 6. (A) EIS Nyquist plot for Mn_3O_4-MCNT composite.

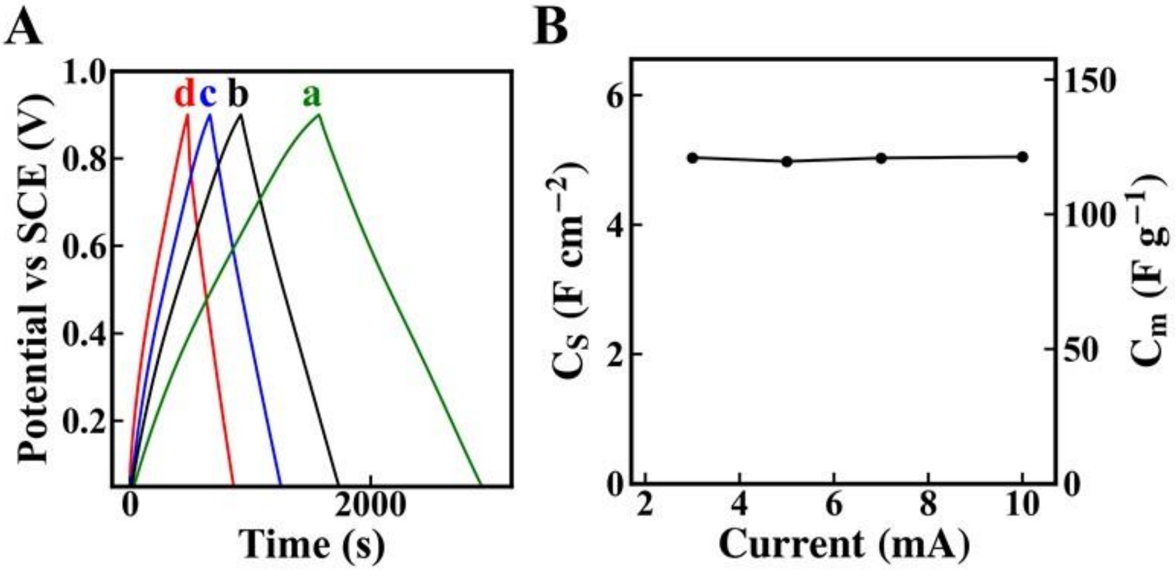

Figure 7. (A) GCD data at (a) 3, (b) 5, (c) 7, and (d) 10 mA cm^{-2} and (B) capacitances versus GCD current density for Mn_3O_4 -MCNT.

Figure 8A shows an SEM image of as-prepared Mn_3O_4-MCNT electrodes. The electrode showed a porous structure, which is beneficial for the electrolyte access to AM. Mn_3O_4 particles and MCNT formed mixed agglomerates, in which MCNT provided a conductive path to the individual

Mn_3O_4 nanoparticles. The size of the mixed agglomerates was ~1 μm. It is important to note that drying of particles inevitably results in agglomeration. However, the segregation of individual Mn_3O_4 and MCNT agglomerates was avoided. The salting-out aided extraction method facilitated dispersion and mixing of Mn_3O_4 and MCNT in suspensions, which provided their good mixing in the dried composite electrodes. Electrochemical cycling resulted in changes in the electrode morphology. Figure 8B shows an SEM image of the electrode after 1000 cycles. Mn_3O_4 formed a flaky structure with embedded MCNT. The changes in microstructure correlated with changes in capacitance. Figure 9 shows capacitance retention during cycling. The capacitance increased to 152% of the initial value during the initial 200 cycles and the total capacitance retention was 148% after 1000 cycles. A similar increase in capacitance of Mn_3O_4 based electrodes was observed in other studies[40].

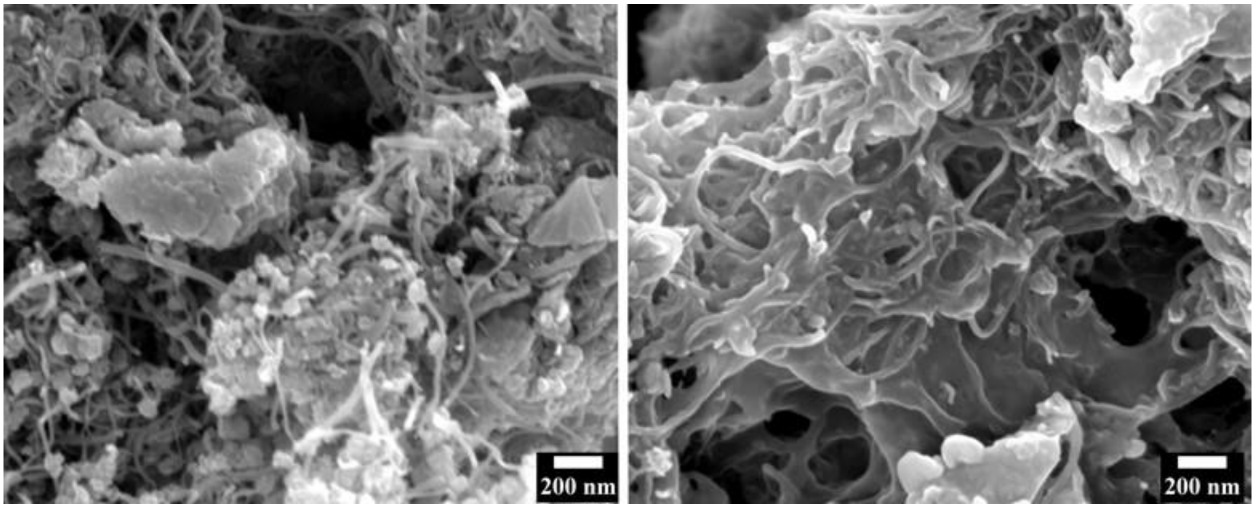

Figure 8. SEM images of Mn_3O_4-MCNT: (A) as-prepared and (B) after 1000 CV cycles.

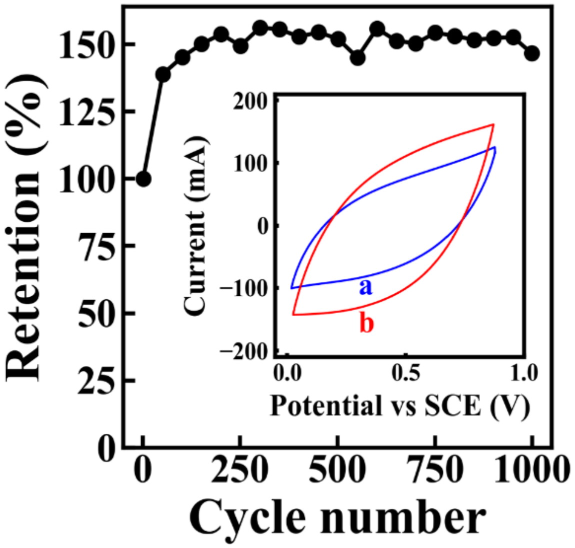

Figure 9. C_S retention for Mn_3O_4-MCNT, inset shows CVs for (a) cycle 1 and (b) cycle 1000.

Conclusions

Mn_3O_4 – MCNT composites were prepared using a conceptually new salting-out aided dispersive extraction method. LG adsorbed on Mn_3O_4 and MCNT and facilitated their extraction to the isopropanol phase and co-dispersion. The method allowed for enhanced mixing of Mn_3O_4 and MCNT by avoiding agglomeration caused by drying. The Mn_3O_4 - MCNT electrodes with HAM of 41 mg cm^{-2} showed a record-high C_S of 6 F cm^{-2} at 2 mV cm^{-2}. The remarkably high C_S was achieved at a low electrical resistance. The Mn_3O_4 - MCNT electrodes are promising for applications in cathodes of electrochemical supercapacitors. The salting-out aided extraction method overcomes limitations of other extraction strategies and can be used for the fabrication of various advanced nanocomposites for supercapacitors, batteries and other applications.

Acknowledgement

This research was funded by NSERC Canada. SEM studies were conducted at the Canadian Centre for Electron Microscopy.

References

[1] J. Zhao, G. Lu, Y. Wu, P. Zhang, J. Yue, Z. Cheng, J. Zhang, X. Kang, Manganeseoxide with rich oxygen vacancies based on plasma modification for high performance supercapacitors, Colloids and Surfaces A: Physicochemical and Engineering Aspects 603 (2020) 125254.
[2] X. Wang, L. Chen, S. Zhang, X. Chen, Y. Li, J. Liu, F. Lu, Y. Tang, Compounding δ-MnO2 with modified graphene nanosheets for highly stable asymmetric supercapacitors, Colloids and Surfaces A: Physicochemical and Engineering Aspects 573 (2019) 57-66.
[3] Q. Li, Y. Li, A.V. Fulari, G.S. Ghodake, D.-Y. Kim, G.M. Lohar, Performance of chemically synthesized Mn3O4/rGO nanocomposite for electrochemical supercapacitor: a cost-effective high-performance electrode, Nanotechnology 31(41) (2020).
[4] M.S. Yadav, Synthesis and characterization of Mn2O3Mn3O4 nanoparticles and activated charcoal based nanocomposite for supercapacitor electrode application, Journal of Energy Storage 27 (2020).
[5] R. Shobana, B. Saravanakumar, G. Ravi, V. Ganesh, R. Yuvakkumar, Synthesis and characterization of Mn3O4/MnSnO3 nanocomposites for supercapacitor applications, International Journal of Plastics Technology 24(1-2) (2020) 9-17.
[6] T. Brousse, D. Bélanger, A Hybrid Fe3O4-MnO2 Capacitor in Mild Aqueous Electrolyte, Electrochemical and solid-state letters 6(11) (2003) A244-A248.
[7] S. Devaraj, N. Munichandraiah, High capacitance of electrodeposited MnO2 by the effect of a surface-active agent, Electrochemical and Solid-State Letters 8(7) (2005) A373-A377.
[8] R. Attias, D. Sharon, A. Borenstein, D. Malka, O. Hana, S. Luski, D. Aurbach, Asymmetric supercapacitors using chemically prepared MnO2 as positive electrode materials, Journal of The Electrochemical Society 164(9) (2017) A2231-A2237.
[9] M. Shi, B. Wang, Y. Shen, J. Jiang, W. Zhu, Y. Su, M. Narayanasamy, S. Angaiah, C. Yan, Q. Peng, 3D assembly of MXene-stabilized spinel ZnMn2O4 for highly durable aqueous zinc-ion batteries, Chemical Engineering Journal 399 (2020) 125627.
[10] M. Shi, M. Narayanasamy, C. Yang, L. Zhao, J. Jiang, S. Angaiah, C. Yan, 3D interpenetrating assembly of partially oxidized MXene confined Mn–Fe bimetallic oxide for superior energy storage in ionic liquid, Electrochimica Acta 334 (2020) 135546.
[11] D.P.M.D. Shaik, P. Rosaiah, O.M. Hussain, Fabrication of the Mn3O4 thin film electrodes by electron beam evaporation for supercapacitor applications, Journal of Electroanalytical Chemistry 851 (2019) 8-18.
[12] A.A. Yadav, S.N. Jadhav, D.M. Chougule, P.D. Patil, U.J. Chavan, Y.D. Kolekar, Spray deposited Hausmannite Mn3O4 thin films using aqueous/organic solvent mixture for supercapacitor applications, Electrochimica Acta 206 (2016) 134-142.
[13] A. Gowrisankar, A.L. Sherryn, T. Selvaraju, Impact of morphological variation by phase-oriented MnO2-based hierarchical ternary composites for the fabrication of solid-state symmetric supercapacitor, Ionics 26(5) (2020) 2563-79.
[14] M. Toupin, T. Brousse, D. Bélanger, Charge Storage Mechanism of MnO2 Electrode Used in Aqueous Electrochemical Capacitor, Chemistry of Materials 16(16) (2004) 3184-3190.
[15] J. Broughton, M. Brett, Investigation of thin sputtered Mn films for electrochemical capacitors, Electrochimica Acta 49(25) (2004) 4439-4446.
[16] R. Chen, M. Yu, R.P. Sahu, I.K. Puri, I. Zhitomirsky, The Development of Pseudocapacitor Electrodes and Devices with High Active Mass Loading, Advanced Energy Materials 10(20) (2020) 1903848.
[17] Y. Gogotsi, P. Simon, True performance metrics in electrochemical energy storage, Science 334(6058) (2011) 917-918.
[18] M.-W. Xu, W. Jia, S.-J. Bao, Z. Su, B. Dong, Novel mesoporous MnO2 for high-rate electrochemical capacitive energy storage, Electrochimica Acta 55(18) (2010) 5117-5122.
[19] Y. Zhu, K. Shi, I. Zhitomirsky, Polypyrrole coated carbon nanotubes for supercapacitor devices with enhanced electrochemical performance, Journal of Power Sources 268 (2014) 233-239.

[20] M. Nawwar, R. Poon, R. Chen, R.P. Sahu, I.K. Puri, I. Zhitomirsky, High areal capacitance of Fe3O4-decorated carbon nanotubes for supercapacitor electrodes, Carbon Energy 1(1) (2019) 124-133.
[21] Y. Liu, I. Zhitomirsky, Electrochemical supercapacitor based on multiferroic BiMn2O5, Journal of Power Sources 284 (2015) 377-382.
[22] R. Chen, R. Poon, R.P. Sahu, I.K. Puri, I. Zhitomirsky, MnO2-carbon nanotube electrodes for supercapacitors with high active mass loadings, Journal of The Electrochemical Society 164(7) (2017) A1673-A1678.
[23] J. Ma, Q. Cheng, V. Pavlínek, P. Sáha, C. Li, Morphology-controllable synthesis of MnO 2 hollow nanospheres and their supercapacitive performance, New Journal of Chemistry 37(3) (2013) 722-728.
[24] C. Wan, L. Yuan, H. Shen, Effects of electrode mass-loading on the electrochemical properties of porous MnO2 for electrochemical supercapacitor, Int. J. Electrochem. Sci 9 (2014) 4024-4038.
[25] Y.-j. Yang, E.-h. Liu, L.-m. Li, Z.-z. Huang, H.-j. Shen, X.-x. Xiang, Nanostructured amorphous MnO2 prepared by reaction of KMnO4 with triethanolamine, Journal of Alloys and Compounds 505(2) (2010) 555-559.
[26] X. Xie, L. Gao, Characterization of a manganese dioxide/carbon nanotube composite fabricated using an in situ coating method, Carbon 45(12) (2007) 2365-2373.
[27] A.G. Naiknaware, J.U. Chavan, S.H. Kaldate, A.A. Yadav, Studies on spray deposited Ni doped Mn3O4 electrodes for supercapacitor applications, Journal of Alloys and Compounds 774 (2019) 787-794.
[28] O. Bayram, M.E. Ertargin, E. Igman, H. Guney, O. Simsek, Synthesis and characterization of Zn-doped Mn3O4 thin films using successive ionic layer adsorption and reaction technique: Its structural, optical and wettability properties, Journal of Materials Science: Materials in Electronics 29(11) (2018) 9466-73.
[29] D.P. Dubal, R. Holze, Self-assembly of stacked layers of Mn3O4 nanosheets using a scalable chemical strategy for enhanced, flexible, electrochemical energy storage, Journal of Power Sources 238 (2013) 274-282.
[30] A.U. Ubale, M.A. Waghmare, K.S. Iqbal, H.M. Pathan, Manganese oxides: promising electrode materials for Li-ion batteries and supercapacitors, Journal of Materials Science: Materials in Electronics 31(17) (2020) 14003-14021.
[31] J. Milne, I. Zhitomirsky, Application of octanohydroxamic acid for liquid-liquid extraction of manganese oxides and fabrication of supercapacitor electrodes, Journal of Colloid and Interface Science 515 (2018) 50-57.
[32] M.S. Ata, J. Milne, I. Zhitomirsky, Fabrication of Mn3O4–carbon nanotube composites with high areal capacitance using cationic and anionic dispersants, Journal of Colloid and Interface Science 512 (2018) 758-766.
[33] R.M.E. Silva, R. Poon, J. Milne, A. Syed, I. Zhitomirsky, New developments in liquid-liquid extraction, surface modification and agglomerate-free processing of inorganic particles, Advances in Colloid and Interface Science 261 (2018) 15-27.
[34] G. Khayati, A. Gholitabar, Liquid–liquid equilibrium of hydrophilic alcohols with three different salts of chloride: experiment and correlation, Journal of Chemical & Engineering Data 61(4) (2016) 1454-1461.
[35] T. Zhigang, Z. Rongqi, D. Zhanting, Separation of isopropanol from aqueous solution by salting-out extraction, Journal of Chemical Technology & Biotechnology 76(7) (2001) 757-763.
[36] L. Yan, Y.-Q. Sun, X.-D. Wang, H.-X. Fu, Y. Mu, Z.-L. Xiu, Partition behavior of monocarboxylic acids in salting-out extraction systems of monohydric alcohols and dipotassium phosphate, Separation and Purification Technology 199 (2018) 351-358.
[37] N.H. Chung, M. Tabata, Salting-out phase separation of the mixture of 2-propanol and water for selective extraction of cobalt (II) in the presence of manganese (II), nickel (II), and copper (II), Hydrometallurgy 73(1-2) (2004) 81-89.
[38] N.H. Chung, M. Tabata, Selective extraction of gold (III) in the presence of Pd (II) and Pt (IV) by salting-out of the mixture of 2-propanol and water, Talanta 58(5) (2002) 927-933.
[39] M. Ata, Y. Liu, I. Zhitomirsky, A review of new methods of surface chemical modification, dispersion and electrophoretic deposition of metal oxide particles, Rsc Advances 4(43) (2014) 22716-22732.
[40] R. Poon, I. Zhitomirsky, Application of Cyrene as a solvent and dispersing agent for fabrication of Mn3O4-carbon nanotube supercapacitor electrodes, Colloid and Interface Science Communications 34 (2020) 100226.

Chapter 7 – Dispersant Molecules with Functional Catechol Groups for Supercapacitor Fabrication

Author's Contributions:

1. Testing and processing of results
2. Synthesis of nanocomposite active material
3. Electrode sample preparation and electrochemical testing
4. SEM imaging
5. Preparation of manuscript draft
6. Literature review

Article

Dispersant Molecules with Functional Catechol Groups for Supercapacitor Fabrication

Kaelan Rorabeck and Igor Zhitomirsky *

Department of Materials Science and Engineering, McMaster University, Hamilton, ON, Canada; rorabeck@mcmaster.ca
* Correspondence: zhitom@mcmaster.ca

Abstract: Cathodes for supercapacitors with enhanced capacitive performance are prepared using MnO_2 as a charge storage material and carbon nanotubes (CNT) as conductive additives. The enhanced capacitive properties are linked to the beneficial effects of catecholate molecules, such as chlorogenic acid and 3,4,5-trihydroxybenzamide, which are used as co-dispersants for MnO_2 and CNT. The dispersant interactions with MnO_2 and CNT are discussed in relation to the chemical structures of the dispersant molecules and their biomimetic adsorption mechanisms. The dispersant adsorption is a key factor for efficient co-dispersion in ethanol, which facilitated enhanced mixing of the nanostructured components and allowed for improved utilization of charge storage properties of the electrode materials with high active mass of 40 mg cm^{-2}. Structural peculiarities of the dispersant molecules are discussed, which facilitate dispersion and charging. Capacitive properties are analyzed using cyclic voltammetry, chronopotentiometry and impedance spectroscopy. A capacitance of 6.5 F cm^{-2} is achieved at a low electrical resistance. The advanced capacitive properties of the electrodes are linked to the microstructures of the electrodes prepared in the presence of the dispersants.

Keywords: catechol; manganese dioxide; carbon nanotube; composite; dispersant; supercapacitor

Citation: Rorabeck, K.; Zhitomirsky, I. Dispersant molecules with functional catechol groups for supercapacitor fabrication. *Molecules* **2021**, *26*, x. https://doi.org/10.3390/xxxxx

Academic Editor:

Received: 27 February 2021
Accepted: 16 March 2021
Published: date

1. Introduction

Organic molecules, containing catechol groups, exhibit exceptionally strong adsorption on inorganic surfaces, which is a key factor for their applications for surface modification of various materials and fabrication of adherent coatings[1]. The adsorption mechanism of such molecules is similar to that of mussel proteins bonding to different surfaces, which results in super strong adhesion[2-4]. It is based on the bidentate chelating or bridging bonding of phenolic OH groups of the catechol ligands [1] to the metal atoms. The structural features of catecholates have rendered them useful in dispersion of various inorganic materials and fabrication of coatings by electrophoretic deposition[1,5]. Various charged dispersants have been developed for nanotechnology of functional materials[1]. The use of catecholate bonding mechanism has been gaining ground in the development of liquid-liquid extraction techniques[6], which facilitate the fabrication of non-agglomerated nanoparticles for diverse applications. Polyaromatic catecholates allowed efficient co-dispersion of inorganic materials and carbon nanotubes for the fabrication of advanced composites [7,8]. Various catecholate molecules were used as capping and structure directing agents for the synthesis of non-agglomerated nanoparticles, coated particles and nanorods with high aspect ratios[9-14]. Moreover, it was found that metastable materials can be synthesized in the presence of catecholate molecules[15].

Significant interest has been generated in the synthesis of polymer adhesives, containing catecholate monomers [16-18] and modification of polymers with catechol molecules[19-20]. The adsorption of catecholates on semiconductors allowed for enhanced charge transfer, advanced optical and photovoltaic properties, which were used for the development of various photovoltaic devices and sensors[21-23]. Catecholate molecules have been utilized for the fabrication of magnetic nanoparticles with enhanced magnetization[24], materials with luminescent properties[25], and quantum dots[26].

Anionic catecholate molecules were utilized for the fabrication of polypyrrole coatings on various non-noble substrates by anodic electropolymerization[27-29]. The role of catecholates in the electropolymerization process was multifunctional. Such molecules acted as anionic dopants for the electropolymerization process, facilitated charge transfer and allowed for electropolymerization at reduced electrode potential, which is critically important for corrosion prevention and fabrication of adherent coatings. Catecholate molecules facilitated incorporation of carbon nanotubes into the polypyrrole coatings[29]. Moreover, the catecholate-type bonding of the molecules to the electrode surface was another important factor for the fabrication of adherent polypyrrole coatings. Antifouling polymer coatings were prepared using catecholate molecules as anchors and initiators for surface-initiated polymerization on metallic substrates[30]. The strong adsorption of catecholates on metal surfaces was an important factor for their applications as corrosion inhibitors for stainless steel[31].

Many applications of catecholates are based on their interesting redox properties[32-34]. Catecholate molecules were used as reducing agents for the synthesis of inorganic nanoparticles by chemical precipitation methods[20,32]. Moreover, there is a growing interest in the applications of redox active catecholates for the fabrication of electrochemical sensors [19,20] and supercapacitors[35]. Chiral catecholate molecules were utilized for the fabrication of sensors for chiral electrochemical recognition of biomolecules[36]. Recently it was discovered that catecholate molecules can be used as charge transfer mediators between charge storage material and current collector of supercapacitor electrodes[9]. As a result, significant improvement in charge storage properties was achieved[9].

The increasing number of successful applications of catecholates and promising results achieved in various research fields have generated interest in fundamental investigation of various catecholate molecules. This interest is fueled by the rich functional properties of catecholate molecules. The investigation of multifunctional catecholate molecules, combining properties of catechol ligands with properties of other functional groups is a promising strategy for the development of advanced materials and composites as well as their surface modification and functionalization. An important task is to analyze the influence of various factors, such as chemical structure and solvent composition on interactions of catecholates with different materials.

Chlorogenic acid and 3,4,5-trihydroxybenzamide are promising molecules for the surface modification of materials by catecholate-type bonding and development of advanced functional materials. Chlorogenic acid is a natural material found in coffee and tea. Previous investigations focused on the rich variety of biomedical and pharmaceutical applications of this molecule[37]. Moreover, chlorogenic acid exhibits interesting functional properties for applications in sensors and photoluminescent devices[38-40]. Investigations revealed strong complexation of metal ions with chlorogenic acid[41]. 3,4,5-Trihydroxybenzamide exhibits interesting redox active and antioxidant properties[42,43].

The goal of this investigation was the application of chlorogenic acid and 3,4,5-trihydroxybenzamide for the fabrication of MnO_2-carbon nanotube (CNT) electrodes for supercapacitors. The approach was based on the catecholate-type bonding of the molecules to the MnO_2 surface which facilitated particle dispersion and charging. An important finding was the possibility to co-disperse MnO_2 and CNT in ethanol, which facilitated their enhanced mixing and allowed for the fabrication of advanced electrodes. Testing results showed good capacitive properties at high active mass, which resulted in high areal capacitance.

2. Results and Discussion

Recent studies on the development of supercapacitors stressed the importance of advanced manufacturing technologies[44-48]. The development of nanostructured electrodes has generated a need for advanced dispersants for active materials[49,50]. Therefore, in this investigation chlorogenic acid and 3,4,5-trihydroxybenzamide were tested as co-dispersants for MnO_2 and CNT.

Figure 1A,B show the chemical structures of chlorogenic acid and 3,4,5-trihydroxybenzamide. The structure of chlorogenic acid includes a catechol group. The anionic properties of this molecule are attributed to a carboxylic group. The adsorption of chlorogenic acid on inorganic surfaces can involve catecholate or carboxylate bonding mechanisms[1,51]. However, catecholate bonding to metal oxide surfaces is usually stronger than that of carboxylate bonding[1]. The structure of 3,4,5-trihydroxybenzamide contains a galloyl group, containing three phenolic OH groups bonded to adjacent carbon atoms of the aromatic ring. The galloyl group allows for catecholate type bonding, which usually involves two phenolic OH groups[1]. Moreover, NH_2 group of the structure can potentially be involved on weak bonding to metal atoms on the inorganic surfaces. Different modes of catecholate bonding are presented in Figure 1(Ca–c), including chelating, bridging inner sphere and bridging outer sphere bonding.

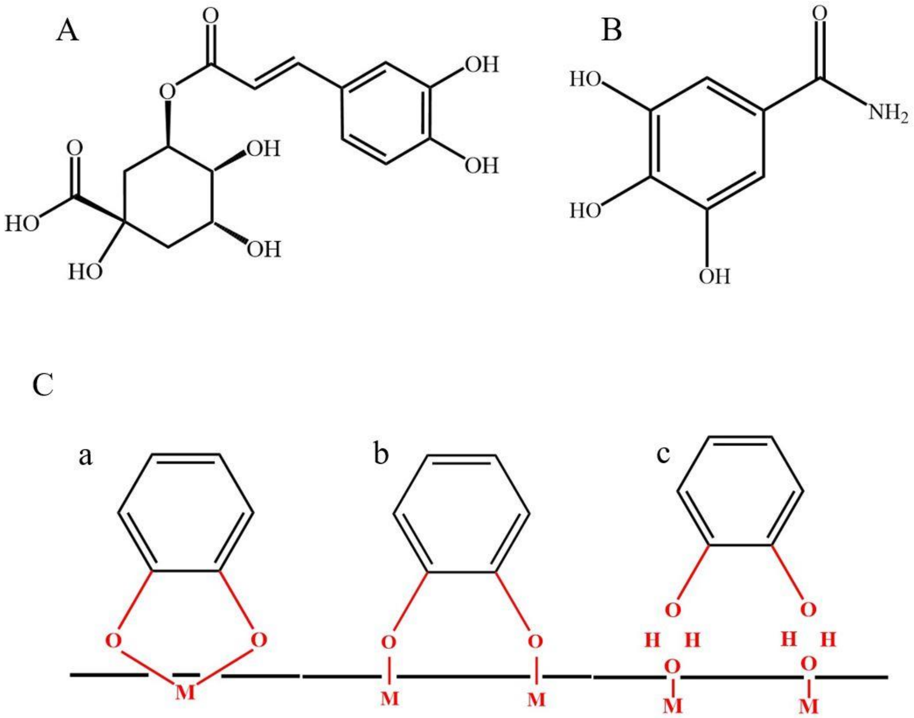

Figure 1. (A,B) Chemical structures of (**A**) chlorogenic acid and (**B**) 3,4,5-trihydroxybenzamide, (**C**) bonding mechanism of catechol to the metal atoms (M) on inorganic surface: (**a**) chelating, (**b**) inner sphere bridging and (**c**) outer sphere bridging.

It was suggested that catecholate bonding of chlorogenic acid and 3,4,5-trihydroxybenzamide to the MnO_2 particle surface will facilitate their dispersion and result in enhanced stability of suspensions for impregnation of current collectors. Sedimentation tests confirmed enhanced stability of the MnO_2 nanoparticles in ethanol solvent (Figure 2). Figure 2 compares MnO_2 suspensions prepared without and with dispersant molecules. The enhanced suspension stability achieved in the presence of the dispersants indicates that the dispersants adsorbed on the MnO_2 particles. Moreover, chlorogenic acid and 3,4,5-trihydroxybenzamide acted as dispersants for CNT in the same solvent. The ability to co-disperse MnO_2 and CNT in ethanol using chlorogenic acid and 3,4,5-trihydroxybenzamide was critically important for the fabrication of electrodes. Polyvinyl butyral (PVB) was dissolved in the same solvent and obtained slurry, containing MnO_2, CNT, and PVB binder, was used for the impregnation of Ni foam current collectors. For comparison, the electrodes were prepared using slurries, which were fabricated without dispersants.

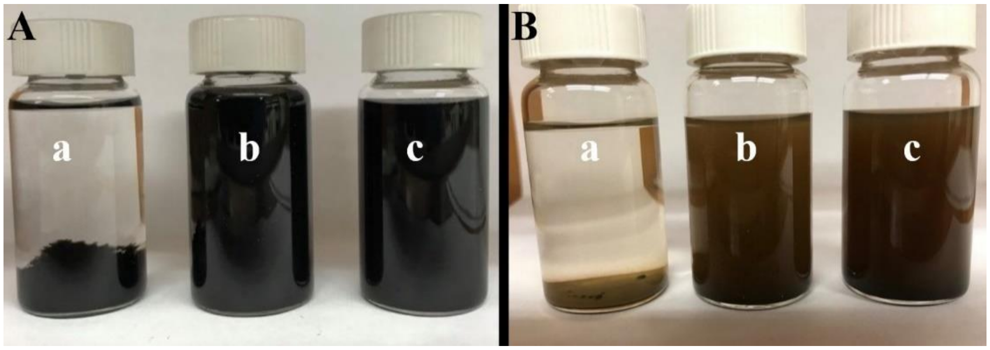

Figure 2. Sedimentation test for (**A**) carbon nanotubes (CNT) and (**B**) MnO_2 prepared (**a**) without dispersants and in the presence of (**b**) chlorogenic acid and (**c**) 3,4,5-trihydroxybenzamide.

Figure 3 shows Scanning Electron Microscopy (SEM) images of electrodes prepared without dispersants. The electrodes contained large agglomerates of MnO_2 (Figure 3A) and CNT (Figure 3B). The SEM images indicate poor mixing of the capacitive MnO_2 material and conductive CNT additives. It will be shown below that such poor mixing resulted in a low capacitance. In contrast, the use of chlorogenic acid and 3,4,5-trihydroxybenzamide dispersants allowed for improved mixing of MnO_2 and CNT. Figure 4 shows SEM images of MnO_2-CNT electrodes prepared using the dispersants. The SEM images at low magnifications show porous microstructures, which are beneficial for electrolyte transport. The high magnification images show MnO_2 particles as well as CNT and indicate enhanced mixing of the components, which allowed for enhanced capacitance.

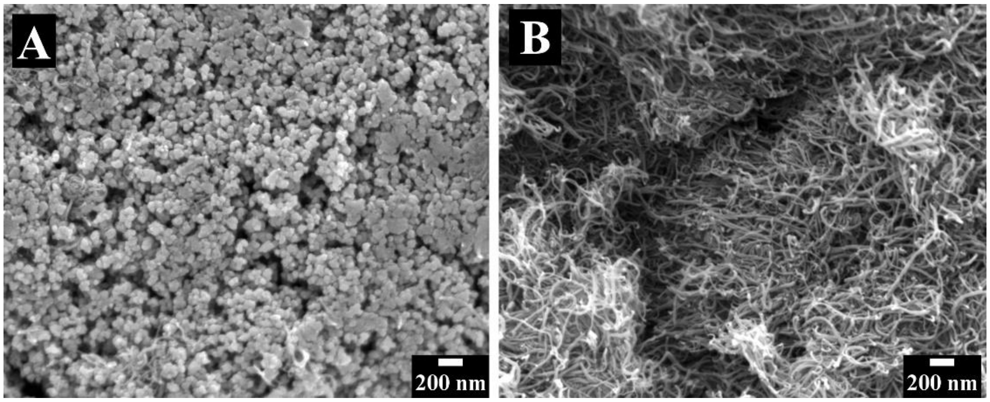

Figure 3. SEM images of electrode prepared without dispersant: (**A**) area of MnO_2 agglomerate and (**B**) area of CNT agglomerate.

Capacitance measurements were taken using cyclic voltammetry (CV) and galvanostatic charge–discharge (GCD) methods, which allowed for analysis of integral capacitance in a voltage window of 0 to 0.9 V. Moreover, components of complex differential capacitances were calculated from the electrochemical impedance spectroscopy (EIS) data at a voltage amplitude of 5 mV at different frequencies. The data obtained by different methods provided information on charging behavior of the electrodes at different conditions. The experimental results presented below indicated that capacitance depends on different factors, such has scan rate, frequency, charge/discharge current and voltage or potential.

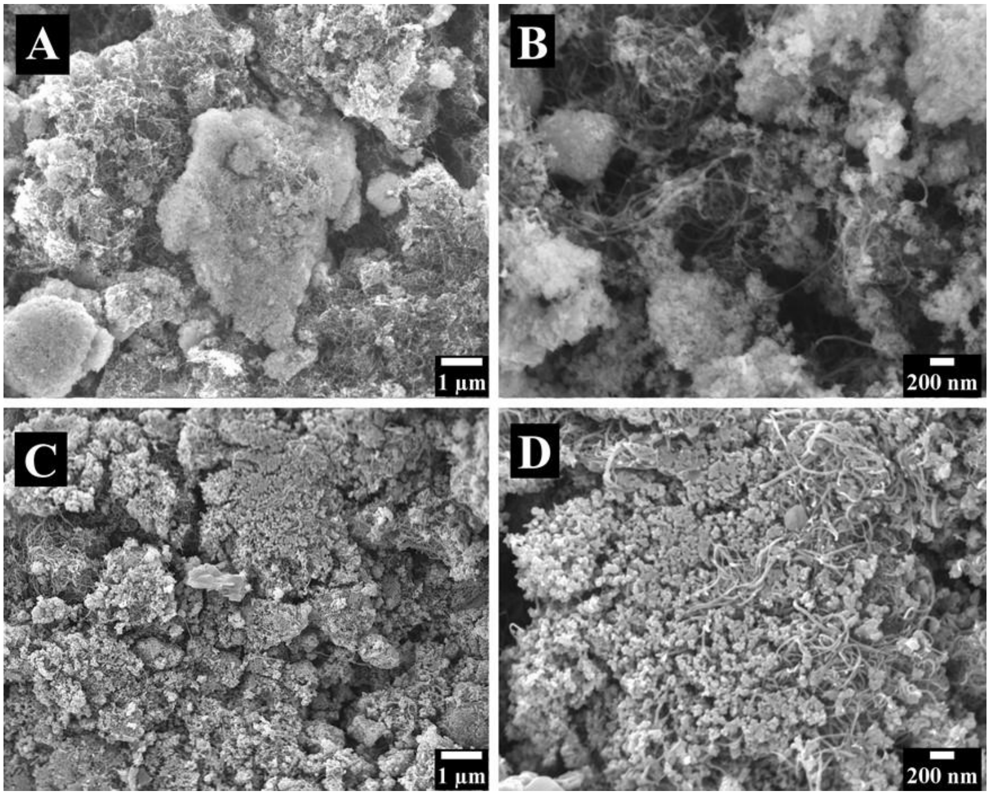

Figure 4. SEM images of different magnifications for electrodes prepared using (**A**,**B**) chlorogenic acid and (**C**,**D**) 3,4,5-trihydroxybenzamide.

Figure 5A–C show CV data at different scan rates for electrodes prepared without and with dispersants. The electrodes prepared using dispersants showed significantly larger areas of CVs, which indicated higher capacitances. The integral capacitances in a voltage window of 0 to 0.9 V were measured at different scan rates and presented in Figure 5D. The electrodes prepared with chlorogenic acid, 3,4,5-trihydroxybenzamide and without dispersants showed areal capacitances of 6.4, 6.5 and 2.1 F cm^{-2}, respectively at a scan rate of 2 mV s^{-1}. The increase in scan rate resulted in the reduced capacitance due to diffusion limitations of an electrolyte in pores. The electrodes prepared using dispersants showed significantly higher capacitance, compared to the electrodes prepared without dispersants. The electrodes, formed using 3,4,5-trihydroxybenzamide, showed higher capacitance retention at 100 mV s^{-1}, compared to the electrodes formed using chlorogenic acid. EIS studies showed higher resistance $R = Z'$ of the electrodes prepared without dispersant, which resulted from poor mixing of CNT with MnO_2. Moreover, the electrodes prepared without dispersant showed lower C_S' and lower relaxation frequency, corresponding to the C_S'' maximum. The electrodes prepared in the presence of chlorogenic acid showed the highest capacitance at 10 MHz. However, the electrodes formed using 3,4,5-trihydroxybenzamide showed higher capacitance at frequencies above 50 Hz, indicating better charge storage properties at higher charge discharge rates in agreement with CV data. The electrodes prepared using 3,4,5-trihydroxybenzamide as a dispersant showed the lowest resistance and the highest relaxation frequency, as indicated by the location of the C'' maximum. It is important to note that capacitances, calculated from the CV data, depended on scan rate, whereas the capacitances calculated from the impedance data depend on frequency. The comparison of the capacitances calculated at the same charge–discharge time scale showed that integral capacitances were higher than differential capacitances. The difference in the differential and integral capacitance was discussed in the literature[52]. It was shown that such difference can result from various reasons, such as the presence of sites with different redox potentials and limited access of the electrolyte to some redox sites at low voltages[52]. Testing results showed beneficial effect of improved mixing of MnO_2 and CNT, which was achieved using dispersant molecules. However, this investigation revealed some difference in electrochemical behavior of the electrodes prepared using chlorogenic acid and 3,4,5-trihydroxybenzamide. Turning again the chemical structures of the molecules (Figure 1) it is seen that the dissociation of the carboxylic group of adsorbed chlorogenic acid can potentially impart a negative charge to MnO_2 and CNT and improve their dispersion and mixing. This can result in better performance of the composite electrodes, which was observed at low frequencies. However, little attention has been paid in the available supercapacitor literature to possible local pH changes at the positive electrode during charge–discharge process.

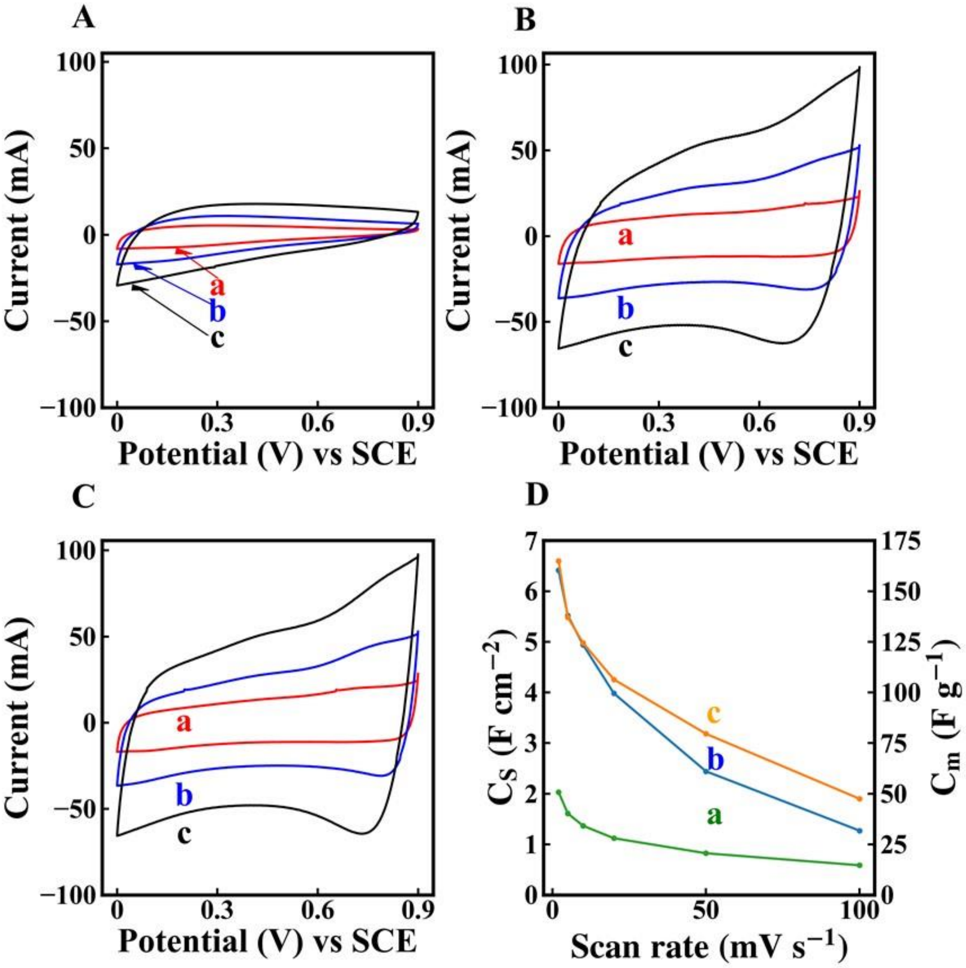

Figure 5. (**A–C**) CVs at scan rates of (a) 2, (b) 5 and (c) 10 mV s^{-1} for electrodes prepared (**A**) without dispersant, (**B**) in the presence of chlorogenic and (**C**) in the presence of 3,4,5-trihydroxybenzamide, (**D**) Cs and Cm versus scan rate for electrodes prepared (a) without dispersant, (b) in the presence of chlorogenic acid and (c) in the presence of 3,4,5-trihydroxybenzamide.

It is known that the application of a positive potential to the electrode usually results in a local pH decrease[53]; therefore, the protonation of amino groups of organic molecules [1,53] can be expected at such conditions. Therefore, it was hypothesized that the protonation of NH_2 groups of adsorbed 3,4,5-trihydroxybenzamide can potentially impart a positive charge to the electrode material.

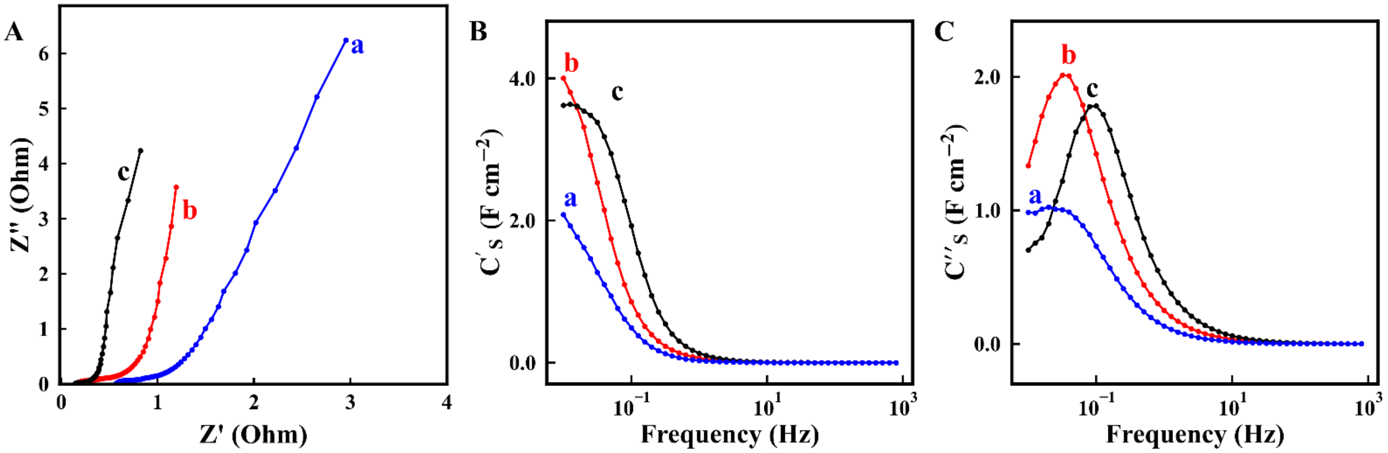

Figure 6. (**A**) Nyquist plot of impedance and (**B**,**C**) components complex capacitance C* = C′ − *i*C″ versus frequency for electrodes prepared (a) without dispersant, (b) in the presence of chlorogenic acid and (c) in the presence of 3,4,5-trihydroxybenzamide.

The charging process of the MnO_2 electrode is given by the reaction, involving MnO_2 oxidation from 3^+ to 4^+ and release of adsorbed Na^+.

$$MnO_2Na \leftrightarrow MnO_2 + e^- + Na^+ \quad (4)$$

It was suggested that the positive charge of the electrodes prepared using 3,4,5-trihydroxybenzamide will facilitate Na^+ desorption and transport. In contrast, the protonation of the carboxylic groups of the carboxylic acid molecules will result in their discharge. Therefore, it was not surprizing that the electrodes prepared using 3,4,5-trihydroxybenzamide showed lower resistance and better capacitive properties at high scan rates and high frequencies. The results of this investigation indicate that the modification of the charge of an active material by adsorption of organic molecules can potentially open a promising avenue for the development of electrodes with enhanced performance.

Figure 7A–C show GCD data for electrodes prepared without and with dispersants. The use of dispersants resulted in significantly longer charge–discharge currents, which was attributed to higher capacitance. The capacitances calculated from the discharge data were presented in Figure 7D. It is seen that the use of dispersants allowed for the fabrication of electrodes with significantly higher capacitances, compared to the electrodes prepared without dispersants. The electrodes showed good cyclic stability (Figure 8). The electrodes prepared without dispersants, with chlorogenic acid and 3,4,5-trihydroxybenzamide showed capacitance retentions of 111, 102 and 113%, respectively. The slight increase in retention during cycling can result form microstructure changes during cycling or enhanced wetting of the electrodes by the electrolyte[54,55]. Obtained cathodes are promising for applications in asymmetric devices operating in Na_2SO_4 electrolyte. However, in order to utilize the benefits of high capacitance of the cathodes in devices, the anodes of similar capacitance must be used. The analysis of literature indicates that reported areal capacitances of some promising anode materials in the same electrolyte are significantly lower and their cyclic stability must be improved[56]. Therefore, further progress must be achieved in the discovery and development of advanced anode materials.

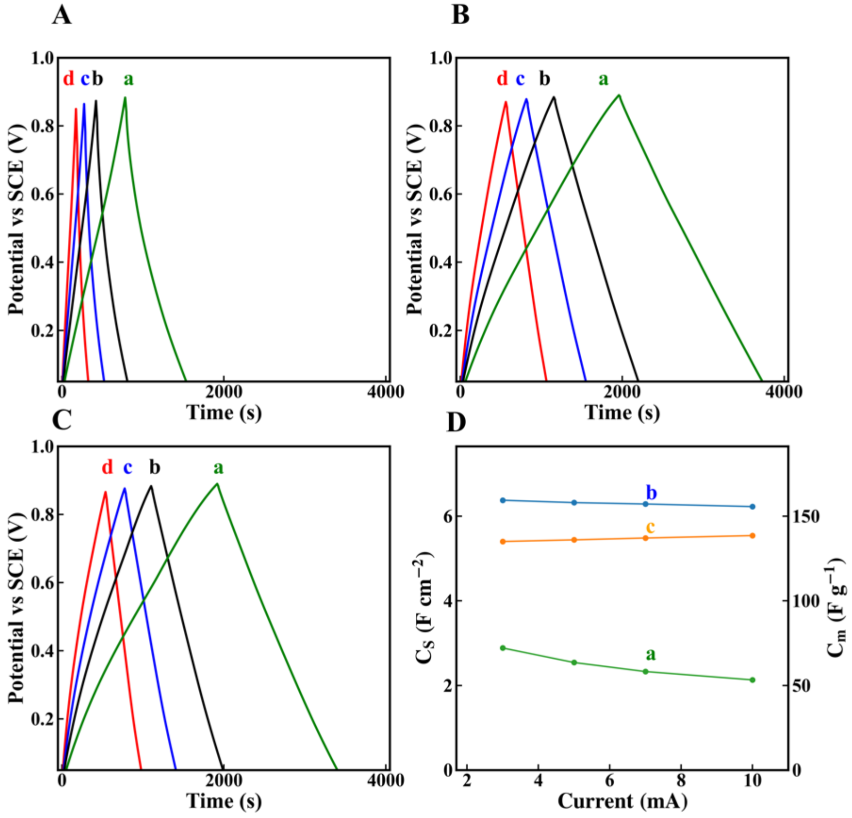

Figure 7. Galvanostatic charge–discharge (GCD) data for electrodes prepared (**A**) without dispersant, (**B**) in the presence of chlorogenic and (**C**) in the presence of 3,4,5-trihydroxybenzamide at current densities of (a) 3, (b) 5, (c) 7 and (d) 10 mA cm^{-2}, (**D**) capacitances calculated from the GCD data for electrodes prepared (a) without dispersant, (b) in the presence of chlorogenic and (c) in the presence of 3,4,5-trihydroxybenzamide versus current density.

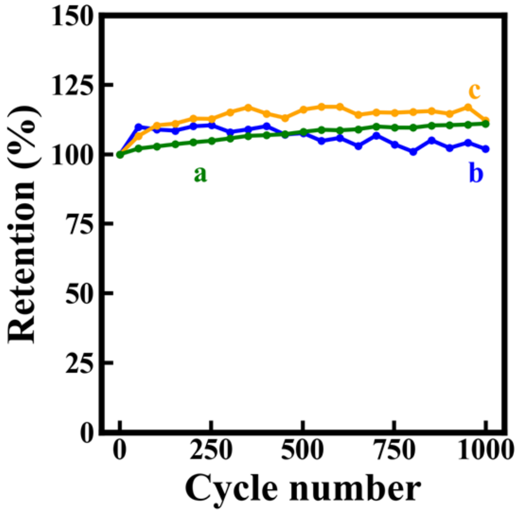

Figure 8. Capacitance retention versus cycle number for electrodes prepared (a) without dispersant, (b) in the presence of chlorogenic and (c) in the presence of 3,4,5-trihydroxybenzamide versus current density.

3. Materials and Methods

$KMnO_4$, polyvinyl butyral (PVB), chlorogenic acid, ethanol, Na_2SO_4, and 3,4,5-trihydroxybenzamide (Aldrich), CNT (multiwalled, Bayer) and Ni foams (Vale) were used. MnO_2 nanoparticles were prepared by a chemical precipitation method described in a previous investigation[49]. This method was based on reduction of Mn^{7+} in an aqueous $KMnO_4$ solution by addition of ethanol as a reducing agent. The method resulted in nearly amorphous MnO_2, which also contained a small amount of a birnessite phase. Previous investigations showed poor stability of prepared MnO_2 in ethanol. It was found that the dispersant, used in the previous investigation for MnO_2 dispersion, failed to disperse CNT. Therefore, in this investigation chlorogenic acid, and 3,4,5-trihydroxybenzamide were tested as co-dispersants for MnO_2 and CNT. The ability to co-disperse MnO_2 and CNT was critical for the fabrication of slurries, containing dissolved PVB as a binder, for impregnation of Ni foam current collectors and fabrication of high active mass electrodes with the mass of impregnated material of 40 mg cm^{-2}. The mass ratio MnO_2:CNT:PVB was 80:20:3.

SEM studies were performed using a microscope JEOL SEM (JSM-7000F). Cyclic voltammetry (CV) and electrochemical impedance spectroscopy (EIS) studies were performed using a potentiostat-impedance analyzer PARSTAT 2273 (Ametek). EIS data were obtained at an open circuit potential using alternating voltage with an amplitude of 5 mV in the frequency range 0.01–10 kHz. Galvanostatic charge–discharge (GCD) investigations in a fixed potential range were performed using BioLogic VMP 300. Testing was performed using a 3-electrode electrochemical cell containing a working electrode (impregnated Ni foam), counter electrode (Pt mesh), and a reference electrode (SCE, saturated calomel electrode). Aqueous 0.5 M Na_2SO_4 solution was used as an electrolyte. Integral capacitances in a potential window of 0 to 0.9 V were calculated from CV and GCD data, as described in previous investigations[56,57]. Mass normalized C_m and area normalized C_S capacitances were analyzed. Differential capacitance was calculated from the EIS data by the methodology described in[56,57]. All the testing results were obtained for 5 electrodes of the same active mass. The capacitances obtained by the same method for different electrodes varied within 3%.

4. Conclusions

For the first time, chlorogenic acid and 3,4,5-trihydroxybenzamide were used as dispersants for MnO_2 and CNT and fabrication of composite cathodes for supercapacitors. The chemical structures of the molecules facilitated their adsorption on MnO_2 and CNT, which allowed for co-dispersion and enhanced mixing. Structural peculiarities of the dispersant molecules facilitate dispersion and charging. This simple strategy allowed for the fabrication of supercapacitor electrodes, which showed a capacitance of 6.5 F cm^{-2} and low resistance at high active mass of 40 mg cm^{-2}. The analysis of microstructures of electrodes prepared without dispersant and with dispersant provides an insight into the influence of chlorogenic acid and 3,4,5-trihydroxybenzamide dispersants on the electrode performance. The electrodes showed good cyclic stability and can be used for the fabrication of asymmetric supercapacitor devices.

Author Contributions: Conceptualization, K.R. and I.Z.; methodology, K.R.; validation, K.R. and I.Z.; formal analysis, K.R.; investigation, K.R.; resources, I.Z.; writing—original draft preparation, I.Z. and K.R.; writing—review and editing, K.R. and I.Z.; supervision, I.Z.; project administration, I.Z.; funding acquisition, I.Z. All authors have read and agreed to the published version of the manuscript.

Funding: This research was funded by the Natural Sciences and Engineering Research Council of Canada, grant number RGPIN-2018-04014.

Institutional Review Board Statement: Not Applicable.

Informed Consent Statement: Not Applicable.

Data Availability Statement: The data presented in this study are available in: Dispersant molecules with functional catechol groups for supercapacitor fabrication.

Acknowledgments: SEM investigations were performed at the Canadian Centre for Electron Microscopy.

Conflicts of Interest: The authors declare no conflict of interest.

References

1. Ata, M.S.; Liu, Y.; Zhitomirsky, I. A review of new methods of surface chemical modification, dispersion and electrophoretic deposition of metal oxide particles. *RSC Adv.* **2014**, *4*, 22716–22732, doi:10.1039/c4ra02218a.
2. Lee, B.P.; Messersmith, P.; Israelachvili, J.; Waite, J. Mussel-Inspired Adhesives and Coatings. *Annu. Rev. Mater. Res.* **2011**, *41*, 99–132, doi:10.1146/annurev-matsci-062910-100429.
3. Lee, H.; Lee, B.P.; Messersmith, P.B. A reversible wet/dry adhesive inspired by mussels and geckos. *Nat. Cell Biol.* **2007**, *448*, 338–341, doi:10.1038/nature05968.
4. Petrone, L. Molecular surface chemistry in marine bioadhesion. *Adv. Colloid Interface Sci.* **2013**, *195*, 1–18.
5. Lebrette, S.; Pagnoux, C.; Abelard, P. Fabrication of titania dense layers by electrophoretic deposition in aqueous media. *J. Eur. Ceram. Soc.* **2006**, *26*, 2727–2734, doi:10.1016/j.jeurceramsoc.2005.05.009.
6. Silva, R.; Poon, R.; Milne, J.; Syed, A.; Zhitomirsky, I. New developments in liquid-liquid extraction, surface modification and agglomerate-free processing of inorganic particles. *Adv. Colloid Interface Sci.* **2018**, *261*, 15–27, doi:10.1016/j.cis.2018.09.005.

7. Ata, M.S.; Poon, R.; Syed, A.M.; Milne, J.; Zhitomirsky, I. New developments in non-covalent surface modification, dispersion and electrophoretic deposition of carbon nanotubes. *Carbon* **2018**, *130*, 584–598, doi:10.1016/j.carbon.2018.01.066.
8. Wang, Y.; Liu, Y.; Zhitomirsky, I. Surface modification of MnO2 and carbon nanotubes using organic dyes for nanotechnology of electrochemical supercapacitors. *J. Mater. Chem. A* **2013**, *1*, 12519–12526, doi:10.1039/c3ta12458d.
9. Nawwar, M.; Poon, R.; Sahu, R.P.; Puri, I.K.; Zhitomirsky, I. Fe3O4 spinel-Mn3O4 spinel supercapacitor prepared using Celestine blue as a dispersant, capping agent and charge transfer mediator. *Ceram. Int.* **2020**, *46*, 18851–18858, doi:10.1016/j.ceramint.2020.04.204.
10. Togashi, T.; Takami, S.; Kawakami, K.; Yamamoto, H.; Naka, T.; Sato, K.; Abe, K.; Adschiri, T. Continuous hydrothermal synthesis of 3,4-dihydroxyhydrocinnamic acid-modified magnetite nanoparticles with stealth-functionality against immunological response. *J. Mater. Chem.* **2012**, *22*, 9041–9045, doi:10.1039/c2jm30325f.
11. Sugimoto, T.; Itoh, H.; Mochida, T. Shape Control of Monodisperse Hematite Particles by Organic Additives in the Gel–Sol System. *J. Colloid Interface Sci.* **1998**, *205*, 42–52, doi:10.1006/jcis.1998.5588.
12. Hori, M.; Pagnoux, C.; Baumard, J.-F.; Nogami, M. Preparation of gold nanoparticles (GNP) aqueous suspensions by a new method involving Tiron. *J. Mater. Sci.* **2006**, *42*, 80–86, doi:10.1007/s10853-006-1048-x.
13. Zhang, T.; Wojtal, P.; Rubel, O.; Zhitomirsky, I. Density functional theory and experimental studies of caffeic acid adsorption on zinc oxide and titanium dioxide nanoparticles. *RSC Adv.* **2015**, *5*, 106877–106885, doi:10.1039/c5ra21511k.
14. Zhu, Y.; Shi, K.; Zhitomirsky, I. Anionic dopant–dispersants for synthesis of polypyrrole coated carbon nanotubes and fabrication of supercapacitor electrodes with high active mass loading. *J. Mater. Chem. A* **2014**, *2*, 14666–14673, doi:10.1039/c4ta02117g.
15. Kim, S.; Park, C.B. Mussel-inspired transformation of CaCO3 to bone minerals. *Biomaterials* **2010**, *31*, 6628–6634, doi:10.1016/j.biomaterials.2010.05.004.
16. Yu, M.; Deming, T.J. Synthetic Polypeptide Mimics of Marine Adhesives. *Macromolecules* **1998**, *31*, 4739–4745, doi:10.1021/ma980268z.
17. Ye, Q.; Zhou, F.; Liu, W., Bioinspired catecholic chemistry for surface modification. *Chem. Soc. Rev.* **2011**, *40*, 4244–4258.
18. Dalsin, J.L.; Hu, B.-H.; Lee, B.P.; Messersmith, P.B. Mussel Adhesive Protein Mimetic Polymers for the Preparation of Nonfouling Surfaces. *J. Am. Chem. Soc.* **2003**, *125*, 4253–4258, doi:10.1021/ja0284963.
19. Winkler, T.E.; Ben-Yoav, H.; Chocron, S.E.; Kim, E.; Kelly, D.L.; Payne, G.F.; Ghodssi, R. Electrochemical Study of the Catechol-Modified Chitosan System for Clozapine Treatment Monitoring. *Langmuir* **2014**, *30*, 14686–14693, doi:10.1021/la503529k.
20. Clifford, A.; Pang, X.; Zhitomirsky, I. Biomimetically modified chitosan for electrophoretic deposition of composites. *Colloids Surf. A Physicochem. Eng. Asp.* **2018**, *544*, 28–34, doi:10.1016/j.colsurfa.2018.02.028.
21. Wang, G.-L.; Xu, J.-J.; Chen, H.-Y. Dopamine sensitized nanoporous TiO2 film on electrodes: Photoelectrochemical sensing of NADH under visible irradiation. *Biosens. Bioelectron.* **2009**, *24*, 2494–2498, doi:10.1016/j.bios.2008.12.031.
22. Varaganti, S.; Ramakrishna, G. Dynamics of Interfacial Charge Transfer Emission in Small Molecule Sensitized TiO2 Nanoparticles: Is It Localized or Delocalized? *J. Phys. Chem. C* **2010**, *114*, 13917–13925, doi:10.1021/jp102629u.
23. Rajh, T.; Chen, L.X.; Lukas, K.; Liu, T.; Thurnauer, M.C.; Tiede, D.M. Surface Restructuring of Nanoparticles: An Efficient Route for Ligand−Metal Oxide Crosstalk. *J. Phys. Chem. B* **2002**, *106*, 10543–10552, doi:10.1021/jp021235v.
24. Nagesha, D.K.; Plouffe, B.D.; Phan, M.; Lewis, L.H.; Sridhar, S.; Murthy, S.K. Functionalization-induced improvement in magnetic properties of Fe3O4 nanoparticles for biomedical applications. *J. Appl. Phys.* **2009**, *105*, 317, doi:10.1063/1.3073654.
25. Huang, W.; Jiang, P.; Wei, C.; Zhuang, D.; Shi, J. Low-temperature one-step synthesis of covalently chelated ZnO/dopamine hybrid nanoparticles and their optical properties. *J. Mater. Res.* **2008**, *23*, 1946–1952, doi:10.1557/jmr.2008.0243.
26. Bloemen, M.; Debruyne, D.; Demeyer, P.-J.; Clays, K.; Gils, A.; Geukens, N.; Bartic, C.; Verbiest, T. Catechols as ligands for CdSe–ZnS quantum dots. *RSC Adv.* **2014**, *4*, 10208, doi:10.1039/c3ra47844k.
27. Tallman, D.E.; Vang, C.; Wallace, G.G.; Bierwagen, G.P. Direct Electrodeposition of Polypyrrole on Aluminum and Aluminum Alloy by Electron Transfer Mediation. *J. Electrochem. Soc.* **2002**, *149*, C173–C179, doi:10.1149/1.1448820.
28. Chen, S.; Zhitomirsky, I. Influence of dopants and carbon nanotubes on polypyrrole electropolymerization and capacitive behavior. *Mater. Lett.* **2013**, *98*, 67–70, doi:10.1016/j.matlet.2013.01.123.
29. Shi, C.; Zhitomirsky, I. Electrodeposition of composite polypyrrole–carbon nanotube films. *Surf. Eng.* **2011**, *27*, 655–661, doi:10.1179/1743294410y.0000000004.
30. Fan, X.; Lin, L.; Dalsin, J.L.; Messersmith, P.B. Biomimetic Anchor for Surface-Initiated Polymerization from Metal Substrates. *J. Am. Chem. Soc.* **2005**, *127*, 15843–15847, doi:10.1021/ja0532638.
31. De Souza, F.; Spinelli, A. Caffeic acid as a green corrosion inhibitor for mild steel. *Corros. Sci.* **2009**, *51*, 642–649, doi:10.1016/j.corsci.2008.12.013.
32. Black, K.C.L.; Liu, Z.; Messersmith, P.B. Catechol Redox Induced Formation of Metal Core−Polymer Shell Nanoparticles. *Chem. Mater.* **2011**, *23*, 1130–1135, doi:10.1021/cm1024487.
33. Marcelo, G.; Fernández-García, M. Direct preparation of PNIPAM coating gold nanoparticles by catechol redox and surface adhesion chemistry. *RSC Adv.* **2014**, *4*, 11740–11749, doi:10.1039/c3ra47880g.
34. Stallings, M.D.; Morrison, M.M.; Sawyer, D.T., Redox chemistry of metal-catechol complexes in aprotic media. 1. Electrochemistry of substituted catechols and their oxidation products. *Inorg. Chem.* **1981**, *20*, 2655–2660.
35. Touzé, E.; Gohier, F.; Daffos, B.; Taberna, P.-L.; Cougnon, C. Improvement of electrochemical performances of catechol-based supercapacitor electrodes by tuning the redox potential via different-sized O-protected catechol diazonium salts. *Electrochim. Acta* **2018**, *265*, 121–130, doi:10.1016/j.electacta.2018.01.115.

36. Fireman-Shoresh, S.; Turyan, I.; Mandler, D.; Avnir, D.; Marx, S. Chiral Electrochemical Recognition by Very Thin Molecularly Imprinted Sol−Gel Films. *Langmuir* **2005**, *21*, 7842–7847, doi:10.1021/la050240y.
37. Naveed, M.; Hejazi, V.; Abbas, M.; Kamboh, A.A.; Khan, G.J.; Shumzaid, M.; Ahmad, F.; Babazadeh, D.; FangFang, X.; Modarresi-Ghazani, F.; et al. Chlorogenic acid (CGA): A pharmacological review and call for further research. *Biomed. Pharmacother.* **2018**, *97*, 67–74, doi:10.1016/j.biopha.2017.10.064.
38. Huang, J.; Li, T.; Chen, Z.; Liu, X.; Liu, S. Rapid electrochemical detection of DNA damage and repair with epigallocatechin gallate, chlorogenic acid and ascorbic acid. *Electrochem. Commun.* **2008**, *10*, 1198–1200, doi:10.1016/j.elecom.2008.06.002.
39. Zhang, X.; Wang, H.; Niu, N.; Chen, Z.; Li, S.; Liu, S.-X.; Li, J., Fluorescent Poly (vinyl alcohol) Films Containing Chlorogenic Acid Carbon Nanodots for Food Monitoring. *ACS Appl. Nano Mater.* **2020**, *3*, 7611–7620.
40. Salimi, A.; Hallaj, R. Adsorption and Reactivity of Chlorogenic Acid at a Hydrophobic Carbon Ceramic Composite Electrode: Application for the Amperometric Detection of Hydrazine. *Int. J. Devoted Fundam. Pract. Asp. Electroanal.* **2004**, *16*, 1964–1971, doi:10.1002/elan.200303030.
41. Andjelkovic, M.; Vancamp, J.; Demeulenaer, B.; Depaemelaere, G.; Socaciu, C.; Verloo, M.; Verhe, R. Iron-chelation properties of phenolic acids bearing catechol and galloyl groups. *Food Chem.* **2006**, *98*, 23–31, doi:10.1016/j.foodchem.2005.05.044.
42. Cheng, M.-C.; Lu, Y.-C.; Wu, J.; Ma, Y.-H. Gallate-induced nanoparticle uptake by tumor cells: Structure-activity relationships. *Colloids Surf. B Biointerfaces* **2019**, *179*, 28–36, doi:10.1016/j.colsurfb.2019.03.048.
43. Jovanović, I.N.; Miličević, A.; Jadreško, D.; Hranjec, M. Electrochemical oxidation of synthetic amino-substituted benzamides with potential antioxidant activity. *J. Electroanal. Chem.* **2020**, *870*, 114244, doi:10.1016/j.jelechem.2020.114244.
44. Vangari, M.; Pryor, T.; Jiang, L. Supercapacitors: Review of Materials and Fabrication Methods. *J. Energy Eng.* **2013**, *139*, 72–79, doi:10.1061/(asce)ey.1943-7897.0000102.
45. Mao, N.; Wang, H.; Sui, Y.; Cui, Y.; Pokrzywinski, J.; Shi, J.; Liu, W.; Chen, S.; Wang, X.; Mitlin, D. Extremely high-rate aqueous supercapacitor fabricated using doped carbon nanoflakes with large surface area and mesopores at near-commercial mass loading. *Nano Res.* **2017**, *10*, 1767–1783, doi:10.1007/s12274-017-1486-6.
46. Pant, B.; Pant, H.R.; Park, M. Fe1−xS Modified TiO2 NPs Embedded Carbon Nanofiber Composite via Electrospinning: A Potential Electrode Material for Supercapacitors. *Molecules* **2020**, *25*, 1075, doi:10.3390/molecules25051075.
47. Chen, G.; Zhang, X.; Ma, Y.; Song, H.; Pi, C.; Zheng, Y.; Gao, B.; Fu, J.; Chu, P.K. In-Situ Synthesis of Heterostructured Carbon-Coated Co/MnO Nanowire Arrays for High-Performance Anodes in Asymmetric Supercapacitors. *Molecules* **2020**, *25*, 3218, doi:10.3390/molecules25143218.
48. Malkova, A.N.; Sipyagina, N.A.; Gozhikova, I.O.; Dobrovolsky, Y.A.; Konev, D.V.; Baranchikov, A.E.; Ivanova, O.S.; Ukshe, A.E.; Lermontov, S.A. Electrochemical Properties of Carbon Aerogel Electrodes: Dependence on Synthesis Temperature. *Molecules* **2019**, *24*, 3847, doi:10.3390/molecules24213847.
49. Li, J.; Zhitomirsky, I. Cathodic electrophoretic deposition of manganese dioxide films. *Colloids Surf. A Physicochem. Eng. Asp.* **2009**, *348*, 248–253, doi:10.1016/j.colsurfa.2009.07.035.
50. Zhu, Y.; Shi, K.; Zhitomirsky, I. Polypyrrole coated carbon nanotubes for supercapacitor devices with enhanced electrochemical performance. *J. Power Sources* **2014**, *268*, 233–239, doi:10.1016/j.jpowsour.2014.06.046.
51. Biswas, N.; Kapoor, S.; Mahal, H.S.; Mukherjee, T. Adsorption of CGA on colloidal silver particles: DFT and SERS study. *Chem. Phys. Lett.* **2007**, *444*, 338–345, doi:10.1016/j.cplett.2007.07.049.
52. Liu, Y.; Shi, K.; Zhitomirsky, I. Asymmetric supercapacitor, based on composite MnO2-graphene and N-doped activated carbon coated carbon nanotube electrodes. *Electrochim. Acta* **2017**, *233*, 142–150, doi:10.1016/j.electacta.2017.03.028.
53. Sikkema, R.; Baker, K.; Zhitomirsky, I. Electrophoretic deposition of polymers and proteins for biomedical applications. *Adv. Colloid Interface Sci.* **2020**, *284*, 102272, doi:10.1016/j.cis.2020.102272.
54. Su, Y.; Zhitomirsky, I. Hybrid MnO2/carbon nanotube-VN/carbon nanotube supercapacitors. *J. Power Sources* **2014**, *267*, 235–242.
55. Rorabeck, K.; Zhitomirsky, I. Application of Octanohydroxamic Acid for Salting out Liquid–Liquid Extraction of Materials for Energy Storage in Supercapacitors. *Molecules* **2021**, *26*, 296, doi:10.3390/molecules26020296.
56. Chen, R.; Yu, M.; Sahu, R.P.; Puri, I.K.; Zhitomirsky, I. The Development of Pseudocapacitor Electrodes and Devices with High Active Mass Loading. *Adv. Energy Mater.* **2020**, *10*, 1903848, doi:10.1002/aenm.201903848.
57. Shi, K.; Zhitomirsky, I. Fabrication of Polypyrrole-Coated Carbon Nanotubes Using Oxidant–Surfactant Nanocrystals for Supercapacitor Electrodes with High Mass Loading and Enhanced Performance. *ACS Appl. Mater. Interfaces* **2013**, *5*, 13161–13170, doi:10.1021/am404159b.

Chapter 8 – Conclusions and Future Works

The conceptually different, colloidal extraction technique based on the salting out phenomenon, using OHA and LG was successful, and the materials showed a good capacitive and cyclic properties when compared with materials prepared by the PELLI technique. Similarly, to PELLI, the salting out technique avoids the drying stage, which is beneficial to the electrode fabrication process. This technique removes the need for hydrophobic solvents, removing the possibility that these hydrophobic solvents may remain adsorbed to the electrode surfaces. It was found that electrodes fabricated using LG in the salting out process showed a capacitance increase of 1.7 F cm^{-2} at a scan rate of 2 mV s^{-1}, for similar mass loadings. SEM analysis of both electrode samples indicated a change in morphology from before to after electrochemical testing, and the significant increase in cyclic stability over 1000 cycles has been attributed to this morphological change.

The co-dispersion of MnO_2 and MWCNTs using chlorogenic acid and 3,4,5-trihydroxybenzamide, was shown to increase in the specific capacitance three-fold at a scan rate of 2 mV s^{-1} ,when compared to electrodes fabricated without these co-dispersing agents. Images taken using SEM, showed an improvement in the mixing of MnO_2 with the MWCNTs, as well as providing good overall dispersion of both compounds. This improved mixing and dispersion compared to the electrodes fabricated without the co-dispersants, is hypothesized to be the major contributing factor to the increase in the specific capacitance.

Future works in this domain, should immediately consider the development of electrodes that can operate with similar capacitance values in the potential range from -0.9 to 0V, so that these electrodes may be used to fabricate supercapacitor devices, and report on their performance. The significant increases in cyclic stability and capacitance, could become a diminished success if negative electrodes could not be fabricated with similar capacitive properties. To facilitate the development of negative electrodes, XPS may be beneficial in providing surface chemical oxidation states during electrochemical testing. Further studies with SEM for the qualitative observation of new active materials and dispersants with conducting additives, would help streamline the selection process.